PL-TR-96-2279

ATMOSPHERIC ULTRAVIOLET RADIANCE INTEGRATED CODE (AURIC): AIRGLOW PORTION PROVIDING DAYGLOW AND NIGHTGLOW SPECTRAL RADIANCES FROM 100 TO 900 nm

D. J. Strickland   T. Majeed
J. S. Evans   P. M. Shen
J. E. Bishop   R. Link

Computational Physics, Inc
2750 Prosperity Avenue, Suite 600
Fairfax, VA 22031

27 January 1997

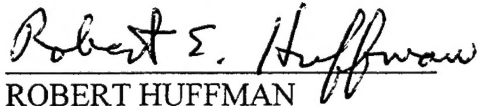Final Report
30 December 1991-30 March 1996

19970305 063

PHILLIPS LABORATORY
Directorate of Geophysics
AIR FORCE MATERIEL COMMAND
HANSCOM AFB, MA 01731-3010

DTIC QUALITY INSPECTED 3

"This technical report has been reviewed and is approved for publication"

ROBERT HUFFMAN
Contract Manager

DAVID N. ANDERSON
Branch Chief

DAVID A. HARDY
Division Director

This report has been reviewed by the ESC Public Affairs (PA) and is releasable to the National Technical Information Service (NTIS)

Qualified requesters may obtain additional copies from the Defense Technical Information Center (DTIC). All others should apply to the National Technical Information Service (NTIS)

If your address has changed, if you wish to be removed from the mailing list, or if the addressee is no longer employed by your organization, please notify PL/IM, 29 Randolph Road, Hanscom AFB, MA 01731-3010. This will assist us in maintaining a current mailing list.

Do not return copies of this report unless contractual obligations or notices on a specific document require that it be returned.

REPORT DOCUMENTATION PAGE

Form Approved
OMB No. 0704-0188

Public reporting burden for this collection of information is estimated to average 1 hour per response, including the time for reviewing instructions, searching existing data sources, gathering and maintaining the data needed, and completing and reviewing the collection of information. Send comments regarding this burden estimate or any other aspect of this collection of information, including suggestions for reducing this burden, to Washington Headquarters Services, Directorate for Information Operations and Reports, 1215 Jefferson Davis Highway, Suite 1204, Arlington, VA 22202-4302, and to the Office of Management and Budget, Paperwork Reduction Project (0704-0188), Washington, DC 20503.

1. AGENCY USE ONLY *(Leave blank)*	2. REPORT DATE	3. REPORT TYPE AND DATES COVERED
	January 27, 1997	Final Report (30 Dec 91 - 30 Mar 96)

4. TITLE AND SUBTITLE
Atmospheric Ultraviolet Radiance Integrated Code (AURIC): Airglow Portion
Providing Dayglow and Nightglow Spectral Radiances From 100 to 900 nm

5. FUNDING NUMBERS
PE 63215C
PR S321   TA 06   WU AP

Contract #F19628-92-C-0016

6. AUTHOR(S)

D. J. Strickland, J. S. Evans, J. E. Bishop, T. Majeed, P. M. Shen, R. Link

7. PERFORMING ORGANIZATION NAME(S) AND ADDRESS(ES)

Computational Physics, Inc.
2750 Prosperity Avenue   Suite 600
Fairfax, Virginia 22031

8. PERFORMING ORGANIZATION REPORT NUMBER

9. SPONSORING/MONITORING AGENCY NAME(S) AND ADDRESS(ES)
Phillips Laboratory
29 Randolph Street
Hanscom AFB, MA 01731-5000
Contract Manager: Dr. Robert Huffman/GPIM

10. SPONSORING/MONITORING AGENCY REPORT NUMBER

PL-TR-96-2279

11. SUPPLEMENTARY NOTES

12a. DISTRIBUTION AVAILABILITY STATEMENT

APPROVED FOR PUBLIC RELEASE
DISTRIBUTION UNLIMITED

12b. DISTRIBUTION CODE

13. ABSTRACT *(Maximum 200 words)*

The work reported let to a suite of codes for characterizing dayglow and nightglow and for ingesting Rayleigh scattered radiances (solar and lunar) from MODTRAN. The key outputs are spectral radiances at satellite altitudes for any viewing angle. The wavelength range is from ~100 to ~900 nm and, for dayglow, contains all prominent band systems and lines, including HI 121.6 nm and OI 130.4 nm. Chemistry models are available for calculating a variety of ion and neutral densities under sunlit conditions and excitation rates at night for O atom recombination (lower thermosphere and upper thermosphere) and O+ recombination (F region).

AURIC was originally developed to provide the ballistic missile defense community with a tool for realistically characterizing terrestrial backgrounds from the far UV to the near IR on both the Earth's dayside and nightside. Recent enhancements make AURIC of interest to a wider community by enabling the user to conduct scientific studies in addition to predictions of optical backgrounds. Detailed investigations may be performed that relate emissions to composition for remote sensing purposes. Studies may also be undertaken of ion and neutral species with detailed examiniation of densities of these species as functions of background compostion, solar EUV, cross sections, rate coefficients, etc. AURIC is easy to run through either a user-interface or direct submission of batch files. Furthermore, I/O files are formatted for easy inspection of their contents and numerous IDL procedures are available for graphical display of inputs and outputs. Contract deliverables include this report, two science papers, AURIC's rate coefficients, the software itself, and a user's manual.

14. SUBJECT TERMS

Aeronomy, Dayglow, Nightglow, Photochemistry, Optical Backgrounds

15. NUMBER OF PAGES
94

16. PRICE CODE

17. SECURITY CLASSIFICATION OF REPORT	18. SECURITY CLASSIFICATION OF THIS PAGE	19. SECURITY CLASSIFICATION OF ABSTRACT	20. LIMITATION OF ABSTRACT
Unclassified	Unclassified	Unclassified	SAR

Standard Form 298 (Rev. 2-89) (EG)
Prescribed by ANSI Std. 239.18
Designed using Perform Pro, WHS/DIOR, Oct 94

CONTENTS

1. INTRODUCTION

This is the final report on Air Force Phillips Laboratory/Geophysics Directorate Contract F19628-92-C-0016. Work emphasized the conversion of a suite of CPI research codes into a new suite using modern programming standards involving redesign, software implementation, testing, and validation. The original statement-of-work (SOW) called for a new suite of codes that would model spectral radiances for dayglow, nightglow, and electron aurora. Due to interruptions in funding and associated uncertainty about the needed support to complete the original SOW, the program was de-scoped to exclude auroral modules. The final products are a suite of codes that model dayglow and nightglow along with documentation. The latter includes a User's manual and two science papers. The papers follow this introduction. We have just received word that the second paper titled "New Survey of Electron Impact Cross Sections for Photoelectron and Auroral Electron Energy Loss Calculations" as been accepted for publication in *J. Phys. Chem., Ref. Data*.

The delivered software is to be part of a larger set of models called AURIC which stands for Atmospheric Ultraviolet Radiance Integrated Code. The term Integrated refers to original plans to develop a user interface behind which would lie the delivered software along with MODTRAN and associated software. The combined capability would allow users to calculate spectral radiances from the upper atmosphere (airglow), from the middle and lower atmospheres (Rayleigh scattering of sunlight and moonlight), as well combinations of these emissions. Plans are uncertain at this time with regard to this integration.

The delivered software offers a stand-alone capability to calculate airglow spectral radiances from 100 to 900 nm. Viewing is from satellite altitudes and includes the limb and hard disk. The software was redesigned in Fortran and is available for running on Unix, VMS, and PC systems. All input and output files are formatted with standard formats wherever possible. The suite of codes is comprised of 27 members containing approximately 35,000 lines of coding. It provides the user with the capability to characterize optical backgrounds and conduct detailed scientific studies. Studies include interpretation of space-based radiance measurements and theoretical investigations of a variety of optical features, neutral densities, and ion densities.

Table 1 lists atomic dayglow and nightglow features presently contained in AURIC. Similar information for band systems is given in Table 2. Emission for some of the dayglow and nightglow features arises from metastable states. Densities of these states are calculated by AURIC's photochemistry and nightglow chemistry models. Table 3 lists the dayglow metastables which are part of a larger list that includes ground state ion species and $N(^4S)$.

The original funding for this project came from the Ballistic Missile Defense Office with the intent of providing analysts with a tool for accurately calculating optical

backgrounds as seen from space. The delivered software achieves this goal for two of the three upper atmospheric emission components (dayglow and nightglow). Since first-principles rather than empirical approaches have been used to characterized the radiances, the software has a broader use. Quantitative analysis of satellite and rocket data may be undertaken for optical emissions as well as ion and neutral densities. The software may also be used in the development of remote sensing algorithms. An example is an algorithm developed by Strickland et al. (*J. Geophys. Res., 100,* 12,217, 1995) for deriving the abundance of atomic oxygen and an integrated value of the solar EUV flux from N_2 Lyman-Birge-Hopfield and OI 135.6 nm disk viewing dayglow data.

Table 1. Atomic lines, transitions, type of airglow (day/night) modeled, and identification of those features affected by scattering or requiring chemistry modeling (metastables)

Species	Transition	Wavelength (nm)	Region	Comment
H	$^2P^\circ \to {}^2S$	121.6	Global	Requires multi-dimensional photon transport model
N	$^2P \to {}^2D^\circ$	149.3	Day	
N	$^2P \to {}^2P^\circ$	174.3	"	
N		346.6	"	Metastable
N	$^2P^\circ \to {}^4S^\circ$	520.0	"	Metastable
	$^2D^\circ \to {}^4S^\circ$			
N^+	$^3D^\circ \to {}^3P$	108.5	Day	
N^+	$^5S^\circ \to {}^3P$	214.3	"	Metastable
O	$^3S^\circ \to {}^3P$	130.4	Day/Night	Requires photon transport model
O	$^5S^\circ \to {}^3P$	135.6	"	Requires photon transport model
O	$^1S \to {}^3P$	297.2	"	Metastable
O	$^1S \to {}^1D$	557.7	"	Metastable
O	$^1D \to {}^3P$	630.0	"	Metastable
O	$^5P \to {}^5S^\circ$	777.4	"	
O	$^3P \to {}^3S^\circ$	844.6	"	
O^+	$^2P^\circ \to {}^4S^\circ$	247.0	Day	Metastable
O^+	$^2D^\circ \to {}^4S^\circ$	372.7	"	Metastable
O^+	$^2P^\circ \to {}^2D^\circ$	732.0	"	Metastable

A conscientious effort was made to test and validate the software. Testing included extensive code reviews and cross platform verification of outputs. Validation included comparisons with results from the original research codes (which themselves have been validated over the years through model/data comparisons) and comparisons to selected emission and composition data.

Considerable effort was directed to the User's manual. Every I/O file and code including a user interface is discussed. Detailed information is provided on how to run the codes on each of the three types of platforms. Detailed I/O information is also given in the form of plots of key input parameters and calculated quantities such as the photoelectron source function, the photoelectron flux, volume production rates, limb intensity profiles, spectral radiances, and densities of ions and neutrals.

Table 2. Band systems, transitions, type of airglow, and wavelength regions covered.

Species	Transition	Band system	Region	Wavelength range (nm)
N_2	$a^1\Pi_g \rightarrow X^1\Sigma_g^+$	Lyman-Birge-Hopfield	Day	125 - 240
N_2	$A^3\Sigma_u^+ \rightarrow X^1\Sigma_g^+$	Vegard-Kaplan	"	150 - 690
N_2	$C^3\Pi_u \rightarrow B^3\Pi_g$	Second Positive	"	280 - 460
N_2	$B^3\Pi_g \rightarrow A^3\Sigma_u^+$	First Positive	"	600 to beyond 1000
N_2^+	$B^2\Sigma_u^+ \rightarrow X^2\Sigma_g^+$	First Negative	Day	360 - 520
N_2^+	$A^2\Pi_u \rightarrow X^2\Sigma_g^+$	Meinel	"	500 to beyond 1000
NO	$A^2\Sigma^+ \rightarrow X^2\Pi$	γ	Day	200 - 310
NO	$C^2\Pi \rightarrow X^2\Pi$	δ	"	190 - 250
NO	$D^2\Sigma^+ \rightarrow X^2\Pi$	ε	"	180 - 260
O_2	$b^1\Sigma_g^+ \rightarrow X^3\Sigma_g^-$	Atmospheric	Night	680 - 1000
O_2	$A'^3\Delta_u \rightarrow a^1\Delta_g$	Chamberlain	"	300 - 440
O_2	$A^3\Sigma_u^+ \rightarrow X^3\Sigma_g^-$	Herzberg I	"	250 - 480
O_2	$c^1\Sigma_u^- \rightarrow X^3\Sigma_g^-$	Herzberg II	"	260 - 470

As a concluding introductory comment, much more information on the overall capability of the delivered software may be seen in the first of the following two papers.

We would like to acknowledge Dr. Robert Huffman of AFPL/GP who has been the COTR of this project during its entire lifetime. His support and comments have strengthen the program and helped lead to completion of the revised SOW.

Table 3. Species treated by the photochemistry module and identification of dominant production mechanisms

Species	Dominant Production Mechanisms
Slow reacting species (time integrated)	
NO^+	Charge transfer
O_2^+	photoionization, charge transfer
O^+	e^- impact, photoionization
$N(^4S)$	$N(^2D)$ quenching by O
Fast reacting species	
N^+	e^- impact, photoionization
N_2^+	e^- impact, photoionization
$O^+(^2D)$	e^- impact, photoionization
$O^+(^2P)$	e^- impact, photoionization
$N(^2D)$	e^- impact, photodissociation
$N(^2P)$	e^- impact, photodissociation
$O(^1D)$	e^- impact, O_2^+ recombination
$O(^1S)$	e^- impact, quenching of $N_2(A)$ state
$N_2(A)$	e^- impact

APPENDIX A: AURIC THERMOSPHERIC-IONOSPHERIC CHEMISTRY RATE COEFFICIENTS

Modeling of thermospheric-ionospheric chemistry within AURIC is geared primarily towards evaluation of volume excitation rates of prominent metastable species and associated volume emission rates from radiative relaxation. The chemical reaction scheme is fairly complete with regard to N, O and O^+ metastables; of the molecular species, the only metastable explicitly followed is $N_2(A)$. The reaction rate coefficients and pertinent references are given in Tables A1–A4. Alternate recent discussions of ionospheric-thermospheric chemistry within the context of aeronomic data analyses are provided by *Link et al.* [1983], *Fox and Dalgarno* [1985], *Link and Cogger* [1988], *Solomon et al.* [1988], *Buonsanto et al.* [1992], and *Torr et al.* [1995].

By-and-large, reaction rate coefficient expressions have been taken from laboratory measurements where available, even in those cases where past aeronomic data analyses may have suggested reassessment of these rates. Pertinent rate coefficients for some reactions (*i.e.*, rate coefficients for genuine thermal distributions at temperatures 250 K $\lesssim T \lesssim$ 1500 K), however, have not been experimentally determined; in these cases, rates derived from aeronomic data analyses have been used where available (*e.g.*, *Constantinides et al.* [1979]). In several cases, reaction rate coefficients that have been treated as "standard" in aeronomic modeling have been questioned in recent laboratory investigations. Examples are: *Flesch and Ng* [1991] *vs Johnsen and Biondi* [1980a,b], *Schultz and Armentrout* [1991] *vs McFarland et al.* [1973], and *Burley et al.* [1987] *vs Chen et al.* [1978]. We have retained the "standard" rate coefficients in these cases, in part because the more recent laboratory results are not convenient and in part because the "standard" rates have been adequate for previous aeronomic applications.

Since the vibrational distributions of several molecular species are not well characterized (*e.g.*, N_2^+, O_2^+, NO^+, $N_2(A)$), the rates adopted here are biased towards the relevant ground vibrational level. For example, the dissociative recombination rate and branching ratios for production of product metastable species for

$$
\begin{aligned}
O_2^+ + e^- \quad &\rightarrow \quad O(^1D) + O(^3P) \\
& O(^1D) + O(^1D) \\
& O(^1D) + O(^1S)
\end{aligned}
$$
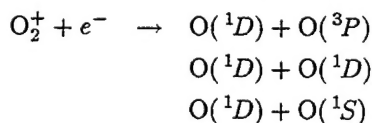
are from *Meyr and Biondi* [1969] with the branching ratios for the product channels taken from *Guberman* [1988] for the O_2^+ $v'' = 0$ state. There is no tracking of translationally excited species.

Miscellaneous Thermospheric-Ionospheric Chemistry References

Buonsanto, M. J., S. C. Solomon, and W. K. Tobiska, Comparison of measured and modeled solar EUV flux and its effect on the *E-F1* region ionosphere, *J. Geophys. Res.*, *97*, 10513–10524, 1992.

Fox, J. L., and A. Dalgarno, The vibrational distribution of N_2^+ in the terrestrial ionosphere, *J. Geophys. Res.*, *90*, 7557–7567, 1985.

Link, R., and L. L. Cogger, A reexamination of the OI 6300-Å nightglow, *J. Geophys. Res.*, *93*, 9883–9892, 1988.

Solomon, S. C., P. B. Hays, and V. J. Abreu, The auroral 6300 Å emission: Observations and modeling, *J. Geophys. Res.*, *93*, 9867–9882, 1988.

Torr, M. R., D. G. Torr, T. Chang, P. Richards, W. Swift, and N. Li, Thermospheric nitric oxide from the ATLAS 1 and Spacelab 1 missions, *J. Geophys. Res.*, *100*, 17389–17413, 1995.

Table A1: AURIC Chemical Reactions

REACTION			RATE COEFFICIENT (cm^3 s^{-1})	REFERENCES
$N_2^+ + O_2$	$\rightarrow O_2^+ + N_2$	k_1	$= 5.0 \times 10^{-11}\, \tau_i^{-0.8}$	*McFarland et al.* [1973] *Lindinger et al.* [1974] *Smith et al.* [1978]
$N_2^+ + NO$	$\rightarrow NO^+ + N_2$	k_2	$= 3.3 \times 10^{-10}$	*Fehsenfeld et al.* [1970]
$N_2^+ + O$	$\rightarrow$ products	k_3	$= 1.4 \times 10^{-10}\, \tau_i^{-0.44},\ T_i \leq 1500°\mathrm{K}$ $= 5.2 \times 10^{-11}\, \tau_i^{0.2},\ T_i > 1500°\mathrm{K}$	*McFarland et al.* [1974] *Knutsen et al.* [1988]
	$\rightarrow NO^+ + N(^2D°)$	k_{3a}	$= (1 - 0.07\, \tau_i^{0.21}) \cdot k_3$	
	$\rightarrow O^+ + N_2$	k_{3b}	$= 0.07\, \tau_i^{0.21} \cdot k_3$	
$O_2^+ + NO$	$\rightarrow NO^+ + O_2$	k_4	$= 4.4 \times 10^{-10}$	*Lindinger et al.* [1975] *Glosik et al.* [1978] *Lindinger et al.* [1974]
$O_2^+ + N(^4S°)$	$\rightarrow NO^+ + O$	k_5	$= 1.2 \times 10^{-10}$	*Fehsenfeld* [1977]
$O^+ + N_2$	$\rightarrow NO^+ + N(^4S°)$	k_6	$= 2.78 \times 10^{-13} \exp(2.07/\tau_i - 0.608/\tau_i^2)$	*Chen et al.* [1978] *Smith et al.* [1978] *Lindinger et al.* [1974] *McFarland et al.* [1973]
$O^+ + O_2$	$\rightarrow O_2^+ + O$	k_7	$= 3.25 \times 10^{-11} - 1.30 \times 10^{-11}\, \tau_i$ $\quad + 1.60 \times 10^{-12}\, \tau_i^2$	*Chen et al.* [1978] *Smith et al.* [1978] *Rakshit et al.* [1978] *Lindinger et al.* [1974] *McFarland et al.* [1973]
$O^+ + NO$	$\rightarrow NO^+ + O$	k_8	$= 8.0 \times 10^{-13}$	*Graham et al.* [1975]

$N^+ + O_2$	$\rightarrow$ products	k_9	$= 6.1 \times 10^{-10}$	*Adams et al. [1980]*
				Rakshit et al. [1978]
				Lindinger et al. [1974]
				McFarland et al. [1973]
	$\rightarrow NO^+ + O$	k_{9a}	$= 0.3 \cdot 0.43 \cdot k_9$	*Adams et al. [1980]*
				Langford et al. [1986]
	$\rightarrow NO^+ + O(^1D)$	k_{9b}	$= 0.7 \cdot 0.43 \cdot k_9$	
	$\rightarrow O_2^+ + N(^4S^\circ)$	k_{9c}	$= 0.7 \cdot 0.51 \cdot k_9$	*Adams et al. [1980]*
				O'Keefe et al. [1986]
	$\rightarrow O_2^+ + N(^2D^\circ)$	k_{9d}	$= 0.3 \cdot 0.51 \cdot k_9$	
	$\rightarrow O^+ + NO$	k_{9e}	$= 0.06 \cdot k_9$	*Adams et al. [1980]*
$N^+ + NO$	$\rightarrow$ products	k_{10}	$= 5.3 \times 10^{-10}$	*Adams et al. [1980]*
				Fahey et al. [1981]
	$\rightarrow NO^+ + N(^4S^\circ)$	k_{10a}	$= 0.85 \cdot k_{10}$	
	$\rightarrow N_2^+ + O$	k_{10b}	$= 0.15 \cdot k_{10}$	
$N^+ + O$	$\rightarrow N(^4S^\circ) + O^+$	k_{11}	$= 2.2 \times 10^{-12}$	*Constantinides et al. [1979]*
				Bates [1989]
$O^+(^2P^\circ) + N_2$	$\rightarrow N_2^+ + O$	k_{12}	$= 4.8 \times 10^{-10}$	*Rusch et al. [1977]*
$O^+(^2P^\circ) + O_2$	$\rightarrow O_2^+ + O$	k_{13}	$= 4.8 \times 10^{-10}$	*Link et al. [1983]*
$O^+(^2P^\circ) + O$	$\rightarrow O^+(^2D^\circ) + O$	k_{14}	$= 5.2 \times 10^{-11}$	*Rusch et al. [1977]*
				Rusch and Gerard [1980]
$O^+(^2D^\circ) + N_2$	$\rightarrow N_2^+ + O$	k_{15}	$= 8.0 \times 10^{-10}$	*Johnsen and Biondi [1980a,b]*
				Rowe et al. [1980]
$O^+(^2D^\circ) + O_2$	$\rightarrow O_2^+ + O$	k_{16}	$= 7.0 \times 10^{-10}$	*Johnsen and Biondi [1980a,b]*
				Rowe et al. [1980]
$O^+(^2D^\circ) + NO$	$\rightarrow NO^+ + O$	k_{17}	$= 1.2 \times 10^{-9}$	*Glosik et al. [1978]*
$O^+(^2D^\circ) + O$	$\rightarrow O^+ + O$	k_{18}	$= 5.0 \times 10^{-12}$	*Abdou et al. [1984]*

$$N(^2P^o) + N_2 \rightarrow N(^4S^o) + N_2 \qquad k_{19} = 2.0 \times 10^{-18}$$

Schofield [1979]

$$N(^2P^o) + O_2 \rightarrow NO + O(^1D) \qquad k_{20} = 2.2 \times 10^{-12}$$

Piper [1993a]
Schofield [1979]

$$N(^2P^o) + NO \rightarrow N(^2D^o) + NO \qquad k_{21} = 3.0 \times 10^{-11}$$

Schofield [1979]

$$N(^2P^o) + O \rightarrow N(^2D^o) + O \qquad k_{22} = 1.7 \times 10^{-11}$$

Piper [1993a]
Bates [1989]

$$N(^2P^o) + N(^4S^o) \rightarrow N(^2D^o) + N(^4S^o) \qquad k_{23} = 6.0 \times 10^{-13}$$

Young and Dunn [1975]
Taghipour and Brennen [1979]

$$N(^2D^o) + N_2 \rightarrow N(^4S^o) + N_2 \qquad k_{24} = 1.0 \times 10^{-13} \exp(-510/T_n)$$

Slanger and Black [1976]

$$N(^2D^o) + O_2 \rightarrow NO + O \qquad k_{25a} = 5.9 \times 10^{-12}$$

Fell et al. [1990]
Schofield [1979]

$$\rightarrow NO + O(^1D) \qquad k_{25b} = 6.0 \times 10^{-13}$$

Link [1983]
Link and Swaminathan [1992]

$$N(^2D^o) + NO \rightarrow N_2 + O \qquad k_{26} = 6.7 \times 10^{-11}$$

Fell et al. [1990]

$$N(^2D^o) + O \rightarrow N(^4S^o) + O \qquad k_{27a} = 6.9 \times 10^{-13}$$

Fell et al. [1990]
Piper [1989b]

$$\rightarrow NO^+ + e^- \qquad k_{27b} = 2.5 \times 10^{-18} T_n^{1/2} (2205 + T_n) \exp(-4410/T_n)$$

Ringer and Gentry [1979]

$$N(^2D^o) + O^+ \rightarrow N^+ + O \qquad k_{28} = 1.3 \times 10^{-10}$$

Constantinides et al. [1979]
Bates [1989]

$$N(^4S^o) + O_2 \rightarrow NO + O \qquad k_{29} = 5.48 \times 10^{-12} \exp(-3221/T_n)$$

Becker et al. [1969]

$$N(^4S^o) + NO \rightarrow N_2 + O \qquad k_{30} = 2.2 \times 10^{-11} \exp(160/T_n),\ T_n \leq 400^\circ K$$
$$= 3.3 \times 10^{-11},\ T_n > 400^\circ K$$

Wennberg et al. [1994]
Lee et al. [1978]

$$N(^4S^o) + O \rightarrow NO + h\nu(NO\ IR) \qquad k_{31} = 3.33 \times 10^{-16} T_n^{-1/2} (1 - 0.567 T_n^{-1/2})$$

Sun and Dalgarno [1992]

$O(^1S) + O_2$	$\rightarrow$ products	k_{32}	$= 2.32 \times 10^{-12} \exp[-\frac{6750 - 0.0151T_n^2}{8.314T_n}]$	*Capetanakis et al.* [1993]
	$\rightarrow O + O_2$	k_{32a}	$= 0.69 \cdot k_{32}$	*Slanger and Black* [1978b]
	$\rightarrow O(^1D) + O_2$	k_{32b}	$= 0.31 \cdot k_{32}$	

$O(^1S) + NO$	$\rightarrow$ products	k_{33}	$= 8.0 \times 10^{-11}$	*Filseth et al.* [1970]
	$\rightarrow O + NO$	k_{33a}	$= 0.36 \cdot k_{33}$	*Slanger and Black* [1978a]
	$\rightarrow O(^1D) + NO$	k_{33b}	$= 0.64 \cdot k_{33}$	

| $O(^1S) + O$ | $\rightarrow O + O$ | k_{34} | $= 2.0 \times 10^{-14}$ | *Krauss and Neumann* [1975] |

| $O(^1D) + N_2$ | $\rightarrow O + N_2$ | k_{35} | $= 2.0 \times 10^{-11} \exp(108/T_n)$ | *Streit et al.* [1976] |

| $O(^1D) + O_2$ | $\rightarrow O + O_2$ | k_{36} | $= 2.9 \times 10^{-11} \exp(67.4/T_n)$ | *Streit et al.* [1976] |

| $O(^1D) + NO$ | $\rightarrow O + NO$ | k_{37} | $= 1.5 \times 10^{-10}$ | *Young et al.* [1968] |

| $O(^1D) + O$ | $\rightarrow O + O$ | k_{38} | $= 7.0 \times 10^{-12}$ | *Abreu et al.* [1986] |
| | | | | *Yee et al.* [1990] |

$N_2(A) + O_2$	$\rightarrow N_2 + O_2$	k_{39}	$= 2.5 \times 10^{-12}$	*Thomas and Kaufman* [1985]
				Thomas et al. [1987]
				Piper et al. [1981a]

| $N_2(A) + NO$ | $\rightarrow N_2 + NO$ | k_{40} | $= 5.6 \times 10^{-11}$ | *Thomas et al.* [1987] |

$N_2(A) + O$	$\rightarrow$ products	k_{41}	$= 2.8 \times 10^{-11}$	*Piper et al.* [1981b]
	$\rightarrow N_2 + O(^1S)$	k_{41a}	$= 0.75 \cdot k_{41}$	*Thomas and Kaufman* [1985]
				Piper [1982]
	$\rightarrow N_2 + O$	k_{41b}	$= 0.25 \cdot k_{41}$	*De Souza et al.* [1985]

$N_2(A) + N(^4S^o)$	$\rightarrow$ products	k_{42}	$= 4.0 \times 10^{-11}$	*Piper* [1989a]
	$\rightarrow N_2 + N(^2P^o)$	k_{42a}	$= 0.9 \cdot k_{42}$	
	$\rightarrow N_2 + N(^2D^o)$	k_{42b}	$= 0.1 \cdot k_{42}$	

Notes:

$\tau_i = \frac{T_i}{300}$, where T_i is ion temperature. T_n is neutral temperature.

k_1: *Alge and Lindinger* [1981] indicate rate is insensitive to v' value. See *Schultz and Armentrout* [1991] for recent laboratory results suggesting a need for revision in adopted rate.

k_{3a}: *Frederick and Rusch* [1977] suggest $N(^2D^o)$ production must be maximum allowable.

k_4: *Lindinger and Ferguson* [1983] indicate rate is insensitive to v' value.

k_5: Possible $O(^1S)$ production ignored.

k_6: See *Burley et al.* [1987] for recent laboratory results suggesting a need for revision in adopted rate.

k_9: Small branching ratio for $O(^1S)$ production ignored.

k_{10}: Possible production of O^+ ignored.

k_{12}, k_{14}: *Rusch et al.* [1977] inferred $O^+(^2P^o)$ loss rates only.

k_{12}, k_{15}: See *Flesch and Ng* [1991] for measured cross sections at above-thermal energies indicating a need to reevaluate the commonly accepted rate coefficient values. Possible NO^+ [*Glosik et al.*, 1978] and N^+ production channels ignored.

k_{13}: Assigned by analogy with $O^+(^2P^o) + N_2$ [*Rusch et al.*, 1977].

k_{17}: *Glosik et al.* [1978] did not distinguish between $O^+(^2P^o)$ and $O^+(^2D^o)$; here taking their rate as applying to $O^+(^2D^o)$.

k_{18}: Estimated upper limit. Possible $O(^1D)$ production ignored.

k_{19}: Simple quenching assumed.

k_{20}: Possible $O(^1S)$ production ignored.

k_{21}: Simple quenching assumed.

k_{22}: Following arguments of *Bates* [1989] regarding allowed product channels.

k_{25b}: Estimated upper limit.

k_{26}: Possible $O(^1D)$ and $O(^1S)$ production ignored.

k_{27a}: Possible $O(^1D)$ production ignored.

k_{34}: Simple quenching assumed.

k_{36}: Production of $O_2(b)$ currently ignored.

k_{38}: Estimate consistent with *Baluja and Zeippen* [1988] transition probabilities and *Guberman* [1988] $v'' = 0$ $O(^1D)$ branching ratio.

$k_{39} - k_{42}$: Assuming $N_2(A)$ in the $v'' = 0$ state; dayside mean vibrational population not known.

k_{39}: Simple quenching assumed; *Golde and Moyle* [1985] indicate $N_2 + O + O$ to be a major product channel.

k_{40}: Simple quenching assumed.

k_{42}: Branching ratios assigned somewhat arbitrarily; *Piper* [1989a] indicates $N(^2P^o)$ production channel is dominant.

Table A2: AURIC Molecular Ion Dissociative Recombination Rates

REACTION	RATE COEFFICIENT ($cm^3 s^{-1}$)	REFERENCES
$O_2^+ + e^- \rightarrow$ products	$\alpha_1 = 1.95 \times 10^{-7} \tau_e^{-0.7}$, $T_e \leq 1200°K$ $= 1.61 \times 10^{-7} \tau_e^{-0.56}$, $T_e > 1200°K$	*Mehr and Biondi* [1969] *Alge et al.* [1983]
$\rightarrow O(^1D) + O(^3P)$	$\alpha_{1a} = 0.609 \cdot \alpha_1$	*Guberman* [1988]
$\rightarrow O(^1D) + O(^1D)$	$\alpha_{1b} = 0.389 \cdot \alpha_1$	
$\rightarrow O(^1S) + O(^1D)$	$\alpha_{1c} = 0.002 \cdot \alpha_1$	
$NO^+ + e^- \rightarrow$ products	$\alpha_2 = 4.20 \times 10^{-7} \tau_e^{-0.75}$	*Dulaney et al.* [1987] *Davidson and Hobson* [1987] *Alge et al.* [1983]
$\rightarrow N(^4S°) + O$	$\alpha_{2a} = 0.24 \cdot \alpha_2$	*Kley et al.* [1977]
$\rightarrow N(^2D°) + O$	$\alpha_{2b} = 0.76 \cdot \alpha_2$	
$N_2^+ + e^- \rightarrow$ products	$\alpha_3 = 1.80 \times 10^{-7} \tau_e^{-0.39}$	*Mehr and Biondi* [1969]
$\rightarrow N(^2D°) + N(^4S°)$	$\alpha_{3a} = 0.88 \cdot \alpha_3$	*Guberman* [1991]
$\rightarrow N(^2D°) + N(^2D°)$	$\alpha_{3b} = 0.12 \cdot \alpha_3$	

Notes:

T_e = electron temperature; $\tau_e = T_e/300°K$.

α_1: Branching ratios from *Guberman* [1988] for $v'' = 0$ state; dayside mean vibrational population not reliably known.

α_3: Branching ratios from *Guberman* [1991] for $v'' = 0$ state; dayside mean vibrational population not reliably known. See *Queffelec et al.* [1985] for laboratory studies indicating a total $N(^2D°)$ yield $\gtrsim 1.8$. See *Noren et al.* [1989] for recent laboratory results suggesting a need for revision of the adopted rate.

Table A3: AURIC Metastable-Electron Quenching Rates

Quenching Channel		Rate Coefficient ($cm^3 s^{-1}$)	References
$O^+(^2P^o) + e^-$	$\rightarrow O^+(^4S^o) + e^-$	$q_{1a} = 3.31 \times 10^{-8}\tau_e^{-1/2}$	*Pradhan* [1976]
	$\rightarrow O^+(^2D^o) + e^-$	$q_{1b} = 1.39 \times 10^{-7}\tau_e^{-1/2}$	
$O^+(^2D^o) + e^-$	$\rightarrow O^+(^4S^o) + e^-$	$q_2 = 6.60 \times 10^{-8}\tau_e^{-1/2}$	
$N(^2P^o) + e^-$	$\rightarrow N(^4S^o) + e^-$	$q_{3a} = 1.60 \times 10^{-12} T_e^{0.85}$	*Berrington and Burke* [1981]
	$\rightarrow N(^2D^o) + e^-$	$q_{3b} = 9.50 \times 10^{-9}$	
$N(^2D^o) + e^-$	$\rightarrow N(^4S^o) + e^-$	$q_4 = 3.80 \times 10^{-12} T_e^{0.81}$	
$O(^1S) + e^-$	$\rightarrow O(^3P) + e^-$	$q_{5a} = 7.30 \times 10^{-13} T_e^{0.94}$	*Berrington and Burke* [1981]
	$\rightarrow O(^1D) + e^-$	$q_{5b} = 8.50 \times 10^{-9}$	
$O(^1D) + e^-$	$\rightarrow O(^3P) + e^-$	$q_6 = 1.60 \times 10^{-12} T_e^{0.91}$	

Notes:
T_e = electron temperature; $\tau_e = T_e/300°K$.

Here and in Table A4, $O^+(^4S^o)$ designation for ground state oxygen ions is used for clarity; elsewhere, the designation is simply O^+.

Table A4: AURIC Radiative Decay Channels

CHANNEL		A COEFFICIENT (s^{-1})	REFERENCES
$O^+(^2P^o)$	$\rightarrow O^+(^4S^o) + h\nu(2470\text{Å})$	$A_{2470} = 4.53 \times 10^{-2}$	*Zeippen* [1982]
	$\rightarrow O^+(^2D^o) + h\nu(7320\text{Å})$	$A_{7320} = 9.85 \times 10^{-2}$	
	$\rightarrow O^+(^2D^o) + h\nu(7330\text{Å})$	$A_{7330} = 7.49 \times 10^{-2}$	
$O^+(^2D^o)$	$\rightarrow O^+(^4S^o) + h\nu(3727\text{Å})$	$A_{3727} = 8.89 \times 10^{-5}$	
$N(^2P^o)$	$\rightarrow N(^4S^o) + h\nu(3466\text{Å})$	$A_{3466} = 5.31 \times 10^{-3}$	*Butler and Zeippen* [1984]
	$\rightarrow N(^2D^o) + h\nu(10400\text{Å})$	$A_{10400} = 8.05 \times 10^{-2}$	
$N(^2D^o)$	$\rightarrow N(^4S^o) + h\nu(5200\text{Å})$	$A_{5200} = 1.28 \times 10^{-5}$	
$O(^1S)$	$\rightarrow O(^3P) + h\nu(2972\text{Å})$	$A_{2972} = 7.63 \times 10^{-2}$	*Baluja and Zeippen* [1988]
	$\rightarrow O(^1D) + h\nu(5577\text{Å})$	$A_{5577} = 1.215$	
$O(^1D)$	$\rightarrow O(^3P) + h\nu(6300\text{Å})$	$A_{6300} = 5.63 \times 10^{-3}$	
	$\rightarrow O(^3P) + h\nu(6364\text{Å})$	$A_{6364} = 1.82 \times 10^{-3}$	
$N_2(A)$	$\rightarrow N_2(X) + h\nu(\text{VK})$	$A_{\text{VK}} = 0.422$	*Piper* [1993b]

Notes:

A_{VK}: Assuming $N_2(A)$ in the $v'' = 0$ state; dayside mean vibrational population not reliably known.

Here and in Table A3, $O^+(^4S^o)$ designation for ground state oxygen ions is used for clarity; elsewhere, the designation is simply O^+.

AURIC Thermospheric-Ionospheric Chemistry References

Abdou, W. A., D. G. Torr, P. G. Richards, M. R. Torr, and E. L. Breig, Results of a comprehensive study of the photochemistry of N_2^+ in the ionosphere, *J. Geophys. Res.*, *89*, 9069–9079, 1984.

Abreu, V. J., J. H. Yee, S. C. Solomon, and A. Dalgarno, The quenching rate of $O(^1D)$ by $O(^3P)$, *Planet. Space Sci.*, *34*, 1143–1145, 1986.

Adams, N. G., D. Smith, and J. F. Paulson, An experimental survey of the reactions of NH_n^+ ions ($n = 0$ to 4) with several diatomic and polyatomic molecules at 300 K, *J. Chem. Phys.*, *72*, 288–297, 1980.

Alge, E., and W. Lindinger, Laboratory investigations of the ionospheric $N_2^+(X, ^2\Sigma_g^+, \nu \neq 0)$ reaction with O_2, *J. Geophys. Res.*, *86*, 871–873, 1981.

Alge, E., N. G. Adams, and D. Smith, Measurements of the dissociative recombination coefficients of O_2^+, NO^+ and NH_4^+ in the temperature range 200–600 K, *J. Phys. B: At. Mol. Phys.*, *16*, 1433–1444, 1983.

Baluja, K. L., and C. J. Zeippen, M1 and E2 transition probabilities for states within the $2p^4$ configuration of the OI isoelectronic sequence, *J. Phys. B: At. Mol. Opt. Phys.*, *21*, 1455–1471, 1988.

Bates, D. R., Theoretical considerations regarding some inelastic atomic collision processes of interest in aeronomy: Deactivation and charge transfer, *Planet. Space Sci.*, *37*, 363–368, 1989.

Becker, K. H., W. Groth, and D. Kley, The rate constant of the aeronomic reaction $N + O_2$, *Z. Naturforsch. Teil A*, *24*, 1280–1281, 1969.

Berrington, K. A., and P. G. Burke, Effective collision strengths for forbidden transitions in e–N and e–O scattering, *Planet. Space Sci.*, *29*, 377–381, 1981.

Burley, J. D., K. M. Ervin, and P. B. Armentrout, Translational energy dependence of $O^+(^4S) + N_2 \rightarrow NO^+ + N$ from thermal energies to 30 eV c.m., *J. Chem. Phys.*, *86*, 1944–1953, 1987.

Butler, K., and C. J. Zeippen, NI forbidden lines revisited, *Astron. Astrophys.*, *141*, 274–278, 1984.

Capetanakis, F. P., F. Sondermann, S. Höser, and F. Stuhl, Temperature dependence of the quenching of $O(^1S)$ by simple inorganic molecules, *J. Chem. Phys.*, *98*, 7883–7887, 1993.

Chen, A., R. Johnsen, and M. A. Biondi, Measurements of the $O^+ + N_2$ and $O^+ + O_2$ reaction rates from 300 to 900 K, *J. Chem. Phys.*, *69*, 2688–2691, 1978.

Constantinides, E. R., J. H. Black, A. Dalgarno, and J. H. Hoffman, The photochemistry of N^+ ions, *Geophys. Res. Lett.*, *6*, 569–572, 1979.

Davidson, D. F., and R. M. Hobson, The shock tube determination of the dissociative recombination rate of NO^+, *J. Phys. B: At. Mol. Phys.*, *20*, 5753–5756, 1987.

De Souza, A. R., G. Gousset, M. Touzeau, and T. Khiet, Note on the determination of the efficiency of the reaction $N_2(A^3\Sigma) + O(^3P) \rightarrow N_2 + O(^1S)$, *J. Phys. B: At. Mol. Phys.*, *18*, L661–L666, 1985.

Dulaney, J. L., M. A. Biondi, and R. Johnsen, Electron temperature dependence of the recombination of electrons with NO^+ ions, *Phys. Rev. A, 36*, 1342–1350, 1987.

Fahey, D. W., I. Dotan, F. C. Fehsenfeld, D. L. Albritton, and L. A. Viehland, Energy dependence of the rate constant of the reaction $N^+ + NO$ at collision energies 0.04 to 2.5 eV, *J. Chem. Phys., 74*, 3320–3323, 1981.

Fehsenfeld, F. C., The reaction of O_2^+ with atomic nitrogen and $NO^+ \cdot H_2O$ and NO_2^+ with atomic oxygen, *Planet. Space Sci., 25*, 195–196, 1977.

Fehsenfeld, F. C., D. B. Dunkin, and E. E. Ferguson, Rate constants for the reaction of CO_2^+ with O, O_2 and NO; N_2^+ with O and NO; and O_2^+ with NO, *Planet. Space Sci., 18*, 1267–1269, 1970.

Fell, C., J. I. Steinfeld, and S. Miller, Quenching of $N(^2D)$ by $O(^3P)$, *J. Chem. Phys., 92*, 4768–4777, 1990.

Filseth, S. V., F. Stuhl, and K. H. Welge, Collisional deactivation of $O(^1S)$, *J. Chem. Phys., 52*, 239–243, 1970.

Flesch, G. D., and C. Y. Ng, Absolute state-selected total cross sections for the $O^+(^2D, ^2P) + N_2$ reactions, *J. Geophys. Res., 96*, 21407–21410, 1991.

Frederick, J. E., and D. W. Rusch, On the chemistry of metastable atomic nitrogen in the *F* region deduced from simultaneous satellite measurements of the 5200-Å airglow and atmospheric composition, *J. Geophys. Res., 82*, 3509–3517, 1977.

Glosik, J., A. B. Rakshit, N. D. Twiddy, N. G. Adams, and D. Smith, Measurement of the rates of reaction of the ground and metastable excited states of O_2^+, NO^+ and O^+ with atmospheric gases at thermal energy, *J. Phys. B: At. Mol. Phys., 11*, 3365–3379, 1978.

Golde, M. F., and A. M. Moyle, Study of the products of the reactions of $N_2(A\,^3\Sigma_u^+)$: The effect of vibrational energy in $N_2(A)$, *Chem. Phys. Lett., 117*, 375–380, 1985.

Graham, E., IV, R. Johnsen, and M. A. Biondi, The $O^+ + NO \rightarrow O + NO^+$ reaction rate from 300°K to 0.55-eV ion mean energy, *J. Geophys. Res., 80*, 2338–2339, 1975.

Guberman, S. L., The production of $O(^1D)$ from dissociative recombination of O_2^+, *Planet. Space Sci., 36*, 47–53, 1988.

Guberman, S. L., Dissociative recombination of the ground state of N_2^+, *Geophys. Res. Lett., 18*, 1051–1054, 1991.

Johnsen, R., and M. A. Biondi, Laboratory measurements of the $O^+(^2D) + N_2$ and $O^+(^2D) + O_2$ reaction rate coefficients and their ionospheric implications, *Geophys. Res. Lett., 7*, 401–403, 1980a.

Johnsen, R., and M. A. Biondi, Charge transfer coefficients for the $O^+(^2D) + N_2$ and $O^+(^2D) + O_2$ excited ion reactions at thermal energy, *J. Chem. Phys., 73*, 190–193, 1980b.

Kley, D., G. M. Lawrence, and E. J. Stone, The yield of $N(^2D)$ atoms in the dissociative recombination of NO^+, *J. Chem. Phys., 66*, 4157–4165, 1977.

Knutsen, K., V. M. Bierbaum, and S. R. Leone, Remeasurement of the rate constant and branching ratio for the $N_2^+ + O$ reaction, *Planet. Space Sci.*, *36*, 307–310, 1988.

Krauss, M., and D. Neumann, On the interaction of $O(^1S)$ with $O(^3P)$, *Chem. Phys. Lett.*, *36*, 372–374, 1975.

Langford, A. O., V. M. Bierbaum, and S. R. Leone, Branching ratios for electronically excited oxygen atoms formed in the reaction of N^+ with O_2 at 300 K, *J. Chem. Phys.*, *84*, 2158–2166, 1986.

Lee, J. H., J. V. Michael, W. A. Payne, and L. J. Stief, Absolute rate of the reaction of $N(^4S)$ with NO from 196–400 K with DF–RF and FP–RF techniques, *J. Chem. Phys.*, *69*, 3069–3076, 1978.

Lindinger, W., and E. E. Ferguson, Laboratory investigation of the ionospheric $O_2^+(X\,^2\Pi_g, \nu \neq 0)$ reaction with NO, *Planet. Space Sci.*, *31*, 1181–1182, 1983.

Lindinger, W., F. C. Fehsenfeld, A. L. Schmeltekopf, and E. E. Ferguson, Temperature dependence of some ionospheric ion-neutral reactions from 300°–900° K, *J. Geophys. Res.*, *79*, 4753–4756, 1974.

Lindinger, W., D. L. Albritton, F. C. Fehsenfeld, and E. E. Ferguson, Laboratory measurements of the ionospheric $O_2^+(X\,^2\Pi_g)$ and $O_2^+(a\,^4\Pi_u)$ reactions with NO, *J. Geophys. Res.*, *80*, 3725–3726, 1975.

Link, R., A rocket observation of the 6300 Å/5200 Å intensity ratio in the dayside aurora: Implications for the production of $O(^1D)$ via the reaction $N(^2D) + O_2 \rightarrow NO + O(^1D)$, *Geophys. Res. Lett.*, *10*, 225–228, 1983.

Link, R., and P. K. Swaminathan, $N(^2D) + O_2$: A source of thermospheric 6300 Å emission? *Planet. Space Sci.*, *40*, 699–705, 1992.

Link, R., J. C. McConnell, and G. G. Shepherd, An analysis of the spatial distribution of dayside cleft optical emissions, *J. Geophys. Res.*, *88*, 10145–10162, 1983.

McFarland, M., D. L. Albritton, F. C. Fehsenfeld, E. E. Ferguson, and A. L. Schmeltekopf, Flow-drift technique for ion mobility and ion-molecule reaction rate constant measurements. II. Positive ion reactions of N^+, O^+, and N_2^+ with O_2 and O^+ with N_2 from thermal to $\sim$2 eV, *J. Chem. Phys.*, *59*, 6620–6628, 1973.

McFarland, M., D. L. Albritton, F. C. Fehsenfeld, E. E. Ferguson, and A. L. Schmeltekopf, Energy dependence and branching ratio of the $N_2^+ + O$ reaction, *J. Geophys. Res.*, *79*, 2925–2926, 1974.

Mehr, F. J., and M. A. Biondi, Electron temperature dependence of recombination of O_2^+ and N_2^+ ions with electrons, *Phys. Rev.*, *181*, 264–271, 1969.

Noren, C., F. B. Yousif, and J. B. A. Mitchell, Dissociative recombination and excitation of N_2^+, *J. Chem. Soc., Faraday Trans. 2*, *85*, 1697–1703, 1989.

O'Keefe, A., G. Mauclaire, D. Parent, and M. T. Bowers, Product energy disposal in the reaction of $N^+(^3P)$ with $O_2(X\,^3\Sigma)$, *J. Chem. Phys.*, *84*, 215–219, 1986.

Piper, L. G., The excitation of $O(^1S)$ in the reaction between $N_2(A\,^3\Sigma_u^+)$ and $O(^3P)$, *J. Chem. Phys.*, *77*, 2373–2377, 1982.

Piper, L. G., The excitation of N(^2P) by N$_2$($A^3\Sigma_u^+$, $v' = 0,1$), *J. Chem. Phys.*, *90*, 7087–7095, 1989a.

Piper, L. G., The rate coefficient for quenching N(^2D) by O(^3P), *J. Chem. Phys.*, *91*, 3516–3524, 1989b.

Piper, L. G., The reactions of N(^2P) with O$_2$ and O, *J. Chem. Phys.*, *98*, 8560–8564, 1993a.

Piper, L. G., Reevaluation of the transition-moment function and Einstein coefficients for the N$_2$($A^3\Sigma_u^+$–$X^1\Sigma_g^+$) transition, *J. Chem. Phys.*, *99*, 3174–3181, 1993b.

Piper, L. G., G. E. Caledonia, and J. P. Kennealy, Rate constants for deactivation of N$_2$(A) $v' = 0,1$ by O$_2$, *J. Chem. Phys.*, *74*, 2888–2895, 1981a.

Piper, L. G., G. E. Caledonia, and J. P. Kennealy, Rate constants for deactivation of N$_2$($A^3\Sigma_u^+$, $v' = 0,1$) by O, *J. Chem. Phys.*, *75*, 2847–2852, 1981b.

Pradhan, A. K., Collision strengths for [OII] and [SII], *Mon. Not. R. Astr. Soc.*, *177*, 31–38, 1976.

Queffelec, J. L., B. R. Rowe, M. Morlais, J. C. Gomet, and F. Vallee, The dissociative recombination of N$_2^+$ ($v = 0,1$) as a source of metastable atoms in planetary atmospheres, *Planet. Space Sci.*, *33*, 263–270, 1985.

Rakshit, A. B., H. M. P. Stock, D. P. Wareing, and N. D. Twiddy, Some ion-molecule reaction rate coefficient measurements at 300 and 100 K in a temperature-variable flowing-afterglow apparatus, *J. Phys. B: At. Mol. Phys.*, *11*, 4237–4247, 1978.

Ringer, G., and W. R. Gentry, A merged molecular beam study of the endoergic associative ionization reaction N(^2D) + O(^3P) $\rightarrow$ NO$^+$ + e^-, *J. Chem. Phys.*, *71*, 1902–1909, 1979.

Rowe, B. R., D. W. Fahey, F. C. Fehsenfeld, and D. L. Albritton, Rate constants for the reactions of metastable O^{+*} ions with N$_2$ and O$_2$ at collision energies 0.04 to 0.2 eV and the mobilities of these ions at 300 K, *J. Chem. Phys.*, *73*, 194–205, 1980.

Rusch, D. W., and J.-C. Gérard, Satellite studies of N(^2D) emission and ion chemistry in aurorae, *J. Geophys. Res.*, *85*, 1285–1290, 1980.

Rusch, D. W., D. G. Torr, P. B. Hays, and J. C. G. Walker, The OII (7319–7330 Å) dayglow, *J. Geophys. Res.*, *82*, 719–722, 1977.

Schofield, K., Critically evaluated rate constants for gaseous reactions of several electronically excited species, *J. Phys. Chem. Ref. Data*, *8*, 723–798, 1979.

Schultz, R. H., and P. B. Armentrout, Reactions of N$_2^+$ and N$_4^+$ with O$_2$ from thermal to 20 eV center of mass, *J. Chem. Phys.*, *95*, 121–129, 1991.

Slanger, T. G., and G. Black, Quenching of N(^2D) by N$_2$ and H$_2$O, *J. Chem. Phys.*, *64*, 4442–4444, 1976.

Slanger, T. G., and G. Black, O(^1S) interactions – the product channels, *J. Chem. Phys.*, *68*, 989–997, 1978a.

Slanger, T. G., and G. Black, Products of the O(^1S)–O$_2$ interaction, *J. Chem. Phys.*, *68*, 998–1000, 1978b.

Smith, D., N. G. Adams, and T. M. Miller, A laboratory study of the reactions of N^+, N_2^+, N_3^+, N_4^+, O^+, O_2^+, and NO^+ ions with several molecules at 300 K, *J. Chem. Phys.*, *69*, 308–318, 1978.

Streit, G. E., C. J. Howard, A. L. Schmeltekopf, J. A. Davidson, and H. I. Schiff, Temperature dependence of $O(^1D)$ rate constants for reactions with O_2, N_2, CO_2, O_3, and H_2O, *J. Chem. Phys.*, *65*, 4761–4764, 1976.

Sun, Y., and A. Dalgarno, Radiative association of N and O atoms at low temperatures, *J. Geophys. Res.*, *97*, 6537–6539, 1992.

Taghipour, A., and W. Brennen, $N(2p^3\ ^2P^\circ)$ in the nitrogen afterglow, *Chem. Phys.*, *37*, 363–368, 1979.

Thomas, J. M., and F. Kaufman, Rate constants of the reactions of metastable $N_2(A^3\Sigma_u^+)$ in $v = 0,1,2$, and 3 with ground state O_2 and O, *J. Chem. Phys.*, *83*, 2900–2903, 1985.

Thomas, J. M., F. Kaufman, and M. F. Golde, Rate constants for electronic quenching of $N_2(A^3\Sigma_u^+, v = 0\text{--}6)$ by O_2, NO, CO, N_2O, and C_2H_4, *J. Chem. Phys.*, *86*, 6885–6892, 1987.

Wennberg, P. O., J. G. Anderson, and D. K. Weisenstein, Kinetics of reactions of ground state nitrogen atoms ($^4S_{3/2}$) with NO and NO_2, *J. Geophys. Res.*, *99*, 18839–18846, 1994.

Yee, J.-H., S. L. Guberman, and A. Dalgarno, Collisional quenching of $O(^1D)$ by $O(^3P)$, *Planet. Space Sci.*, *38*, 647–652, 1990.

Young, R. A., and O. J. Dunn, The excitation and quenching of $N(^2P)$, *J. Chem. Phys.*, *63*, 1150–1153, 1975.

Young, R. A., G. Black, and T. G. Slanger, Reaction and deactivation of $O(^1D)$, *J. Chem. Phys.*, *49*, 4758–4768, 1968.

Zeippen, C. J., Transition probabilities for forbidden lines in the $2p^3$ configuration, *Mon. Not. R. Astr. Soc.*, *198*, 111–125, 1982.

APPENDIX B: 1996 AURIC SPIE PAPER

Atmospheric Ultraviolet Radiance Integrated Code (AURIC): Current Capabilities for Rapidly Modeling Dayglow from the Far UV to the Near IR

D. J. Strickland, J. S. Evans, J. E. Bishop, T. Majeed, P. M. Shen, and R. Link
Computational Physics, Inc., Fairfax, VA 22031

R. E. Huffman
Phillips Laboratory/GPIM, Hanscom AFB, MA 01731

Reprinted from

Ultraviolet Atmospheric and Space Remote Sensing: Methods and Instrumentation

Volume 2831

Atmospheric Ultraviolet Radiance Integrated Code (AURIC): Current Capabilities for Rapidly Modeling Dayglow from the Far UV to the Near IR

D. J. Strickland, J. S. Evans, J. E. Bishop, T. Majeed, P. M. Shen, and R. Link[†]
Computational Physics, Inc., Fairfax, VA 22031

R. E. Huffman
Phillips Laboratory/GPIM, Hanscom AFB, MA 01731

[†] now at SouthWest Research Institute, San Antonio, TX 78228

ABSTRACT

Computational Physics, Inc. (CPI) has been under contract to the Air Force Phillips Laboratory/Geophysics Directorate to re-engineer CPI dayglow and nightglow codes conforming to modern programming standards, followed by testing and validation of these codes. The software and associated input files comprise that portion of AURIC for the modeling of dayglow and nightglow from 100 to about 900 nm (MODTRAN comprises the other portion). This paper will describe the current capabilities of the dayglow portion of AURIC and present selected dayglow results. The dayglow portion models photoionization, photodissociation, photoelectron energy degradation, photoelectron impact excitation, chemistry, solar resonance and resonant fluorescence scattering, and multiple scattering of optically thick lines. Calculated observables are ion and neutral densities and radiances of atomic lines and molecular band systems. AURIC is currently being used to analyze satellite optical data, perform studies of production and loss processes, and support satellite experiments through data simulations.

Keywords: UV-visible optical backgounds, remote sensing, dayglow

1. INTRODUCTION

This paper discusses the model AURIC that has been under development by Computational Physics, Inc. (CPI) for the Air Force Phillips Laboratory/Geophysics Directorate (PL/GP). A more detailed version of the paper[1] is in progress for submission to *J. Geophys. Res.* That paper will include descriptions of both dayglow and nightglow capabilities, a complete reference list, a more detailed mathematical description of the photoelectron flux model, and details about electron impact cross sections and rate coefficients. Under the work being documented, an AURIC User's Manual has also been written[2]. The manual contains detailed information on how to run AURIC on Unix, VMS, and PC systems and includes numerous tables and figures of inputs and outputs. AURIC stands for Atmospheric Ultraviolet Radiance Integrated Code; the term Integrated refers to the coupling of the suite of models to be discussed here with MODTRAN. The integrated package allows one to calculate spectral radiances that contain dayglow and Rayleigh scattering of sunlight (where appropriate) or nightglow and Rayleigh scattering of moonlight (again, where appropriate). MODTRAN's overall capabilities include rapid molecular band model calculations of radiances in the IR, transmittances from the IR to the UV, and Rayleigh scattering of sunlight and moonlight[4-6]. Early work by CPI was reported in a 1992 SPIE paper by Link et al.[7] The models being provided by CPI calculate dayglow, nightglow, and an assortment of densities above 90 km. The dayglow portion of the software has its origin in codes developed by CPI and the Naval Research Laboratory (NRL) under the name PEGFAC[8]. The PEGFAC software has been rewritten using modern programming standards. In addition, major improvements have been made in the handling of I/O. Beyond these improvements, the dayglow portion of AURIC also has many enhancements over PEGFAC. Examples include the addition of a global H Lyman α model (contributed by one of us - JEB) and major revisions to 1) various sets of electron impact cross sections, 2) rate coefficients, and 3) synthetic spectra of various molecular band systems. The nightglow portion of AURIC also has its origins in CPI software that has been rewritten in the same spirit as the dayglow software. There are two modules. One calculates emission from the F2 region of the ionosphere (arising from recombination of O^+ and O_2^+ with electrons); the other

calculates emission from the upper mesosphere/lower thermosphere (arising from O atom recombination). The total number of codes calculating dayglow and nightglow is 27. Included is a code that provides a text-based user interface to executing the dayglow and nightglow codes and another that serves as an interface to MODTRAN. The CPI software within AURIC is comprised of approximately 35,000 lines of code.

The primary sponsor of the work described in this paper is the DoD Ballistic Missile Defense Office with technical monitoring through PL/GP. The interest on the part of the sponsor is to provide a tool to the optical backgrounds community for characterizing naturally occurring atmospheric emissions from the far ultraviolet (FUV) to the near infrared as seen from space. As noted above, present capability allows for the characterization of emission on both the dayside and nightside. Future capability will include the modeling of auroral and twilight emissions. In addition to characterizing dayglow and nightglow, AURIC can also be used to perform analyses of satellite and rocket data and studies of a variety of neutral and ion species on the dayside. An example of such a study was recently published by Siskind et al.[9] addressing the effects of enhanced solar soft X-ray fluxes on the density of nitric oxide (NO) in the lower thermosphere.

Table 1 lists atomic dayglow and nightglow features presently contained in AURIC. Similar information for band systems is given in Table 2. Emission for some of the dayglow and nightglow features arises from metastable states. Densities of these states are calculated by AURIC's photochemistry and nightglow chemistry models. Table 3 lists the dayglow metastables which are part of a larger list that includes ground state ion species and $N(^4S)$.

Table 1. Atomic lines, transitions, type of airglow (day/night) modeled, and identification of those features affected by scattering or requiring chemistry modeling (metastables)

Species	Transition	Wavelength (nm)	Region	Comment
H	$^2P^\circ \to {}^2S$	121.6	Global	Requires multi-dimensional photon transport model
N	$^2P \to {}^2D^\circ$	149.3	Day	
N	$^2P \to {}^2P^\circ$	174.3	"	
N	$^2P^\circ \to {}^4S^\circ$	346.6	"	Metastable
N	$^2D^\circ \to {}^4S^\circ$	520.0	"	Metastable
N^+	$^3D^\circ \to {}^3P$	108.5	Day	
N^+	$^5S^\circ \to {}^3P$	214.3	"	Metastable
O	$^3S^\circ \to {}^3P$	130.4	Day/Night	Requires photon transport model
O	$^5S^\circ \to {}^3P$	135.6	"	Requires photon transport model
O	$^1S \to {}^3P$	297.2	"	Metastable
O	$^1S \to {}^1D$	557.7	"	Metastable
O	$^1D \to {}^3P$	630.0	"	Metastable
O	$^5P \to {}^5S^\circ$	777.4	"	
O	$^3P \to {}^3S^\circ$	844.6	"	
O^+	$^2P^\circ \to {}^4S^\circ$	247.0	Day	Metastable
O^+	$^2D^\circ \to {}^4S^\circ$	372.7	"	Metastable
O^+	$^2P^\circ \to {}^2D^\circ$	732.0	"	Metastable

Table 2. Band systems, transitions, type of airglow, and wavelength regions covered.

Species	Transition	Band system	Region	Wavelength range (nm)
N_2	$a^1\Pi_g \rightarrow X^1\Sigma_g^+$	Lyman-Birge-Hopfield	Day	125 - 240
N_2	$A^3\Sigma_u^+ \rightarrow X^1\Sigma_g^+$	Vegard-Kaplan	"	150 - 690
N_2	$C^3\Pi_u \rightarrow B^3\Pi_g$	Second Positive	"	280 - 460
N_2	$B^3\Pi_g \rightarrow A^3\Sigma_u^+$	First Positive	"	600 to beyond 1000
N_2^+	$B^2\Sigma_u^+ \rightarrow X^2\Sigma_g^+$	First Negative	Day	360 - 520
N_2^+	$A^2\Pi_u \rightarrow X^2\Sigma_g^+$	Meinel	"	500 to beyond 1000
NO	$A^2\Sigma^+ \rightarrow X^2\Pi$	γ	Day	200 - 310
NO	$C^2\Pi \rightarrow X^2\Pi$	δ	"	190 - 250
NO	$D^2\Sigma^+ \rightarrow X^2\Pi$	ε	"	180 - 260
O_2	$b^1\Sigma_g^+ \rightarrow X^3\Sigma_g^-$	Atmospheric	Night	680 - 1000
O_2	$A'^3\Delta_u \rightarrow a^1\Delta_g$	Chamberlain	"	300 - 440
O_2	$A^3\Sigma_u^+ \rightarrow X^3\Sigma_g^-$	Herzberg I	"	250 - 480
O_2	$c^1\Sigma_u^- \rightarrow X^3\Sigma_g^-$	Herzberg II	"	260 - 470

Table 3. Species treated by the photochemistry module and identification of dominant production mechanisms

Species	Dominant Production Mechanisms
Slow reacting species (time integrated)	
NO^+	Charge transfer
O_2^+	photoionization, charge transfer
O^+	e^- impact, photoionization
$N(^4S)$	$N(^2D)$ quenching by O
Fast reacting species	
N^+	e^- impact, photoionization
N_2^+	e^- impact, photoionization
$O^+(^2D)$	e^- impact, photoionization
$O^+(^2P)$	e^- impact, photoionization
$N(^2D)$	e^- impact, photodissociation
$N(^2P)$	e^- impact, photodissociation
$O(^1D)$	e^- impact, O_2^+ recombination
$O(^1S)$	e^- impact, quenching of $N_2(A)$ state
$N_2(A)$	e^- impact

2. SOFTWARE MODULES

Figure 1 shows a flow diagram that contains the AURIC dayglow modules. Table 4 gives a brief description of each module. The basic steps are: (1) specifying needed inputs that include parameters for specifying a model atmosphere, ionosphere, and solar EUV flux, (2) evaluating these latter inputs, (3) calculating photoelectron fluxes, (4) calculating volume production rates by electron impact, photoionization, photodissociation, and resonant fluorescence, (5) calculating densities affected by chemistry, (6) calculating intensity profiles for disk-to-limb viewing, and (7) representing these intensities in spectral radiance form (Rayleighs nm^{-1}) using molecular synthetic spectral routines.
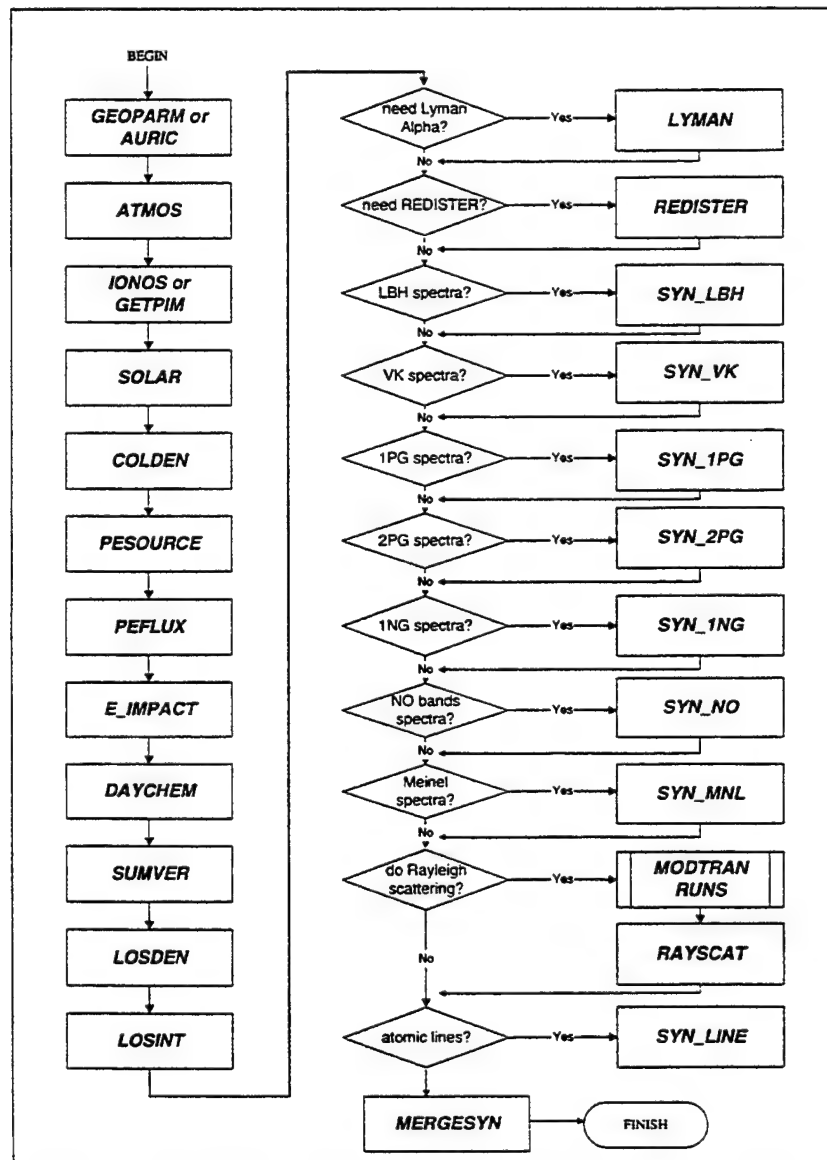
Figure 1. Flow diagram of modules contained in dayglow portion of AURIC.

26

Table 4. Brief description of dayglow modules appearing in Figure 1.

Module	Description
GEOPARM	Calculates selected geophysical parameters
ATMOS	Specifies model atmosphere (MSISE-90 + SHARC atmospheric generator)
IONOS	Specifies model ionosphere using FAIM
SOLAR	Specifies solar EUV flux using Hinteregger algorithm
COLDEN	Calculates slant column densities of N_2, O_2, O, NO, and O_3 for given SZA
PESOURCE	Calculates photoelectron source functions
PEFLUX	Calculates photoelectron fluxes
e_IMPACT	Calculates volume production rates due to electron impact excitation
DAYCHEM	Calculates ion and neutral densities
SUMVER	Places all volume emission rates in a single file
LOSDEN	Calculates line-of-sight column densities of N_2^+ and NO needed for calculation of N_2^+ 1NG, N_2^+ Meinel, and NO γ, δ, ε band intensities
LOSINT	Performs line-of-sight integrations to obtain intensities
LYMAN	Calculates HI 121.6 nm intensity
REDISTER	Calculates intensities of OI 130.4 nm and OI 135.6 nm features
Synthetic spectral routines for molecular band systems	Distributes total molecular band system intensities among appropriate bands
RAYSCAT	Converts MODTRAN output to AURIC synthetic spectral file format for Rayleigh scattering of sunlight
MERGESYN	Merges all synthetic spectra

3. DAYSIDE MODELING

Non-resonant excitation mechanisms

Solar EUV model

The states associated with dayglow and species introduced in Section 1 are produced by one or more of the following processes: photoionization, photodissociation, solar resonance and resonant fluorescence scattering, photoelectron impact, photochemistry, and multiple scattering for optically thick lines. The starting point for all of these processes is the unattenuated solar flux as a function of wavelength λ. The wavelength range of interest is from ~100 nm down to X-ray wavelengths. The shortest wavelength presently treated by AURIC is 1 nm. Most of the solar energy deposited at shorter wavelengths occurs below 100 km and is insignificant except under extreme solar storm conditions. AURIC uses a discrete version of the solar spectrum from Hinteregger et al.[10] extended by us from 1.8 down to 1 nm (see Siskind et al.[9]).

Photoelectron model

AURIC calculates the photoelectron flux in the local approximation. Numerous local models have been published over the past 20 years. Examples are Victor et al.[11], Jasperse[12], Richards and Torr[13], and Strickland and Meier[1]. The solution is adequate for most applications involving photochemistry and dayglow. Transport effects should be taken into account if one is concerned with dayglow above about 300 km. The usual situation where this concern exists is in modeling twilight photochemistry and emissions. The form of the local equation treated by AURIC is:

$$
\begin{aligned}
0 = & -\sum_\ell n_\ell(z)\sigma_\ell(E)\phi(z,E) \\
& + \sum_\ell n_\ell(z)\sigma_\ell(E)\int_E^{E_{max}} dE' \, R_\ell(E' \to E)\phi(z,E') \\
& + n_e(z)\frac{\partial}{\partial E}\Big[L_e(z,E)\phi(z,E)\Big] \\
& + S_{\lambda \to e}(z,E)
\end{aligned}
\tag{1}
$$

Terms include:

ϕ spherical electron flux ($e \, cm^{-2}s^{-1}eV^{-1}$)
n_ℓ density of ℓth species (N_2, O_2, or O)
σ_ℓ total cross section of ℓth species (ionization plus excitation)
R_ℓ energy redistribution function (eV^{-1})
L_e loss function for energy loss to thermal electrons.
$S_{\lambda \to e}$ source function for photoelectron production by solar EUV flux ($e \, cm^{-3}s^{-1}eV^{-1}$).

The dependence on the solar zenith angle (SZA) is not displayed in eq. 1 nor in the remaining equations in this section in order to simplify their appearance. The term explicitly dependent on SZA is the source function. This function contains contributions from both photoelectrons and Auger electrons. The form of R_ℓ is:

$$
R_\ell(E' \to E) = \frac{\sum_k \sigma_{\ell k}(E' \to E)}{\sigma_\ell(E)} \, . \qquad eV^{-1}
\tag{2}
$$

where the sum is over ionization and excitation processes and contains differential cross sections in $cm^2 eV^{-1}$. Eq. 1 is solved on an electron energy grid from 1 to 800 eV. Strickland and Meier[8] discuss the numerical technique used to solve the equation.

Volume production rates

Here, we address production rates by the following processes: photoionization, photodissociation, and electron impact. Rates for the first two processes are obtained from:

28

$$p_{\lambda,lk}(z) = n_l(z) \sum_i \pi F_{\lambda_i}(z) \sigma_{lk}^{photo}(\lambda_i) \qquad cm^{-3} s^{-1} \qquad (3)$$

where πF is the attenuated solar EUV flux at altitude z (accounting for slant paths associated with a non-vertical sun) and σ^{photo} is the photo-cross section for process k involving species l. A similar expression, generalized to integrations over individual lines, is used for resonant fluorescence scattering. The latter process is of interest within the AURIC model for calculating scattering within the bands of the NO γ, δ, and ε systems as well as the N_2^+ 1NG and Meinel systems. Eq. 3 is used to calculate production rates for the species in Table 3 and the photo-component of the NII 108.5 nm emission rate.

Production by electron impact is given by:

$$p_{e,lk}(z) = n_l(z) \int_{W_k}^{E_{max}} \sigma_{lk}(E) \phi(z,E) dE \qquad cm^{-3} s^{-1} \qquad (4)$$

Many of the emission features within the AURIC model are produced exclusively by electron impact. Production rates needed for chemistry modeling are typically comprised of terms from both eqs. 3 and 4.

Photochemistry

Table 3 lists the species for which densities are calculated by AURIC's photochemistry model. The densities of the species labeled as slow reacting are calculated by solving coupled rate equations of the following form:

$$\frac{dn_i}{dt} = p_i(z,t) - l_i(z,t) \qquad cm^{-3} s^{-1} \qquad (5)$$

where p_i and l_i are the total production and loss rates. The derivative is set to zero for calculating the densities of the fast reacting species. The possible terms comprising a given total production rate are rates from eqs. 3 and 4 and one or more rates involving chemical reactions. Loss processes include quenching, spontaneous emission, and reactions such as atom-ion interchange. A detailed description of the chemical scheme with a complete listing of reactions and associated rates is given in reference 1.

Solar resonance and resonant fluorescence scattering features

Features to be addressed are OI 130.4 nm, OI 135.6 nm, HI 121.6 nm, the γ, δ, and ε systems of NO, and the first negative and Meinel systems of N_2^+. The OI 130.4 nm "feature" is actually a triplet (130.2 nm, 130.5 nm, 130.6 nm) arising from the transition $(2p)^4 {}^3P_{2,1,0} \leftarrow (2p)^3(3s)_1 {}^3S$. The initial excitation rate of the ${}^3S$ state, denoted S_0, includes both electron impact and solar resonant absorption terms. For the optically thick OI 130.4 nm triplet, as well as for the much more optically thin OI 135.6 nm feature, the transport equation formulation and solution code of Gladstone[14] is used. This code, named REDISTER, employs the Feautrier technique to solve the radiative transfer equation for resonance multiplet emissions in a plane-parallel planetary atmosphere. Frequency redistribution is handled in the angle-averaged partial redistribution approximation, taking full account of vertical variations in temperature, scatterer density, and the densities of absorbing species (as provided by the MSISE-90[15] atmosphere model). The initial internal (i.e., photoelectron impact) source term is provided by the e_IMPACT module, while the

29

external (i.e., solar resonant absorption) source term is evaluated within REDISTER. Output comprises optical depths, total source functions S, and line-of-sight intensities.

The Lyman α (HI 121.6 nm) radiance calculations within AURIC are performed by the LYMAN module, which is based on a nonisothermal adaptation of the complete frequency redistribution algorithm of Anderson and Hord[16]. As implemented in AURIC, it takes into account the variation of densities and temperature with altitude but assumes spherically symmetric distributions. The temperature, H density, and O_2 (the absorbing species) density profiles are taken from MSISE-90[15] for altitudes 74 - 455 km; at higher altitudes, an analytic formulation[17] is used to estimate H-atom densities. The default incident solar line center Lyman α flux is estimated using the same $F_{10.7}$ scaling of the reference Hinteregger SC21REFW spectrum as is used for specifying the incident solar EUV flux, taking the integrated and line center fluxes to be numerically equal. The anisotropic scattering phase function is included in the calculation of the single scattering component of the total intensity.

Resonant fluorescence g-factors for the γ, δ, and ε band systems of NO are currently computed using scaled solar fluxes from Mount and Rottman[18] with oscillator strengths from Huber and Herzberg[19], as described in Cleary[20]. NO densities are obtained from an empirical model[21]. The total system g-factors for the γ (v' = 0 - 4 progressions), δ (v' = 0 progression), and ε (v' = 0 - 2 progressions) are 2.9×10^{-5} s^{-1}, 3.1×10^{-6} s^{-1}, and 5.8×10^{-6} s^{-1}, respectively. For the N_2^+ 1NG (first negative) system, optically thin g-factors have been computed using the 1985 high resolution SUSIM solar irradiance spectrum[22] and the molecular constants compiled by Laux and Kruger[23]; the total system g-factor is 0.148 s^{-1}. The g-factor for the N_2^+ Meinel system adopted for AURIC is 0.114 s^{-1}, derived using the oscillator strengths of Cartwright[24] and the MODTRAN reference solar irradiance spectrum. Opacity and albedo effects are currently ignored for all these systems.

Dayglow spectral radiances

The intensity equation

AURIC calculates spectral radiances in units of Rayleighs nm^{-1} for user specified look angles from 0° (zenith) to 180° (nadir). The emission is comprised of molecular bands and atomic lines. Rotational lines within these bands along with the atomic lines are smoothed to the user specified wavelength resolution. The spectral radiance, designated by $4\pi I_\lambda$ is:

$$4\pi I_\lambda = 10^{-6} \int j(s,\lambda) T(s,\lambda) e^{-t(s,\lambda)} ds \qquad \text{Rayleighs nm}^{-1} \qquad (6)$$

with terms as follows:

j   volume emission rate in photons cm^{-3} s^{-1} nm^{-1}
T   transmission function for self absorption (dimensionless)
t   pure absorption optical depth (dimensionless)
s   distance from observing point along line-of-sight.

Line-of-sight integration is through a spherically stratified atmosphere. The solar zenith angle is assumed constant along the line-of-sight and thus, the present version of AURIC is not suitable for calculating intensities near the terminator.

The transmission function T is unity for most of AURIC's emission features. Exceptions are OI 130.4 nm, OI 135.6 nm, and HI 121.6 nm. The T functions for these features are treated by the transport models described in the previous section. The exponential term is unity longward of ~175 nm. Below this wavelength, t is non-zero due to Schumann-Runge continuum absorption by O_2 which peaks at ~140 nm.

30

Spectral radiances in nm^{-1} are not calculated by AURIC from eq. 6. Instead, total intensities by line, band, or band system are first calculated followed by separate procedures for distributing these intensities in wavelength for the selected resolution. More details follow below about the synthetic spectral routines that produce the wavelength dependence of bands and band systems. From eq. 6, the total intensity of a line, band, or band system is:

$$4\pi I_i = 10^{-6} \int j_i(s) e^{-t_i(s)} ds \qquad \text{Rayleighs} \qquad (7)$$

where T has been set to unity (applicable except for those features treated by the transport models), the subscript i refers to a line, band, or system, and units of j_i are photons $cm^{-3} s^{-1}$. Three forms of j are treated by AURIC. The first is given by eq. 4 for electron impact excitation with unit probability of emission. The second is given by:

$$j_i(z) = A_i n(z) \qquad (8)$$

which is appropriate to metastable states where n is the density of a given state calculated by AURIC's photochemistry model and A_i is the transition rate associated with the given feature. The third form refers to solar resonant fluorescence:

$$j_i = g_i n(z) \qquad (9)$$

where g_i is the g-factor discussed in the previous section. This form of j is used to calculate the total volume emission rates for the NO and N_2^+ systems.

Molecular band synthetic spectral models

To incorporate molecular emissions in total atmospheric radiance spectra, it is necessary to distribute the system emission rate among the observable bands; in turn, the distribution of emission within a single band is dictated by the rotational line spectrum. For the band systems listed in Table 2, spectral synthesis routines have been adopted from numerous sources. In all cases, spectra are evaluated at 0.1 nm resolution and subsequently smoothed to the user-specified resolution. Spectral synthesis routines for the bands of the NO γ, δ, and ε systems are from Cleary[20], with excitation out of the ground state $v'' = 0$ level. For the N_2^+ band systems, spectral modeling of individual bands is carried out using routines provided by D. Gattinger. Individual band intensities have been evaluated using the solar flux spectra and transition probabilities noted previously, coupled with an assumed N_2^+ ground state vibrational temperature of 6000 K which gives a relative population of 0.40 for the $v'' = 0$ level.

Modeling of the photoelectron impact-produced N_2 LBH, VK, and 2PG emission spectra utilizes the spectral modeling routines of Conway[35] and Conway and Christensen[36]. For the LBH system, progressions $v' = 0 - 6$ are treated with the relative populations estimated from the v'-0 Franck-Condon factors, taking into account wavelength-dependent photoabsorption by O_2. Progressions $v' = 0 - 9$ are included in the modeling of the VK system, using the relative populations of Cartwright[37]. This system is affected by quenching; in AURIC, the dependence of the quenching rate on v' is currently ignored. Modeling of the 2PG system includes progressions $v' = 0 - 4$, again with the v' relative populations estimated from the v'-0 Franck-Condon factors. The N_2 1PG emission system is also generated by photoelectron impact. For this system, spectral modeling of individual bands is done with a routine provided by D. Gattinger; the relative distribution of the total system intensity among system bands is taken from Table 4.12 of Vallance Jones[38].

31

Rayleigh scattering of sunlight

An interface to MODTRAN exists for calculating Rayleigh scattered spectral radiances, saving them to a file, reading the file at an appropriate point within the execution of the sequence of AURIC modules. and adding these radiances to dayglow spectral radiances. Rayleigh scattering must be taken into account longward of ~180 nm at tangent altitudes below ~100 km. MODTRAN's full capability includes rapid molecular band model calculations of radiances in the IR, tranmittances from the IR to the UV, and Rayleigh scattering of sunlight and moonlight (see MODTRAN references in Section 1). The user must provide his/her own copy of MODTRAN for interfacing with that portion of AURIC being discussed in this paper.

Key inputs for dayside modeling

Table 5 lists the key inputs to AURIC's dayglow modules. The first five entries are obtained from models or algorithms as identified in the Reference column. The remaining entries refer to a large volume of data obtained from compilations by either the authors or other investigators. To conserve space, we refer the reader to the papers referenced in the table. Most of the data appear explicitly in several tables appearing in Strickland et al[1] (for example, extensive tables of rate coefficients for AURIC's dayside and nightside chemistry models).

Table 5. Key inputs to dayglow modules and references.

Parameter	Reference
Model atmosphere (N_2, O_2, and O)	MSISE-90 (Hedin[15])
Model atmosphere (NO)	Smith et al.[21]
Model ionosphere	FAIM (Anderson et al.[29])
Geomagnetic field (for relating geomagnetic to geographic coordinates)	IGRF (Peddie[30])
Solar EUV spectrum	Hinteregger et al.[19]
Photoabsorption cross sections	Conway[31]
Photoionization cross sections	Conway[31]
Electron impact energy loss cross sections	Majeed and Strickland[32]
Electron impact cross sections for calculating production rates needed by chemistry model	Strickland et al.[1]
Electron impact cross sections for calculating emission rates	Strickland et al.[1]
Schumann-Runge O_2 continuum photo-absorption cross section	Hudson[33]
Rate coefficients	Strickland et al.[1]
Transition rates	Strickland et al.[1]
Population distributions	Strickland et al.[1]

32

4. SELECTED DAYGLOW RESULTS

A detailed description of the output from AURIC's dayglow modules is available in the AURIC User's Manual[2]. A subset of some of the more interesting results will be illustrated here. Results will be shown in the form of photoelectron fluxes, altitude profiles of volume emission rates, limb intensity profiles, and spectral radiances for selected tangent altitudes as seen from satellite altitudes. Calculations have been performed for an MSISE-90 midlatitude model at moderate solar activity ($F_{10.7}$ = 150) for a solar zenith angle of 60°. The exception to this was the calculation of the photoelectron fluxes for which conditions were chosen to match those of the data to which the fluxes will be compared. Figure 2 shows calculated and measured photoelectron fluxes at an altitude of 167 km. The data were taken from the paper of Lee et al.[34] and have been divided by 1.5 to reproduce the overall magnitude of the model results. The accuracy of the data has been discussed in various papers over the past several years. Richards and Torr[13] argue that the fluxes have the correct magnitude while Strickland and colleagues argue that the fluxes should be reduced by a factor between 1.5 and 2.0 (e.g., Strickland and Anderson[35]). Conway[36] presents independent information that also argues for a reduction in the measured photoelectron fluxes. The different points of view arise from the use of different sets of N_2 excitation cross sections. More details are given in the paper by Majeed and Strickland[32]. Returning to Figure 2, two model spectra are shown for different solar EUV fluxes below 250 Å. A better fit to the data is obtained by increasing the Hinteregger fluxes at short wavelengths. We have chosen a scaling factor of 2 to demonstrate this point. Richards and Torr[13] have also argued for higher fluxes at shorter wavelengths based on the same types of shape comparisons between their model results and the Lee et al. data.
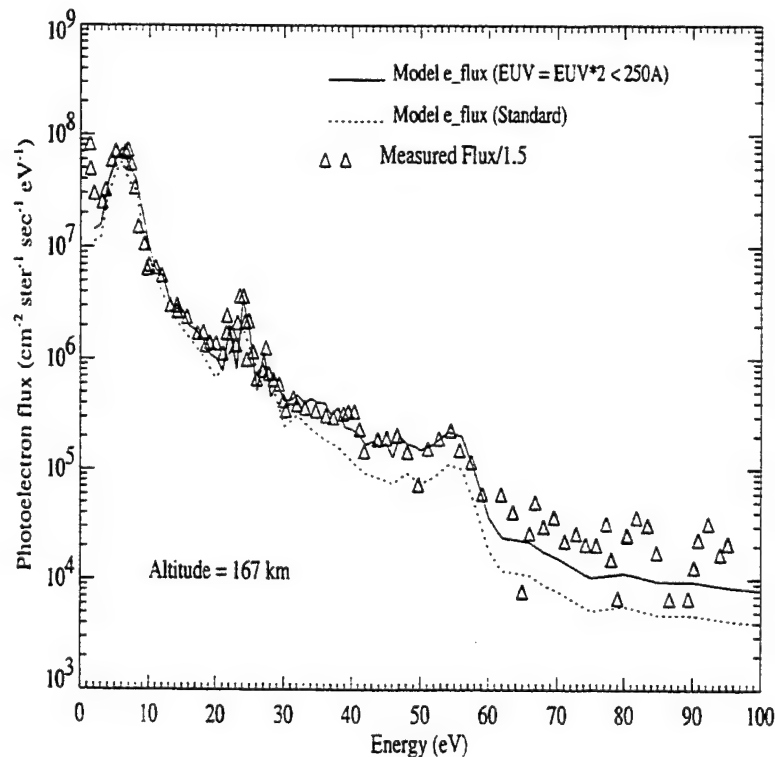

Figure 2. Calculated and measured[34] photoelectron fluxes at 167 km (the latter scaled downward by a factor 1/1.5). The solid curve shows the effect of increasing the solar flux below 25 nm by a factor of two.

33

Figure 3 illustrates the altitude dependence of volume emission rates for selected key emission features. For illustration, we have selected N_2 LBH, N_2 IPG, N_2 VK (includes the effect of quenching), and the lines of atomic oxygen at 135.6 nm and 844.6 nm. The secondary peak at low altitudes is due to the soft X-ray portion of the solar spectrum. Figure 4 shows limb profiles corresponding to the results in Figure 3 plus profiles for the optically thick features OI 130.4 nm and HI 121.6 nm. As noted earlier, the REDISTER model of Gladstone[14] is used to calculate 130.4 radiances (as well as OI 135.6 nm) while a global CFR model by one of us (JEB) is used to calculate 121.6 nm radiances. For LBH, two profiles are shown for emission between 140 - 149 nm and 170 - 180 nm; the difference in shape is caused by differences in O_2 pure absorption between the selected intervals. Spectral radiances from 100 to 1000 nm at tangent altitudes of 80, 100, and 120 km are shown in Figure 5. Rayleigh scattering results are included which begin to exceed the dayglow results as the tangent altitude decreases below 100 km. Tables 1 and 2 list the dayglow features that have contributed to the spectra in Figure 5.
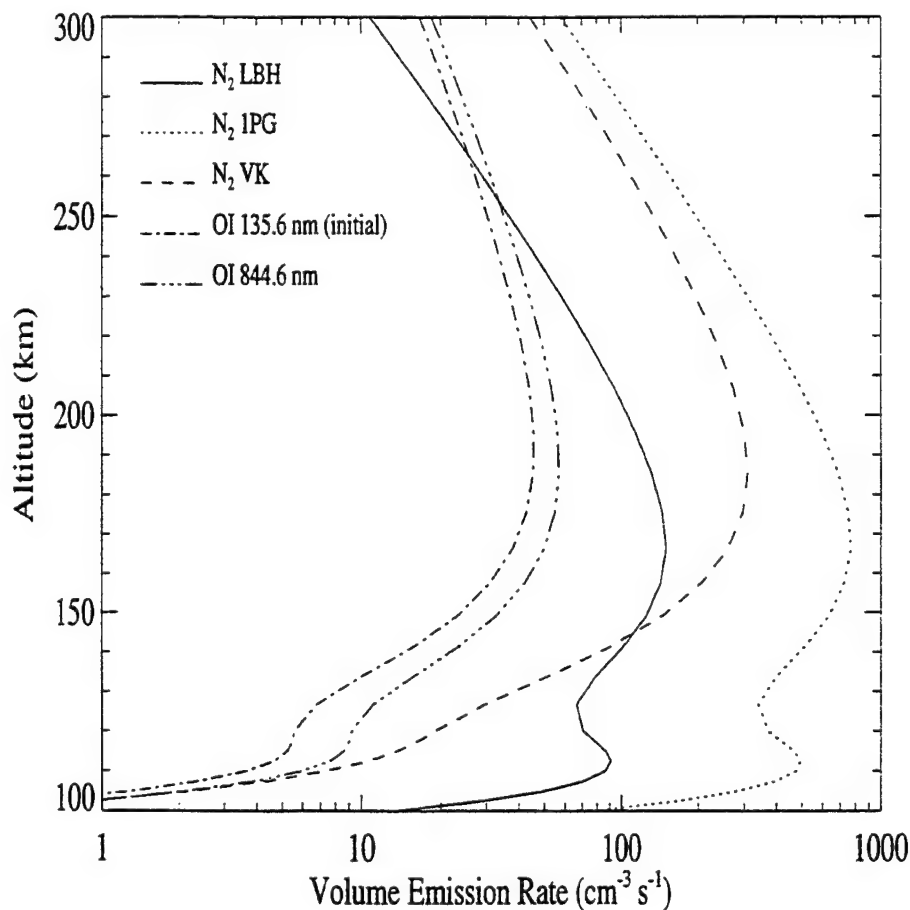

Figure 3. Selected volume emission rates for a 60° solar zenith angle and a Hinteregger solar EUV spectrum based on $F_{10.7}$ = 150. The 135.6 nm rate is the initial rate referred to as S_o in the above section under the heading *Solar resonance and resonant fluorescence scattering features*. X-rays are responsible for the secondary low altitude peaks.
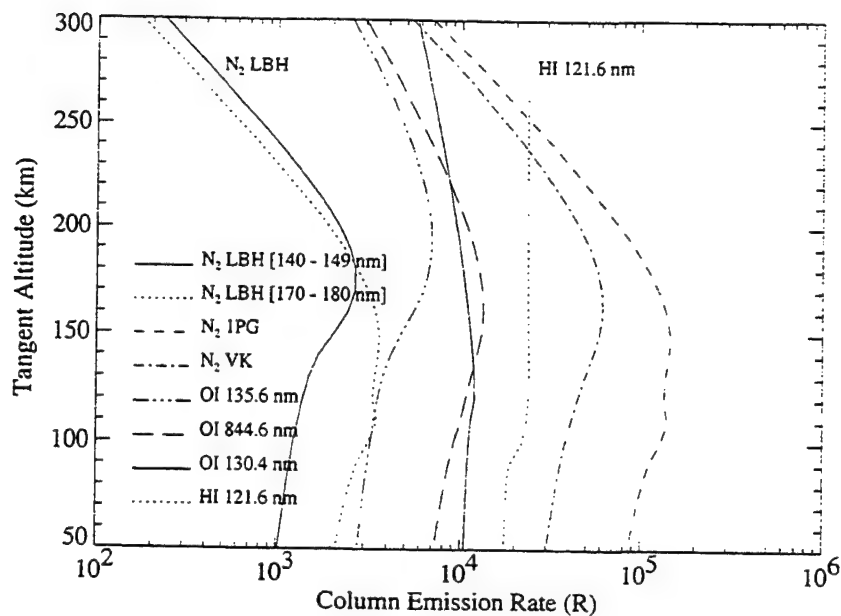
Figure 4. Limb profiles in Rayleighs corresponding to the volume emission rates in Figure 3 plus profiles for the optically thick OI 130.4 nm and HI 121.6 nm features. The differences in the shapes of the two LBH profiles are due to differences in pure absorption by O_2 between these bands.
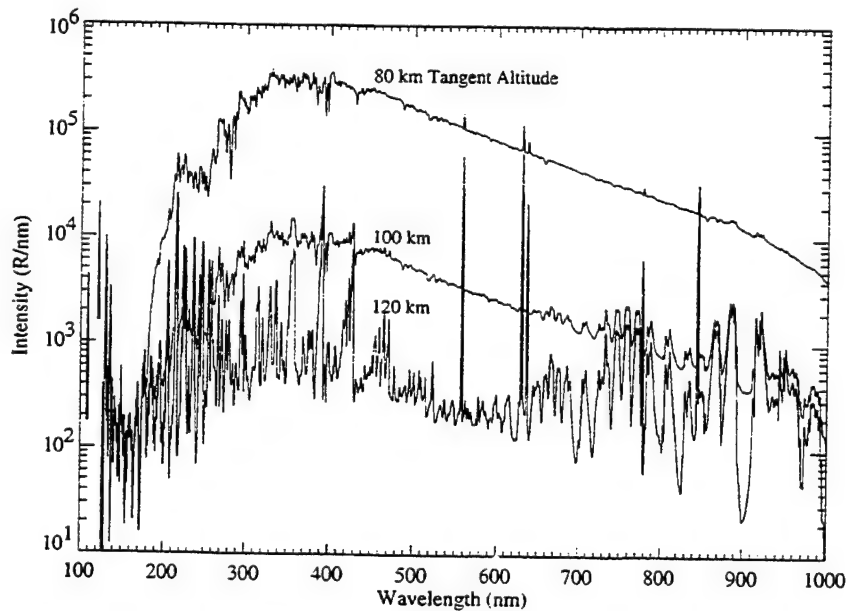

Figure 5. Spectral radiances at a wavelength resolution of 1.0 nm for tangent altitudes of 80, 100, and 120 km. Rayleigh scattering of sunlight dominates the spectrum at 80 km longward of 180 nm.

35

5. DISCUSSION AND SUMMARY

As of this writing, final testing and validation are underway of the software modules introduced in Section 2. An example of validation efforts is presented in Figure 2 where AURIC photoelectron fluxes are compared to the data of Lee et al.[34]. Throughout the project, CPI has made the airglow portion of AURIC available to various DoD affiliated organizations. Executables along with all needed input data files and selected graphics routines have been installed on Unix, VMS, and PC systems as new versions of the software have become available. The AURIC User's Manual has continued to evolve from version to version of the software and has been included with the above installations. Examples of organizations that have been using AURIC are the sponsor (PL/GP), the Naval Research Laboratory, the Applied Physics Laboratory, and selected government contractors.

End-of-project documentation has already been cited in earlier sections. The key documents are a science manual and the user's manual. The science manual is near completion and is being written as a paper[1] for submission to an appropriate journal. This SPIE paper is an abbreviated version of this paper. Present plans are to submit the full paper to *J. Geophys. Res.* within the next two months. Another important documentation effort has been directed to the large number of energy loss cross sections used to calculate photoelectron fluxes. A paper has been completed on this subject and submitted to *J. Phys. Chem. Ref. Data* by two of us (TM and DJS)[32]. The paper was written to document our sets of energy loss cross sections for N_2, O_2, and O which contain many cross sections from recent energy loss measurements. Overall assessments of these sets are made through comparisons with total cross sections obtained from transmission measurements and comparisons of cross-section-based loss functions with the Bethe formula above 100 eV. Discussion includes energy loss cross sections used by other modelers in the field.

The airglow portion of AURIC should prove to be a valuable tool to investigators interested in characterizing optical backgrounds at rocket and satellite altitudes, simulating and analyzing optical data, and studying chemically active species (ions and neutrals) in the thermosphere. The suite of models is easy to use through either the supplied interface or command files. All input files are formatted which allows for easy modification of parameters such as $F_{10.7}$ and arrays containing information such as input densities. Since the modules are first-principles rather than empirically based, the user can conduct detailed investigations of the interrelationships between physical quantities such as the solar EUV flux and composition on the one hand and emissions and chemically active densities on the other.

6. ACKNOWLEDGEMENTS

7. REFERENCES

1. D. J. Strickland, J. S. Evans, J. E. Bishop, T. Majeed, P. M. Shen, R. Link, and R. E. Huffman, Atmospheric Ultraviolet Radiance Integrated Code (AURIC): Airglow segment - theory, software architecture, inputs, and selected results, to be submitted to *J. Geophys. Res.*, 1996.

2. D. J. Strickland, P. M. Shen, J. S. Evans, J. E. Bishop, T. Majeed, and R. Link, AURIC/R User's Guide, Computational Physics, Inc., Fairfax, Va, 1996.

3. F. X. Kneizys, E. P. Shettle, L. W. Abreu, J. H. Chetwynd, G. P. Anderson, W. O. Gallery, J. E. A. Selby, and S. A. Clough, Users guide to LOWTRAN 7, *AFGL Tech. Rep. AFGL-TR-88-0177,* Air Force Geophysics Lab, Hanscom AFB, Mass., 1988. ADA206773

4. A. Berk, L. Bernstein, and D. Robertson, MODTRAN: A moderate resolution model for LOWTRAN 7, AFGL–TR–89–0122, Air Force Geophysics Lab, Hanscom AFB. MA. 1989, ADA214337

5. G. P. Anderson, J. H. Chetwynd, J.-M. Therault, P. Acharya, A. Berk, D. C. Robertson, F. X. Kneizys, M. L. Hoke, L. W. Abreu, and E. P. Shettle, MODTRAN 2: Suitability for remote sensing, *Proc. SPIE Int. Soc. Opt. Eng., 1968*, 514-525, 1993.

6. K. Minschwaner, G. P. Anderson, L. A. Hall, J. H. Chetwynd, R. J. Thomas. D. W. Rusch, A. Berk, and J. A. Conant, Scattered ultraviolet radiation in the upper stratosphere 2: Models and measurements, *J. Geophys. Res., 100*, 11165-11171, 165, 1995.

7. R. Link, D. J. Strickland, and R. E. Daniell, Jr., AURIC airglow modules: phase 1 development and application, *SPIE, Ultraviolet Technology IV, 1764*, 132-141, 1992.

8. D. J. Strickland and R. R. Meier, A photoelectron model for the rapid computation of atmospheric excitation rates, *NRL Memorandum Report 5004*, Naval Research Laboratory, Washington, D.C., 20375-5000, 1982.

9. D. E. Siskind, D. J. Strickland. R. R. Meier, T. Majeed, and F. G. Eparvier, On the relationship between the solar soft X-ray flux and thermospheric nitric oxide: an update with an improved photoelectron model, *J. Geophys. Res., 100*, 19687-19694, 687. 1995.

10. H. E. Hinteregger, K. Fukui, and B.R. Gilson, Observational, reference and model data on solar EUV from measurements of AE-E, *Geophys. Res. Lett., 8*, 1147-1150, 1981.

11. G. A. Victor, K. Kirby-Docken, and A. Dalgarno, Calculations of the equilibrium photoelectron flux in the thermosphere, *Planet. Space Sci., 24*, 679, 1976.

12. J. R. Jasperse, Boltzmann-Fokker-Planck model for the electron distribution function in the Earth's ionosphere, *Planet. Space Sci., 24*, 33, 1976.

13. P. G. Richards and D. G. Torr, An investigation of the consistency of the ionospheric measurements of the photoelectron flux and solar EUV flux, *J. Geophys. Res., 89*, 5625-5635, 1984; P. G. Richards and D. G. Torr, Ratios of photoelectron to EUV ionization rates for aeronomic studies, *J. Geophys. Res., 93*, 4060-4066, 1988.

14. G. R. Gladstone, Radiative transfer with partial frequency redistribution in inhomogeneous atmospheres: Application to the Jovian aurora, *J. Quant. Spectrosc. Radiat. Transfer, 27*, 545-556, 1982; G. R. Gladstone, UV resonance line dayglow emissions on Earth and Jupiter, *J. Geophys. Res., 93*, 14623-14630, 1988.

15. A. E Hedin, Extension of the MSIS thermosphere model into the middle and lower atmosphere, *J. Geophys. Res., 96*, 1159-1172, 1991.

16. D. E. Anderson, Jr., and C. W. Hord, Multidimensional radiative transfer: Applications to planetary coronae, *Planet. Space Sci., 25*, 563-571, 1977.

17. J. Bishop, Analytic exosphere models for geocoronal applications, *Planet. Space Sci., 39*, 885-893, 1991.

18. G. H. Mount and G. J. Rottman, The solar absolute spectral irradiance 1150-3173 Å: 17 May 1982, *J. Geophys. Res., 88*, 5403-5410, 1983.

19. K. P. Huber and G. Herzberg, *Molecular Spectra and Molecular Structure IV. Constants of Diatomic Molecules*, Van Nostrand Reinhold, New York, 1979.

20. D. D. Cleary, Analysis of nitric oxide fluorescence bands from high latitude rocket observations of the thermospheric dayglow, dissertation, Univ. of Colorado, 1985.

21. D. R. Smith, P. De, S. Adler-Golden, and C. Roth, Empirical correlations in thermospheric NO density measured from rockets and satellites, *J. Geophys. Res., 98*, 9453-9458, 1993.

22. G. E. Brueckner, K. L. Edlow, L. E. Floyd IV, J. L. Lean, and M. E. VanHoosier, The solar ultraviolet spectral irradiance monitor (SUSIM) experiment on board the Upper Atmosphere Research Satellite (UARS), *J. Geophys. Res., 98*, 10695-10711, 1993.

23. C. O. Laux and C. H. Kruger, Arrays of radiative transition probabilities for the N$_2$ first and second positive, NO beta and gamma, N$_2^*$ first negative, and O$_2$ Schumann-Runge band systems, *J. Quant. Spectrosc. Radiat. Transfer, 48*, 9-24, 1992.

24. D. C. Cartwright, Transition probabilities for the Meinel band system of N$_2^*$, *J. Chem. Phys., 58*, 178-185, 1973.

25. R. R. Conway, Self-absorption of the N$_2$ Lyman-Birge-Hopfield bands in the far ultraviolet dayglow, *J. Geophys. Res., 87*, 859-866, 1982.

26. R. R. Conway and A. B. Christensen, The ultraviolet dayglow at solar maximum, 2. Photometer observations of N$_2$ second positive (0,0) band emission, *J. Geophys. Res., 90*, 6601-6607, 1985.

27. D. C. Cartwright, Vibrational populations of the excited states of N$_2$ under auroral conditions, *J. Geophys. Res., 83*, 517-531, 1978.

28. A. Vallance Jones, *Aurora*, D. Reidel, Dordrecht, 1974.

29. D. N. Anderson, J. M. Forbes, and M. Codrescu, A fully analytic, low- and middle-latitude ionospheric model, *J. Geophys. Res., 94*, 1520-1524, 1989.

30. N. W. Peddie, International Geomagnetic Reference Field: The third generation, *J. Geomagn. Geoelectr., 34*, 309, 1982.

31. R. R. Conway, Photoabsorption and photoionization cross sections of O, O$_2$, and N$_2$ for photoelectron production calculations: a compilation of recent laboratory measurements, *NRL Memorandum Report 6155*, Naval Research Laboratory, Washington, D.C., 20375-5000, 1988.

32. T. Majeed and D. J. Strickland, New survey of electron impact cross sections for photoelectron and auroral electron energy loss calculations, submitted to *J. Phys. Chem. Ref. Data*, July, 1996.

33. R. D. Hudson, Critical review of ultraviolet photoabsorption cross sections for molecules of astrophysical and aeronomic interest, *Rev. Geophys. Sp. Phys., 9*, 305, 1971.

34. J. S. Lee, J. P. Doering, T. A. Potemra, and L. H. Brace, Measurements of the ambient photoelectron spectrum from Atmosphere Explorer: 1. AE-E measurements below 300 km during solar minimum conditions, *Planet. Space Sci., 28*, 947, 1980.

35. D. J. Strickland and D. E. Anderson, Radiation transport effects on the OI 1356-Å limb intensity profile in the dayglow, *J. Geophys. Res., 88*, 9260-9264, 1983.

36. R. R. Conway, Comments on the interpretation of 3371 A filter-photometer observations and its implications for the AE-E photoelectron fluxes, *Planet. Space Sci., 31*, 1223, 1983.

APPENDIX C: PAPER IN PRESS ON AURIC ENERGY LOSS CROSS SECTIONS

NEW SURVEY OF ELECTRON IMPACT CROSS SECTIONS FOR PHOTOELECTRON AND AURORAL ELECTRON ENERGY LOSS CALCULATIONS

T. Majeed and D. J. Strickland
Computational Physics, Inc., Fairfax, VA 22031

NEW SURVEY OF ELECTRON IMPACT CROSS SECTIONS FOR PHOTOELECTRON AND AURORAL ELECTRON ENERGY LOSS CALCULATIONS

Tariq Majeed and Douglas J. Strickland

Computational Physics, Inc., 2750 Prosperity Avenue, Suite 600, Fairfax, VA 22031

Newly surveyed sets of energy loss cross sections are presented for N_2, O_2, and O. The work was motivated by a number of new electron energy loss measurements in the late 1980s and early 1990s and recent selected review articles. Each set includes a total ionization cross section and excitation cross sections that correspond to all important non-ionizing energy loss channels for that species. A total cross section for each species is constructed by summing the elastic scattering cross section with the ionization and excitation cross sections. The sum is compared to a measured total cross section obtained from electron transmission experiments. Good agreement is achieved for each of the three species. A loss function is also constructed for each species and compared with the Bethe formula above 100 eV. Good agreement is also achieved in energy loss which is dominated by ion and secondary electron production. Fluxes of photoelectrons and auroral electrons have been calculated for the new sets of energy loss cross sections as well as our previous sets. No substantial differences occur using the new description of energy loss.

Key Words: Energy loss cross sections for N_2, O_2 and O, Photoelectron flux, Auroral electron flux, Electron impact, Elastic and total scattering cross sections, Ionization cross section, Bethe formula, Inelastic cross section.

1. INTRODUCTION

The work described below was undertaken as one of several tasks to develop a dayglow/nightglow UV radiance model for the integrated model AURIC (Atmospheric Ultraviolet Radiance Integrated Code). The term *integrated* refers to the joining of this radiance model with the Air Force model MODTRAN. This latter model provides rapid molecular band model calculations of radiances in the IR, transmittances from the IR to the UV and Rayleigh scattering of sunlight and moonlight[1,2,3,4]. The designator AURIC-R will be used to distinguish the UV radiance portion from the integrated model. AURIC-R has been under development by Computational Physics, Inc. (CPI) over the past three years for the Geophysics Directorate of the Air Force Phillips Laboratory (PL/GP). A key task has been the re-engineering of Fortran codes within the PEGFAC (photoelectron g-factor) model[5] using modern programming standards. Another key task has been I/O restructuring and updating of key input parameters. Much of the latter effort has been directed to three sets of electron impact cross sections. These sets are used to 1) perform photoelectron energy loss calculations, 2) calculate volume production rates for chemistry modeling, and 3) calculate volume emission rates for specifying spectral radiances. This paper addresses the first of these sets containing energy loss cross sections for N_2, O_2, and O.

The motivation for this work comes from a number of new cross section measurements in the late 1980*s* and early 1990*s* (references to many of these measurements appear in the recent reviews of Itikawa et al.[6,7], Itikawa and Ichimura[8], Laher and Gilmore[9] and Kanik *et al.*[10]). Our approach has been to gather cross sections

for the important loss channels of each of the three species (a single channel for ionization and several for excitation) and examine them in two ways. First, a total cross section is constructed for each species by summing the total ionization and energy loss cross sections with the elastic scattering cross section for that species. This total cross section is then compared with measurements from electron transmission experiments. Second, a loss function is constructed and compared with the Bethe formula (see Strickland et al.[11] for its form and application to N_2) above 100 eV. While such a test is not useful for accurately assessing a cross section set at energies most important to photoelectron energy loss calculations (below 100 eV), it does place constraints on the total inelastic cross section and differential dependence of the ionization cross section above 100 eV. Assuming good knowledge of the total ionization cross section, the differential dependence dictates the magnitudes of the secondary electron energy loss component of the total loss function. This component dominates above a few hundred eV as will be illustrated later in the paper.

Ionization, elastic, and total cross sections of N_2, O_2, and O appear to be well quantified at this time through both laboratory measurements and calculations. As we shall demonstrate, work still remains to be done in quantifying the many excitation (non-ionizing energy loss) channels of these species, especially near and above the first ionization threshold (Rydberg channels). There is generally good agreement among the various sets of total ionization cross section measurements of N_2, O_2, and O (see Itikawa et al.[6,7], Itikawa and Ichimura[8], and Kanik et al.[10] for specific references). The most recent measurements of total ionization cross sections of N_2 (Krishnakumar and

Srivastava[12]) and O_2 (Krishnakumar and Srivastava[13]) are in close agreement with earlier measurements of Rapp and Englander-Golden[14]. For O, the recent work by Itikawa and Ichimura[8] lends support to the measurements of Brook et al.[15] The total and elastic scattering cross sections of N_2 and O_2 appear to be well characterized based on agreement among the various existing sets of measurements (see reviews of Itikawa et al.[6,7] and Kanik et al.[10] for agreement among the original data sets). For O, the only measurement of the total cross section is by Sunshine et al.[16] The measurements were limited to energies from 1 to 100 eV and possess more scatter than for the corresponding cross sections of N_2 and O_2. Itikawa and Ichimura[8] constructed a total O cross section by summing available components and found agreement with Sunshine et al.[16] within the scatter of the data. The Itikawa and Ichimura[8] cross section spans a larger energy range going to 7000 eV. Within their sum is an elastic scattering cross section based on calculations rather than measurements. The available measurements are by Dehmel et al.[17] which appear to be contaminated by inelastic scattering[8].

Fox and Victor[18] discuss electron energy loss in N_2. Cross section information is in the form of loss function components (for excitation, production of ion states, and kinetic energy of secondaries) with direct cross section information limited to references. Several compiled sets of energy loss cross sections or totals by species have been published over the years in papers addressing the calculation of photoelectron and auroral electron fluxes (e.g., Strickland et al.[11], Victor et al.[19], Oran and Strickland[20], Jackman and Green[21], Mantas[22], Stamnes and Rees[23], Richards and Torr[24,25], Solomon[26], and Strickland et al.[27]). The sources of measured and calculated cross sections from one set

to another are not the same and in turn can lead to different conclusions from analyses of photoelectron data, auroral electron data, and optical data involving emission features produced by electron impact excitation. A further discussion on this topic will be given in Section. 5.

Since this paper addresses energy loss cross sections, there will be limited discussion of the collision products associated with a given loss channel. Collision products are important for the other two cross section sets mentioned above, namely for production rates needed in chemistry calculations and emission rates needed in radiance calculations. Energy loss cross sections, on the other hand, are used to calculate photoelectron and auroral electron fluxes for which the only requirement is that a proper distribution of energy loss be achieved per collision. Here, the important features are excitation thresholds, cross section magnitudes, and in the case of ionization, the initial distribution of secondary electrons (for a discussion of the treatment of secondaries in AURIC-R as well as CPI's auroral model, see Strickland et al.[11]).

The next three sections present our full sets of energy loss cross sections for N_2, O_2, and O, including references to all individual set members. As noted above, total cross sections are constructed and compared to electron transmission data. Loss functions are also constructed and compared to the Bethe formula. A discussion section (Sec. 5) completes the paper.

2. ENERGY LOSS CROSS SECTIONS FOR N_2

Table 1 identifies states or energy loss channels corresponding to individual inelastic cross sections of N_2. For each entry, the table also includes the energy threshold, location of the cross section maximum, the value of this maximum, percent contributing to dissociation, and the source of the cross section. Tabulated values of these cross sections (as well as those to follow in Tables 2 and 3) are given in the Appendices. Figure 1 shows examples of measured energy loss spectra (from two separate measurements as noted below) with an energy level diagram above for states with energy thresholds within the illustrated loss region (6 to 14.6 eV). Such data are obtained by starting with a beam of electrons at a single energy and measuring its energy spectrum at a given scattering angle after passing through a given amount of N_2. High lying states from Table 1 are not included since their thresholds (including ionization) lie above 15 eV. Each of the horizontal line segments in the lower portion of the figure is identified with a given state and shows the excitation threshold along with some indication of the effective range of energy loss. Unlike the localized nature of energy loss for an atomic state, here loss extends to several eV above threshold due to the ability of an impacting electron to leave N_2 in one of several vibrational levels of a given electronic state. The loss spectrum below 12 eV is from S. Trajmar (private communication, 1995) and was obtained for electrons with an incident energy of 40 eV observed at a scattering angle of 20°. The vertical scale is arbitrary since the purpose of showing the data is to simply illustrate energy loss structure. The wings of the Trajmar loss spectrum have been multiplied by 10 to show the structure associated with the various triplet states. The

dominant loss for the given incident energy is seen to be by the $a^1\Pi_g$ state responsible for the Lyman-Birge-Hopfield band system. The loss spectrum above 12 eV is from Ratliff et al.[28] for 100 eV electrons scattering through an angle of 15°. The structure above 12.5 eV is dominated by loss to numerous vibrational levels of the b, b', c, and c' states. The first figure in Ratliff et al.[28] labels the peaks by vibrational level. The magnitude of the Ratliff spectrum is arbitrary and thus no significance is to be placed on its strength relative to the Trajmar spectrum. Cross sections are obtained from data such as these by integrating calibrated spectra over angle and energy loss (see papers such as Ratliff et al.[28] and Doering and Vaughan[29] for more information on the derivation of cross sections from energy loss data).

Figure 2 shows a comparison between the total cross section based on Table 1 and transmission measurements taken from the review by Itikawa et al[6]. The total from our work is comprised of the three curves labeled elastic, total ionization, and total excitation. The elastic cross section was also taken from Itikawa et al[6]. The total and elastic cross sections of Itikawa et al.[6] are based on available measurements with adjustments to account for offsets among the various data sets. References to original data may be seen in the paper of Itikawa et al.[6] (See also Shyn and Carignan[30], who measured the total elastic cross section from 1.5 to 400 eV. This reference is missing in Itikawa et al.[6]). The ionization cross section comes from Rapp and Englander-Golden[14] that has served as the standard for modeling N_2 ionization in the upper atmosphere. Recent measurements by Krishnakumar and Srivastava[12] are in close agreement with Rapp and Englander-Golden[14] (see also for comparison, the derived total ionization cross section by Shyn[31]

from measurements of secondary electrons for primary electron energies from 50 to 400 eV).

The excitation cross section is comprised of the 20 non-ionizing components in Table 1. The next few figures present these components. We start with the triplet state cross sections in Figure 3. The source of these cross sections is Cartwright *et al.*[32] with the exception of that for the *C* state which is Ajello *et al.*[33] As an added note, Brunger and Teubner[34] have recently performed energy loss measurements similar to Cartwright *et al.*[35] but their results are inconclusive with regard to integrated cross section values due to the restricted range of scattering angles. Singlet state cross sections are shown in Figure 4 that include the total vibrational cross section and one for high-lying states. Figure 5 shows the terms comprising this latter cross section, which, from Table 1, are seen to come from Zipf and McLaughlin[36]

In Figure 6 we show a comparison between the total dissociation cross section that we derive from our full set of cross section data (see Table 1) and those measured by Winters[37] and most recently by Cosby[38]. The cross section data of Winters[37] have been corrected for dissociative ionization by using the recommended values of dissociative ionization cross sections from Itikawa *et al*[6]. Although the values of both measured cross sections for energies greater than 15 eV are within the stated error limits, the systematic differences seen in the figure may be due to an additional error from a correction for dissociative ionization. Our cross section is seen to be in overall good agreement with both measurements.

A final figure before discussing O_2 addresses energy loss. The loss function based on Table 1 is compared with the Bethe formula in Figure 7 (see Strickland et al.[11]; Eq. A9 for the form of the Bethe expression). The comparison is restricted to energies above 100 eV since the formula begins to lose its validity at lower energies. The cross section based loss function is calculated from:

$$L(E)=\sum_k W_k \sigma_k(E) + I\sigma_{ioniz} + \int_0^{(E-I)/2} \frac{d\sigma(E,E_s)}{dE_s} E_s dE_s \qquad \text{eV-cm}^2 \qquad (1)$$

Terms are as follows:

W_k threshold in eV of kth excitation process

σ_k k^{th} excitation cross section

I average ionization threshold (taken to be 18 eV)

σ_{ioniz} total ionization cross section

E_s secondary electron energy

$\dfrac{d\sigma(E,E_s)}{dE_s}$ differential ionization cross section in eV^{-1} cm^2

The three components in Eq. 1 are shown in Fig. 7. The importance of the secondary electron component with increasing energy is a reflection of the increase in the average energy of a secondary electron as the energy E of the incident electron increases. The differential form of the ionization cross section is given by Eq. A4 in Strickland et al.[11] with the adjustable parameter $\hat{E} = 13$ eV. The same value has been used for O_2 and O.

Excellent agreement is achieved with the Bethe loss function which gives a strong indication that ionization is being correctly described by its total and differential forms of the cross section. While excitation dominates the loss function below 30 eV, its contribution at higher energies falls below 20% where comparisons with the Bethe loss function become valid. Thus, the test on cross sections using the Bethe formula only weakly addresses excitation.

3. ENERGY LOSS CROSS SECTIONS FOR O_2

Table 2 shows information similar to Table 1 except for O_2. A column has not been included for contributions to dissociation since this is of less interest than for N_2 (this is not to say that the process in not represented within the full set of cross sections presented in the table). Greater interest in N_2 is due to chemistry modeling of $N(^4S)$, $N(^2D)$, $N(^2P)$, and NO within the AURIC model for which production of N in the above states by dissociation (by photoelectrons and solar photons) must be specified. Similar modeling of O is not performed due to O being one of the dominant species in the thermosphere for which its specification is given by a model such as MSIS-90[39]. Like N_2, all excitation cross sections listed in the table are based on energy loss measurements except for those belonging to Rydberg states. Unfortunately, there are no measurements available for these states and consequently we have adopted a theoretical cross section representing total Rydberg excitation as compiled by Oran and Strickland[20].

Figure 8 shows O_2 energy loss spectra similar to those for N_2 in Fig. 1. The spectrum below 2 eV is from Shyn and Sweeney[40] for 10 eV electrons scattered through an angle of 96°. The spectrum above 7 eV is from Shyn et al.[41] for 20 eV electrons scattered through an angle of 156°. Similar to the spectra for N_2, the results in Fig. 8 have arbitrary scales and thus there is no significance in the strength of the low energy portion compared to that above 7 eV.

Figure 9 shows the measured total cross section, the corresponding cross section based on Table 2, and its three components. The measured total and elastic scattering cross sections come from the most recent review of Kanik et al.[10] (see also Sullivan et al.[42], Shyn and Sharp[43] and Wakiya[44] for original studies and other references). Similar to N_2, they are based on several sets of measurements with adjustments for data offsets among these sets. The total ionization cross section also comes from Kanik et al.[10] and includes dissociative ionization. These authors compared available measurements and recommend those recently made by Krishnakumar and Srivastava[13] which are similar to the Rapp and Englander-Golden[14] cross section within the stated uncertainty limits. Similar results are also derived by Shyn and Sharp[45] from secondary electron measurements from threshold to 300 eV. The excitation cross section is the sum of the thirteen from Table 2. Figures 10 and 11 show the individual excitation cross sections where a sum has been performed over the vibrational cross sections. Schumann-Runge dissociation is a well known process for O_2. The responsible states are $1^3\Pi_g$ and $B^3\Sigma_g$ along with the 8.9 eV channel listed in Table 2

Figure 12 presents a comparison between the loss function calculated with eq.1 and the Bethe loss function. The cross-section-based loss function is about 10% below the Bethe loss function and argues for an increase by this amount in the magnitude of the ionization cross section. As with N_2, energy loss by excitation is minor where the comparison is being made. In fact, excitation plays a weaker role in O_2 compared to N_2. As a concluding comment in this section, larger errors in O_2 energy loss cross sections

can be tolerated in photoelectron and auroral electron energy loss calculations compared

to N_2 given the fact that there is much less O_2 in the thermosphere.

4. ENERGY LOSS CROSS SECTIONS FOR O

Table 3 shows information for O similar to that in Tables 1 and 2 for N_2 and O_2.

There are many high lying states of O in addition to those explicitly listed (see, e.g., Fig.

1 in Laher and Gilmore[9]). None of them individually accounts for significant energy loss

based on the measurements of the investigators referenced in the table. The Rydberg

cross sections represent these many states not explicitly accounted for. Figure 13 shows

energy loss spectra for O similar to previous results in Figs. 1 and 8 for N_2 and O_2,

respectively. An important difference, however, is the local nature of energy loss for a

given electronic state compared to states of N_2 and O_2 that can extend over several eV

due to vibrational excitation. The spectrum below 5 eV is from Doering and Gulcicek[46]

for 30 eV electrons scattered through an angle of $120°$. The spectrum at higher energies

is from Doering and Vanghn[29] for 100 eV electrons scattered through an angle of $4°$.

Again, as was the case for N_2 and O_2, the scales for the two spectra are arbitrary. We

have included energy loss data in Fig. 13 above the ionization threshold (13.6 eV). The

slow rise in the underlying continuum above the threshold is due to ionization. The ^{5}S

feature at 9.15 eV has been added based on data from Doering and Gulcicek[47] for 13.9 eV

electrons scattered through an angle of $50°$. Otherwise, this loss feature would not be

discernible given the incident energy (100 eV) associated with rest of the spectrum above

9 eV.

The total cross section for O and its components are shown in Figure 14. The

components are from Itikawa and Ichimura[8] for elastic scattering, Brook et al.[15] (also see

Itikawa and Ichimura[8]) for ionization, and from the references in Table 3 for excitation. Similar to N_2 and O_2, elastic scattering and ionization dominate the total and thus the comparison in the figure demonstrates little about the accuracy of the total excitation cross section. The next three Figures (15 - 17) show the excitation cross sections listed in Table 3. Extrapolations to higher energies beyond those measured are based on expected fall-off for the given transitions.

Similar for O_2, Rydberg cross sections for O are not well characterized experimentally, and consequently, we again rely on theoretical values as compiled by Oran and Strickland[20]. The Rydberg cross section in Figure 15 comes from Oran and Strickland[20]. We are, however, able to compare with other theoretical values produced by Laher and Gilmore[9] who have carried out a critical review of inelastic cross sections for O. They considered more than sixty individual cross sections, including nine allowed and twenty nine forbidden Rydberg series cross sections with transitions to $O^+(^4S_0)$, $O^+(^2D_0)$, and $O^+(^2P_0)$ ion cores of the excited states. Since no cross section measurements were available, they used a semi-empirical formula based on the work of Jackman et al.[48] to estimate individual Rydberg cross sections. Their sum is included in Fig. 15 for comparison with our representation. Good agreement exists below 30 eV while the Laher and Gilmore[9] values are as much as a factor of two higher between 40 and 150 eV. There are large uncertainties associated with either cross section and we thus do not speculate as to which is more accurate based on the respective modeling techniques. Nevertheless, using the Laher and Gilmore[9] cross section, our total cross section then exceeds the measured one by about 10% above 30 eV whereas, agreement to a few percent is

achieved using our representation. This provides an argument, although perhaps weak, for implementing a smaller Rydberg cross section above 30 eV than derived from the many individual terms in Laher and Gilmore[9].

Our calculated loss function for O is shown in Figure 18 along with that based on the Bethe formula. Reasonably good agreement is achieved with the Bethe formula although the differences in shape and magnitude above several hundred eV suggest increasing the total ionization cross section by perhaps 20% and decreasing the average energy of the secondary electron per collision by a similar amount.

5. DISCUSSION

From the information presented in earlier sections, it seems clear that there is much less uncertainty in the ionization, elastic, and total cross sections of a particular species compared to excitation. It is difficult to assign error bars due to the many sources of the information although our own assessment is that 15% or less uncertainty can probably be assigned to the former sets and more than 30% should be assigned to the latter (excitation). The largest source of uncertainty for excitation is in the Rydberg cross sections. The situation appears to be most satisfactory for N_2 among the three species being addressed. As noted earlier, we have used calculated values of Rydberg cross sections for O_2 and O given the paucity of measured values. One approach to specifying the total excitation cross section is to 1) subtract the ionization and elastic scattering cross sections from the total cross section or 2) subtract the ionization cross section from the total inelastic cross section (if available). We do not recommend such subtractions since the calculations involve the differences of similar quantities which demand greater accuracy in these quantities than can be expected at this time. An alternative approach and the one taken in this work is to compile available energy loss measurements for specific states or loss channels, supplement them where necessary with theoretical cross sections, sum this total set along with the ionization and elastic scattering cross sections, and compare with the total obtained from transmission measurements. While such an approach does not assure an accurate description for excitation assuming good agreement between totals, it is nevertheless a worthwhile exercise for assigning some degree of confidence to the overall magnitude of the total excitation cross section.

An important aspect of our N_2 work presented in Sec. 2 was specifying a total dissociation cross section. Based on its magnitude (see Figs. 5 and 6), dissociation accounts for approximately 80% of the energy loss in excitation channels for electron energies above 30 eV. Given the strength of this loss channel and the importance of odd nitrogen to a number of aeronomical problems, we provide further details here to supplement the discussion in Sec. 2. Zipf and Mclaughlin[36] identified nine energy loss channels that provide most of the contribution to the N_2 dissociation cross section (see Table 1). The most important of these are the high-lying states and the family of $^1\Pi_u$ states (terms used by Zipf and Mclaughlin). Cross section values at 100 eV have recently been measured for two members of this family. Ratliff et al.[28] addressed the $b^1\Pi_u$ state and obtained a cross section equal in magnitude to 29% of the value for the family at 100 eV. James et al.[49] reported a value for the $c^1\Pi_u$ state equal to 31%. Since these new measurements are available, we have constructed cross sections for these states using the shape of the cross section for the family along with the reported magnitudes at 100 eV. Having removed these components from the Zipf and McLaughlin[36] cross section, a residual cross section for the remaining members was constructed simply by scaling down the Zipf and McLaughlin[36] cross section by 0.40. While the decomposition into three new members with the same shape does not affect photoelectron or auroral electron energy loss calculations, it was done, nevertheless, in anticipation of further measurements of one or more of the $^1\Pi_u$ states that may lead to some differences in shapes among the components.

In the Introduction, we noted that several investigators have compiled sets of energy loss cross section for the purpose of calculating photoelectron and auroral electron fluxes and that differences exist among these sets. Generally, there is little difference in ionization and elastic scattering cross sections among the sets. The differences occur among the excitation cross sections. Examples of sets that have noteworthy differences are those of Richards and Torr[24, 25] and Strickland and colleagues (e.g., Strickland and Meier[5]; Strickland and Anderson[50]). Specifically, the total N_2 excitation cross section of Richards and Torr[25] is approximately a factor of two smaller above 15 eV in comparison to that of Strickland and colleagues. Richards and Torr[25] use a total N_2 excitation cross section obtained by subtracting a total ionization cross section from the total inelastic cross section of Phelps (private communication) as appears in Stamnes and Rees[23] (more will be said about this in the next paragraph). Strickland and colleagues have relied heavily on measurements of cross sections for specific states or specific energy loss channels (e.g., Zipf and McLaughlin[36]; Cartwright *et al.*[32]; Ajello and Shemansky[51]). Calculated photoelectron fluxes above 15 eV and below the region where ionization begins to dominate (above about 50 eV) by Richards and Torr[24,25] are approximately twice those of Strickland and colleagues due to these differences. This has led to discussions in numerous papers about the accuracy of the satellite measured photoelectron fluxes by Doering and colleagues (e.g., Lee *et al.*[52]). Richards and Torr argue that the fluxes have the correct magnitude while Strickland and colleagues argue that the fluxes should be reduced by a factor between 1.5 and 2.0 (e.g., Strickland and Anderson[50]). Conway[53] presents independent information that also argues for a reduction

in the measured photoelectron fluxes. A resolution to the problem has not been obtained as of this writing. It is important to note that similar results (within 10%) are obtained by us using either the cross sections in this paper or our earlier sets.

Reference was made in the above paragraph to the total excitation cross section of Phelps in the Stamnes and Rees[23] paper. Phelps (in a private communication to Stamnes and Rees) provided several cross sections for triplet states and one for total excitation to singlet states. Most of the contribution to the total comprising these cross sections comes from an analysis of swarm data. Since investigators such as Stamnes and Rees and Richards and Torr[24] have used cross sections of Phelps and colleagues based on swarm data, a brief discussion of recent papers addressing such data is presented here. The N_2 excitation cross sections appearing in Stamnes and Rees are the same as those published by Pitchford and Phelps[54] with the exception of the total singlet cross section. The version appearing in Stamnes and Rees is about twice as large as in Pitchford and Phelps. The increase is explained by Phelps and Pitchford[55] who added selected high threshold singlet cross sections from Zipf and McLaughlin[36]. Richards and Torr[25], as noted above, subtracted a total ionization cross section (from Kieffer and Dunn[56]) from the total inelastic cross section in Stamnes and Rees (based on the ionization and excitation cross sections provided by Phelps) to obtain a total excitation cross section. The result is a smaller cross section above the ionization threshold than would be obtained by adding the excitation components of Phelps since the ionization cross section used by Richards and Torr[25] in the subtraction is larger than assumed by Phelps (Rapp and Englander-Golden[14]). In addition to a larger singlet cross section by Phelps and Pitchford[55]

compared to their 1982 value, the latter paper also gives a larger total triplet cross section due to increasing the C state cross section by a factor of two. The more recent work of Jelenkovic and Phelps[57], based on stronger electric field swarm data, retains the total singlet cross section from the 1985 work, but returns to a total triplet cross similar to that in the 1982 work. Compared to the compilation in this work, the total singlet cross section is ~25% higher while the total triplet cross section is ~35% smaller.

Although more work remains to be done on characterizing excitation cross sections for N_2, O_2, and O, the compilation from this study gives a comprehensive set of the most updated energy loss cross sections that should serve well for performing photoelectron and auroral electron energy loss calculations. In closing, we note areas that most urgently need more attention:

1) Measurements of the total scattering cross section of O to verify and understand the limited measurements available at this time. Also needed is an experimental determination of the O elastic scattering cross section.

2) Measurements to better quantify the Rydberg states of O_2 and O.

3) Additional selected measurements of the excitation cross sections of the first ten states of N_2 ($A^3\Sigma_u^+$, $B^3\Pi_g$, $W^3\Delta_u$, $C^3\Pi_u$, $B'^3\Sigma_u^-$, $E^3\Sigma_g^+$ triplets and $a'^1\Sigma_u^-$, $a^1\Pi_g$, $w^1\Delta_u$, $a''^1\Sigma_g^+$ singlets) to resolve differences between recent[34] and earlier measurements[58,32,35]).

4) Measurements of cross sections for various $^1\Pi_u$ states of N_2 to verify the measurement of Zipf and McLaughlin[36] for the sum of cross sections for these states. As noted earlier, single energy measurements have recently been made for the $b^1\Pi_u$ and $c^1\Pi_u$ states. More measurements are needed, especially near 30 eV where these cross sections peak.

6. ACKNOWLEDGMENTS

7. REFERENCES

[1] F. X. Kneizys, E. P. Shettle, L. W. Abreu, J. H. Chetwynd, G. P. Anderson, W. O. Gallery, J. E. A. Selby, and S. A. Clough, AFGL Tech. Rep. AFGL-TR-88-0177, Air Force Geophysics Laboratory, Hanscom AFB, MA, 1988, ADA206773

[2] A. Berk, L. Bernstein, and D. Robertson, AFGL Tech. Rep., AFGL-TR-89-0122, Air Force Geophysics Laboratory, Hanscom AFB, MA, 1989, ADA214337

[3] G. P. Anderson, J. H. Chetwynd, J.-M. Therault, P. Acharya, A. Berk, D. C. Robertson, F. X. Kneizys, M. L. Hohe, L. W. Abreu, and E. P. Shettle, Proc. SPIE int. Soc. Opt. Eng., **1968**, 514 (1993).

[4] K. Minschwaner, G. P. Anderson, L. A. Hall, J. H. Chetwynd, R. J. Thomas, D. W. Rusch, A. Berk, and J. A. Conant, J. Geophys. Res. **100**, 11,165 (1995).

[5] D. J. Strickland and R. R. Meier, NRL Memorandum Report 5004 (1982).

[6] Y. Itikawa, M. Hayashi, A. Ichimura, K. Onda, K. Sakimoto, K. Takayanagi, M. Nakamura, H. Nishimura, and T. Takayanagi, J. Phys. Chem. Ref. Data **15**, 985 (1986).

[7] Y. Itikawa, A. Ichimura, K. Onda, K. Sakimoto, K Takayanagi, Y. Hatano, M. Hayashi, H. Nishimura, and S. Tsurubuchi, J. Phys. Chem. Ref. Data **18**, 23 (1989).

[8] Y. Itikawa and A. Ichimura, J. Phys. Chem. Ref. Data **19**, 637 (1990).

[9] R. R. Laher and F. R. Gilmore, J. Phys. Chem. Ref. Data **19**, 277 (1990).

[10] I. S. Kanik, S. Trajmar, and J. C. Nickel, J. Geophys. Res. **98**, 7447 (1993).

[11] D. J. Strickland, D. L. Book, T. P. Coffey and J. A. Fedder, J. Geophys. Res. **81**, 2755 (1976).

[12] E. Krishnakumar and S. K Srivastava, J. Phys. B: At. Mol Phys. **23**, 1893 (1990).

[13] E. Krishnakumar and S. K. Srivastava, Int. J. Mass Spectrom. Ion processes **113**, 1, (1992).

[14] D. Rapp and P. Englander-Golden, J. Chem. Phys. **43**, 1464 (1965).

[15] E. M. Brook, F. A. Harrison, and A. C. SH. Smith, J. Phys. B: At. Mol Phys. **11**, 3115 (1978).

[16]G. Sunshine, B. B. Aubrey, and B. Berderson, Phys., Rev. **154**, 1 (1967).

[17]R. C. Dehmel, M. A. Fineman, and D. R. Miller, Phys. Rev. A **13**, 115 (1976).

[18]J. L. Fox and G. A. Victor, Planet Space Sci. **36**, 329 (1988).

[19]G. Victor, K. Kirby-Docken, and A. Dalgarno, Planet. Space Sci. **24**, 679 (1976).

[20]E. S. Oran and D. J. Strickland, Planet. Space Sci. **26**, 1161 (1978).

[21]C. H. Jackman and A. E. S. Green, J. Geophys. Res. **84**, 2715 (1979).

[22]G. P. Mantas, Planet. Space Sci. **29**, 1319 (1981).

[23]K. Stamnes and M. H. Rees, J. Geophys. Res. **88**, 6301 (1983).

[24]P. G. Richards and D. G. Torr, J. Geophys. Res. **93**, 4060 (1988).

[25]P. G. Richards and D. G. Torr, J. Geophys. Res. **89**, 5625 (1984).

[26]S. C. Solomon, P. Hays., and V. J. Abreu, J. Geophys. Res. **93**,9867 (1988).

[27]D. J. Strickland, R. R. Meier, J. H. Hecht and A. B. Christensen, J. Geophys. Res. **94**, 13527 (1989).

[28]J. M. Ratliff, G. K. James, S. Trajmar, J. M. Ajello, and D. E. Shemansky, J. Geophys. Res. **96**, 17559 (1991).

[29]J. P. Doering and S. O. Vaughan, J. Geophys. Res. **91**, 3279 (1986)

[30]T. W. Shyn and G. R. Carignan, Phys. Rev. A **22**, 923 (1980)

[31]T. W. Shyn, Phys. Rev. A **27**, 2388 (1983)

[32]D. C. Cartwright, S. Trajmar, A. Chutjian, and W. Williams, Phy. Rev. A **16**, 1041 (1977).

[33]J. M. Ajello, I. Kanik, E. Bethke, and D. E. Shemansky, Submitted to J. Geophys. Res. (1994).

[34]M. J. Brunger and P. J. O. Teubner, Phys. Rev. A **41**, 1413 (1990).

[35]D. C. Cartwright, S. Trajmar, A. Chutjian, and W. Williams, Phys. Rev. A **16**, 1013 (1977).

[36]E. C. Zipf and R. W. McLaughlin, Planet. Space Sci. **26**, 449 (1978).

[37]H. J. Winters, J. Chem. Phys. **44**, 1472 (1966).

[38]P. C. Cosby, J. Chem. Phys. **98**, 9544 (1993).

[39]A. E. Hedin, J. Geophys. Res. **96**, 1159 (1991).

[40]T. W. Shyn and C. J. Sweeney, Phys. Rev. A **48**, 1214 (1993).

[41]T. W. Shyn, C. J. Sweeney, A. Grafe, and W. E. Sharp, Phys. Rev. A **50**, 4794 (1994).

[42]J. P. Sullivan, J. C. Gibson, R. J. Gulley, and S. J. Buckman, J. Phys. B: At. Mol. Phys. **28**, 4319 (1995).

[43] T. W. Shyn and W. E. Sharp, Phys. Rev. A **26**, 1369 (1982)

[44] K. Wakiya, J. Phys. B: At. Mol. Phys. **11**, 3913 (1978)

[45]T. W. Shyn and W. E. Sharp, Phys. Rev. A **43**, 2300 (1991)

[46]J. P. Doering and E. E. Gulcicek., J. Geophys. Res. **94**, 2733 (1989).

[47]J. P. Doering and E. E. Gulcicek., J. Geophys. Res. **94**, 1541 (1989).

[48]C. H. Jackman, R. M. Garvey, and A. E. S. Green, J. Geophys. Res **82**, 5081 (1977).

[49]G. K. James, J. M. Ajello, B. Franklin, and D. E. Shemansky, J. Phys. : At. Mol. Phys. **23**, 2055 (1990).

[50]D. J. Strickland and D. E. Anderson, J. Geophys. Res. **88**, 9260 (1983).

[51]J. M. Ajello and D. E. Shemansky, J. Geophys. Res **90**, 9845 (1985).

[52]J. S. Lee, J. P. Doering, T. A. Potemra, and L. H. Brace, Planet. Space Sci. **28**, 947 (1980).

[53]R. R. Conway, Planet. Space Sci. **31**, 1223 (1983).

[54]L. C. Pitchford and A. V. Phelps, Phys. Rev. A **25,** 540 (1982).

[55]A. V. Phelps and L. C. Pitchford, Phys. Rev. A **31**, 2932 (1985).

[56]L. J. Kieffer and G. H. Dunn, Rev. Mod. Phys. **38**, 1 (1966).

[57]B. M. Jelenkovic and A. V. Phelps, Phys. Rev. A **36**, 5310 (1987).

[58]S. Trajmar, D. F. Register, and A. Chutjian, Phys. Rept. **97**, 219 (1983).

[59]K. D. Pang, J. M. Ajello, B. Franklin, and D. E. Shemansky, J. Chem. Phys. **86**, 2750 (1987).

[60]N. J. Mason and W. R. Newell, J. Phys. B: At. Mol. Phys. **20**, 3913 (1987).

[61]J. M. Ajello, G. K. James, B. O. Franklin, and D. E. Shemansky, Phys. Rev. A **40**, 3524 (1989).

[62]R. R. Meier, Space Sci. Rev. **58**, 1 (1991).

[63]T. W. Shyn and C. J. Sweeney, Phys., Rev. A **47**, 1006 (1993).

[64]K. Wakiya, (1978), J. Phys. B: At. Mol. Phys. **11**, 3931 (1978)

[65]T. W. Shyn, C. J. Sweeney, and A. Grafe, Phys. Rev. A **49**, 3680 (1994).

[66]E. E. Gulcicek and J. P. Doering, J. Geophys. Res. **93**, 5879 (1988).

[67]E. E. Gulcicek, J. P. Doering, and S. O. Vaughan, J. Geophys. Res. **93**, 5885 (1988).

[68]S. O. Vaughan and J. P. Doering, J. Geophys. Res. **93**, 289 (1988).

[69]T. W. Shyn, J. Geophys. Res. **91**, 1691 (1986)

[70]T. W. Shyn, S. Y. Cho, and W. E. Sharp, J. Geophys. Res. **91**, 13751 (1986)

TABLES

Table 1. Ionization and excitation cross sections for N_2. We are using these to account for all energy loss to electrons impacting on N_2 in calculations of photoelectron and auroral electron fluxes.

Table 2. Ionization and excitation cross sections for O_2. Similar to Table 1, these are intended to account for all energy loss to electrons impacting on O_2.

Table 3. Ionization and excitation cross sections for O. Similar to Table 1, these are intended to account for all energy loss to electrons impacting on O.

FIGURES

Figure 1. Measured energy loss spectra for N_2 and energy level diagram showing electronic states contributing to loss in the given energy range. See text for details on incident electron energies, scattering angles, and references.

Figure 2. Comparison between our derived and measured total N_2 cross section. Also shown are the components of our constructed cross section that include elastic, total ionization, and the sum of excitation cross sections from Table 1.

Figure 3. Excitation cross sections for the six triplet electronic states of N_2.

Figure 4. Excitation cross sections for the ten singlet electronic states of N_2. Vibrational cross sections are summed into a single cross section whose magnitude is reduced by a factor of 10 to be fully displayed in the given panel. Also shown in the lower panel is the sum of the cross sections for the high lying states.

Figure 5. Individual excitation cross sections for the high lying states.

Figure 6. Derived and measured cross sections for dissociation (excluding dissociative ionization). Error bars refer to the Cosby[38] data.

Figure 7. Loss function from this work compared with the Bethe formula. Also shown are its components from this work.

Figure 8. Examples of energy loss spectra for O_2 and identification of states producing the exhibited structure. See text for details on incident electron energies, scattering angles, and references.

Figure 9. Total cross section information similar to Figure 2 except for O_2.

Figure 10. Cross sections for vibration excitation (summed over components identified in Table 2), for the singlet states, and for a combined measurement over the $A^3\Sigma_u^+ + A'^3\Delta_u + c'\Sigma_u^-$ states.

Figure 11. The remaining excitation cross sections from Table 2.

Figure 12. Loss function information similar to that in Figure 7 except for O_2.

Figure 13. Examples of energy loss spectra for O and identification of states producing the exhibited structure. See text for details on incident electron energies, scattering angles, and references.

Figure 14. Total cross section information similar to Figure 2 except for O.

Figure 15. Cross sections for singlet, quintet and Rydberg states of O. Rydberg cross sections (as summed by us) from Laher and Gimore[9] are also shown for comparison.

Figure 16. Cross sections for the triplet states of O.

Figure 17. Autoionization cross sections of O for the following transitions: $^3P \rightarrow 2s\ ^2p^5\ ^3P^0$, $^3P \rightarrow 3s''\ ^3P^0$ and $^3P \rightarrow 4d'\ ^3P^0$.

Figure 18. Loss function information similar to that in Figure 7 except for O.
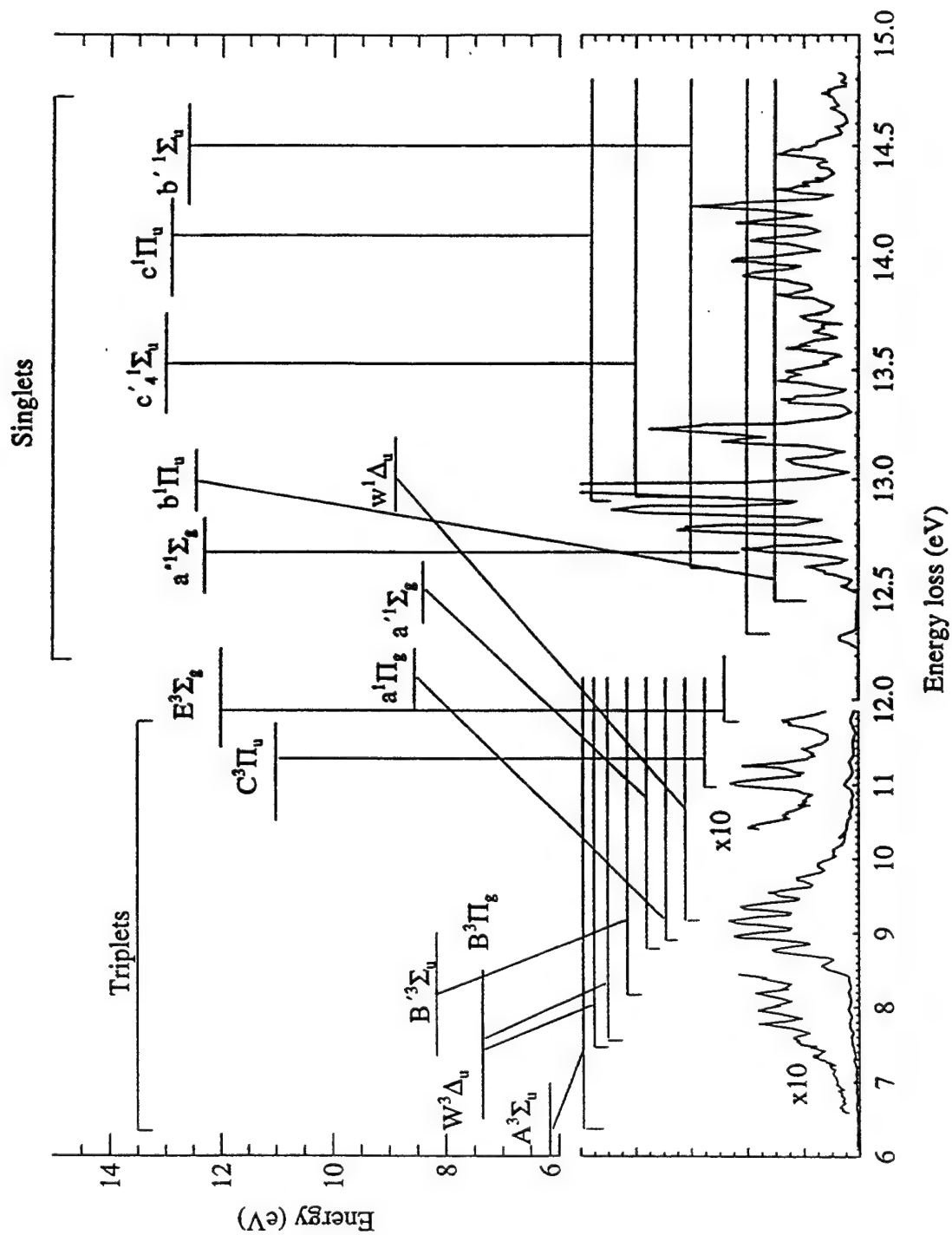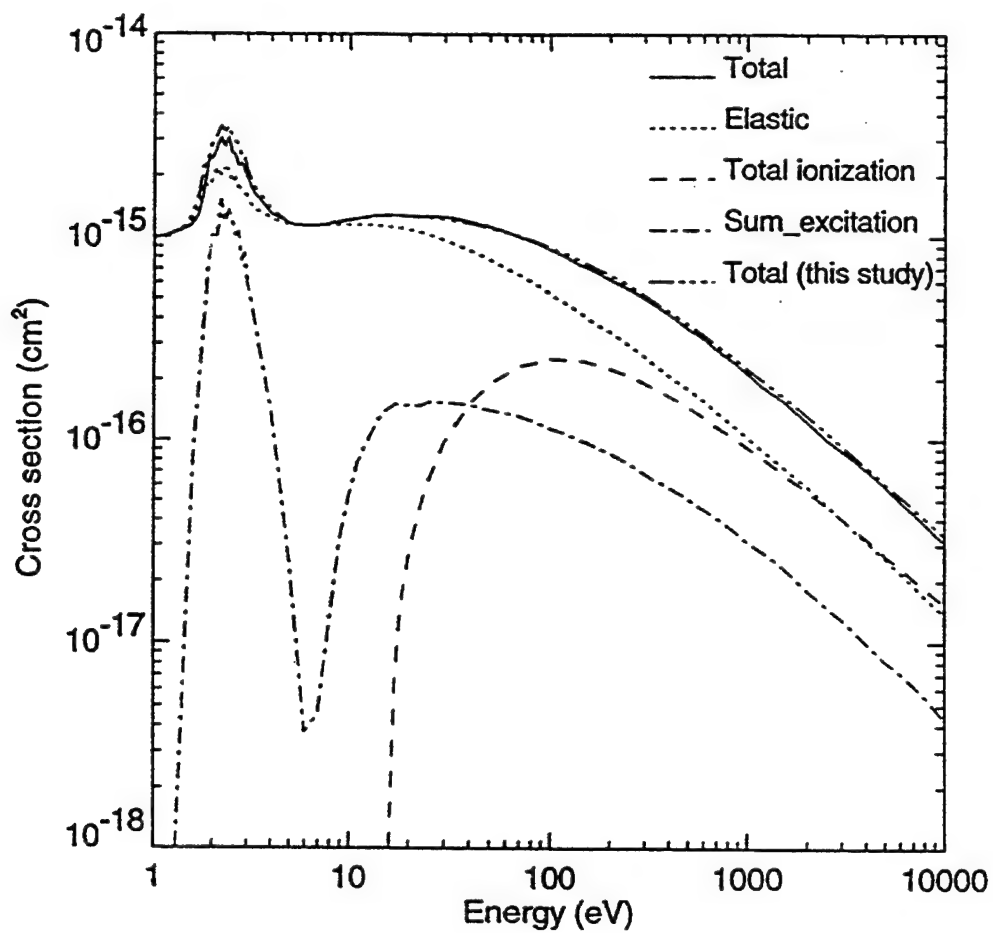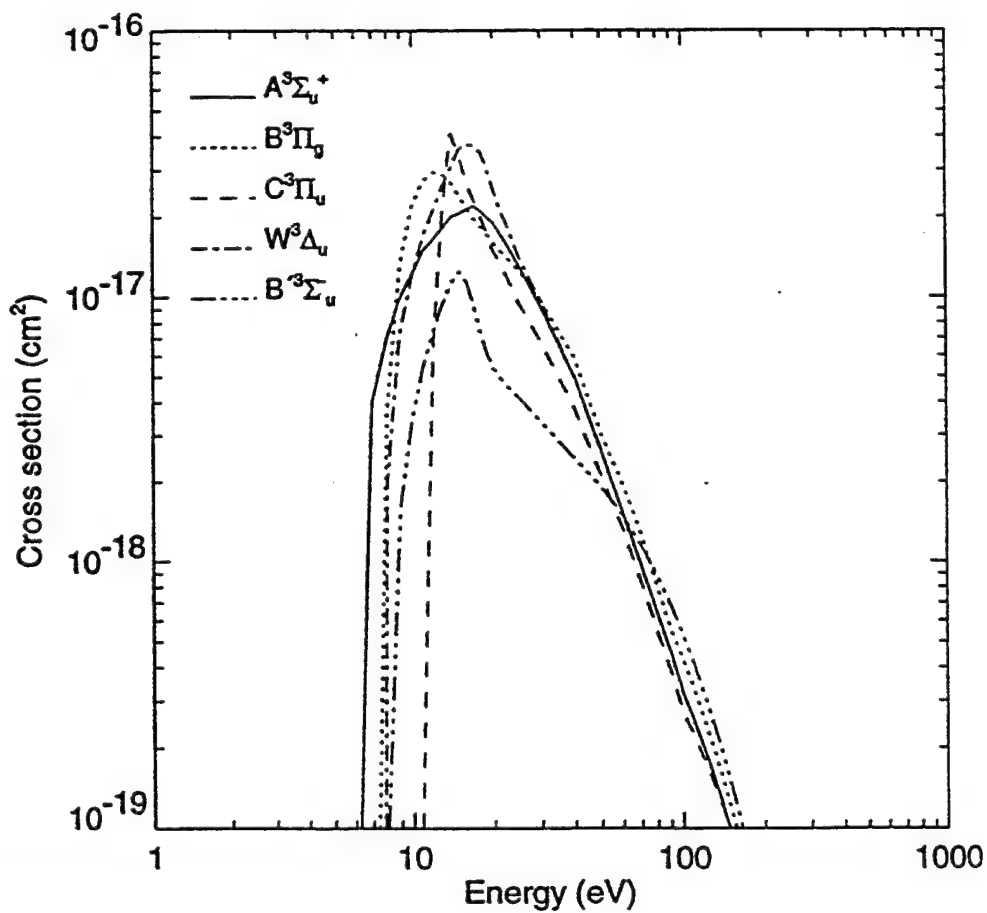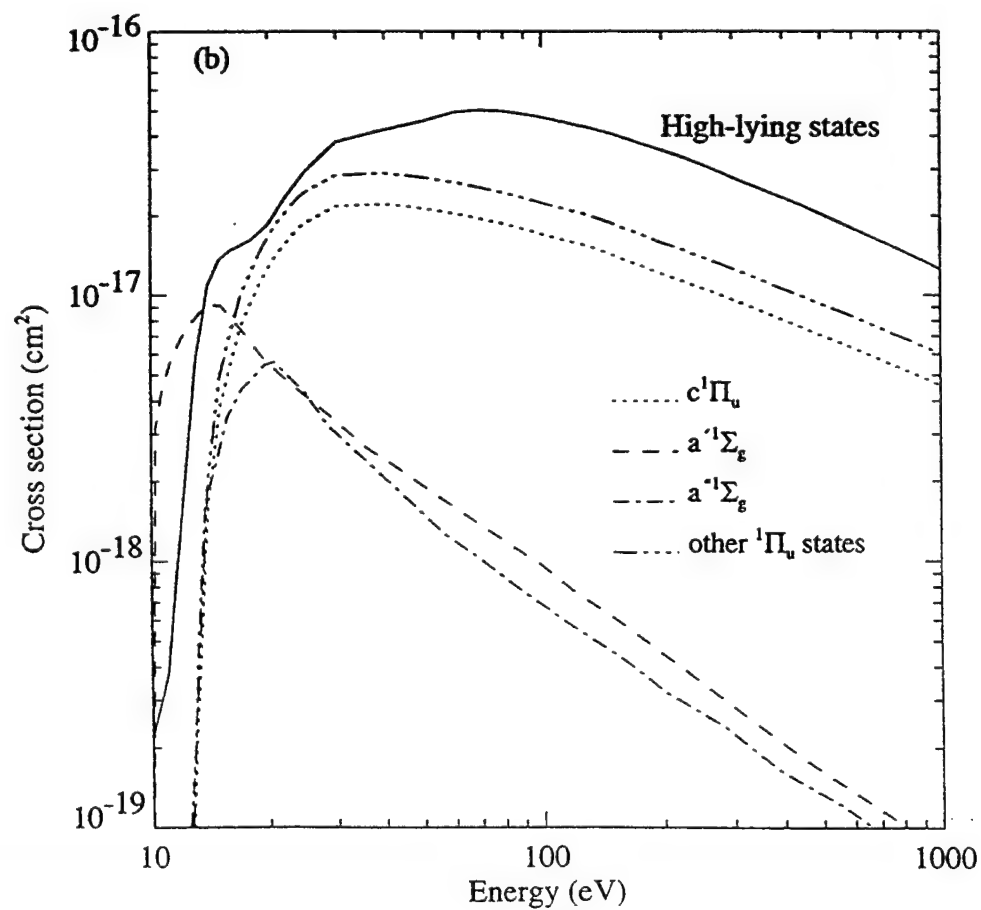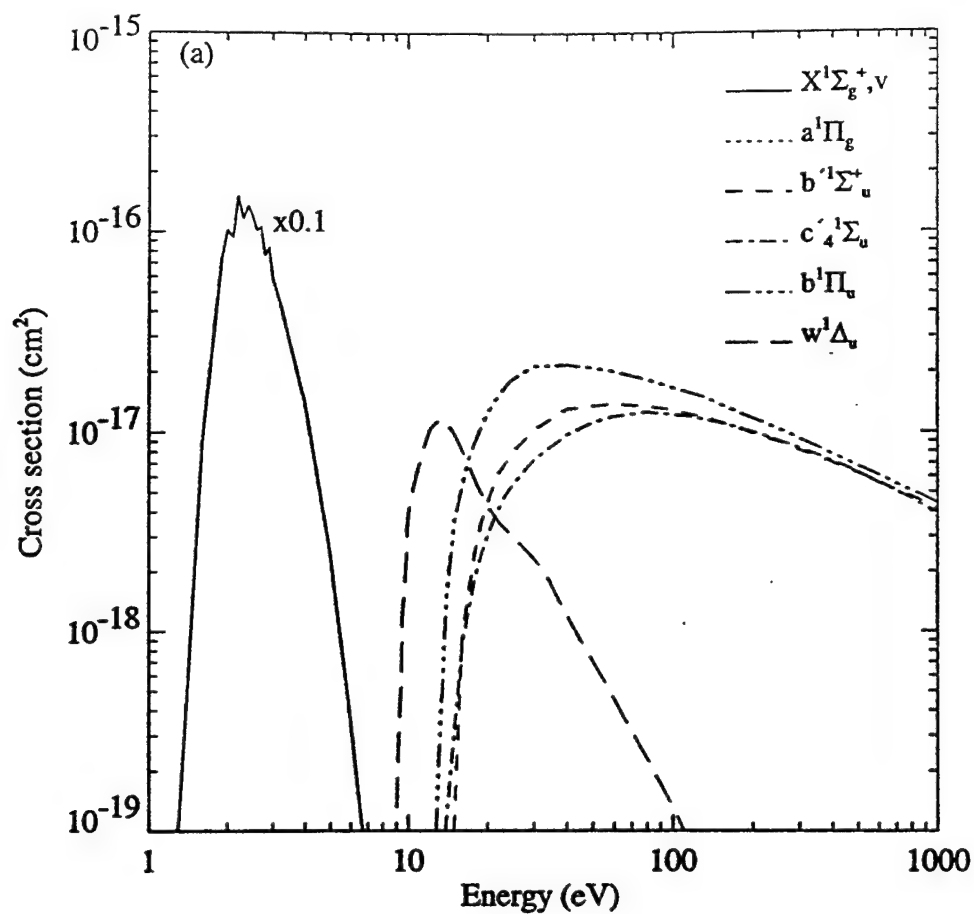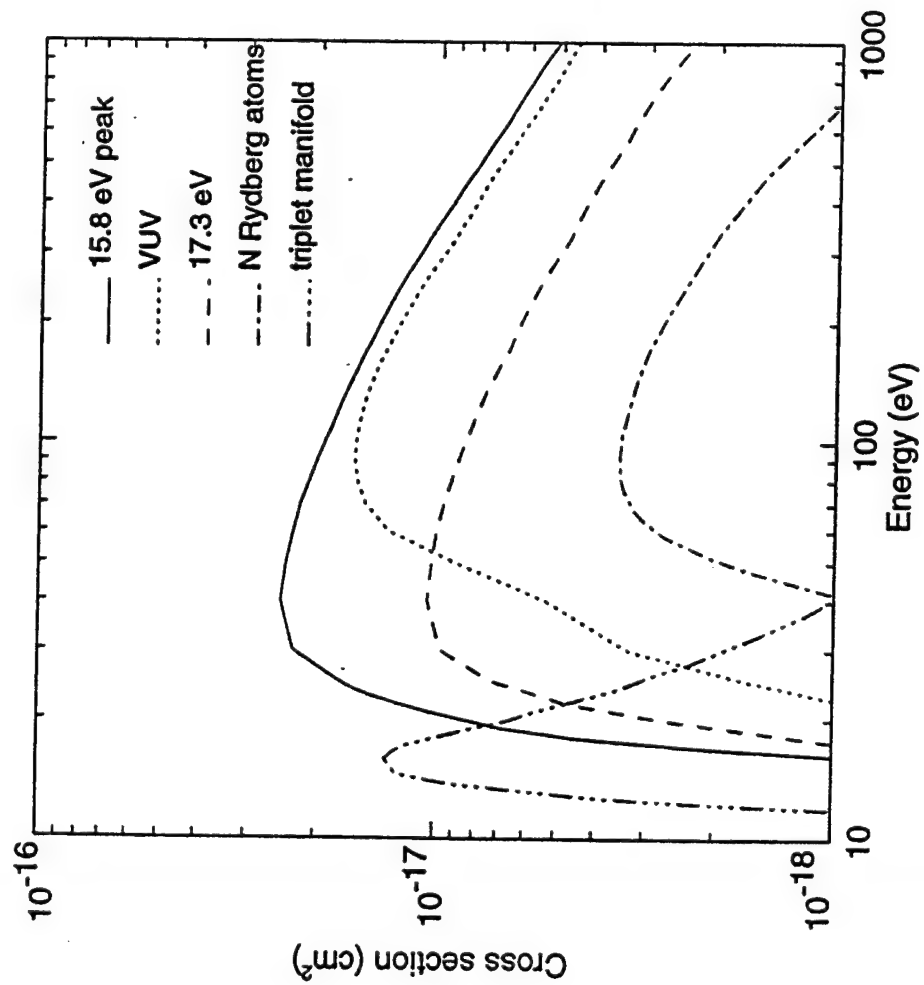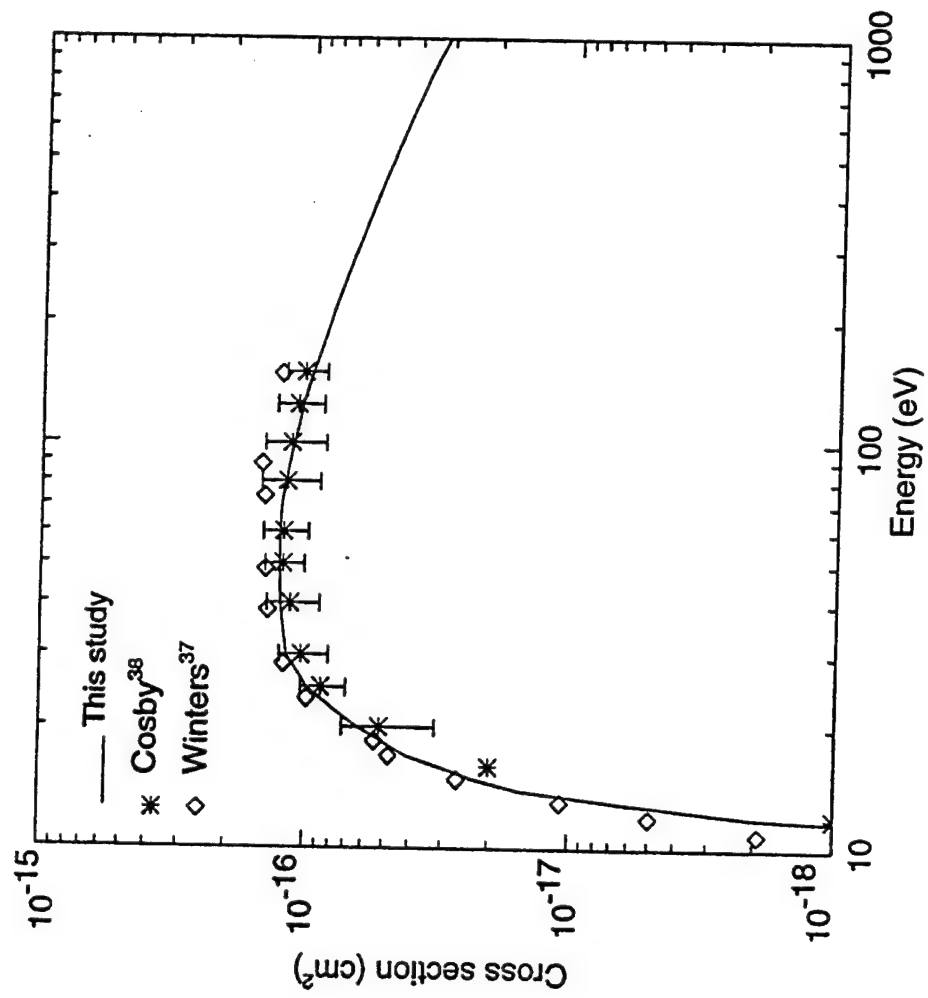
FIGURE 1

68

FIGURE 2

FIGURE 3

69

FIGURE 4

70

FIGURE 6

FIGURE 5

71
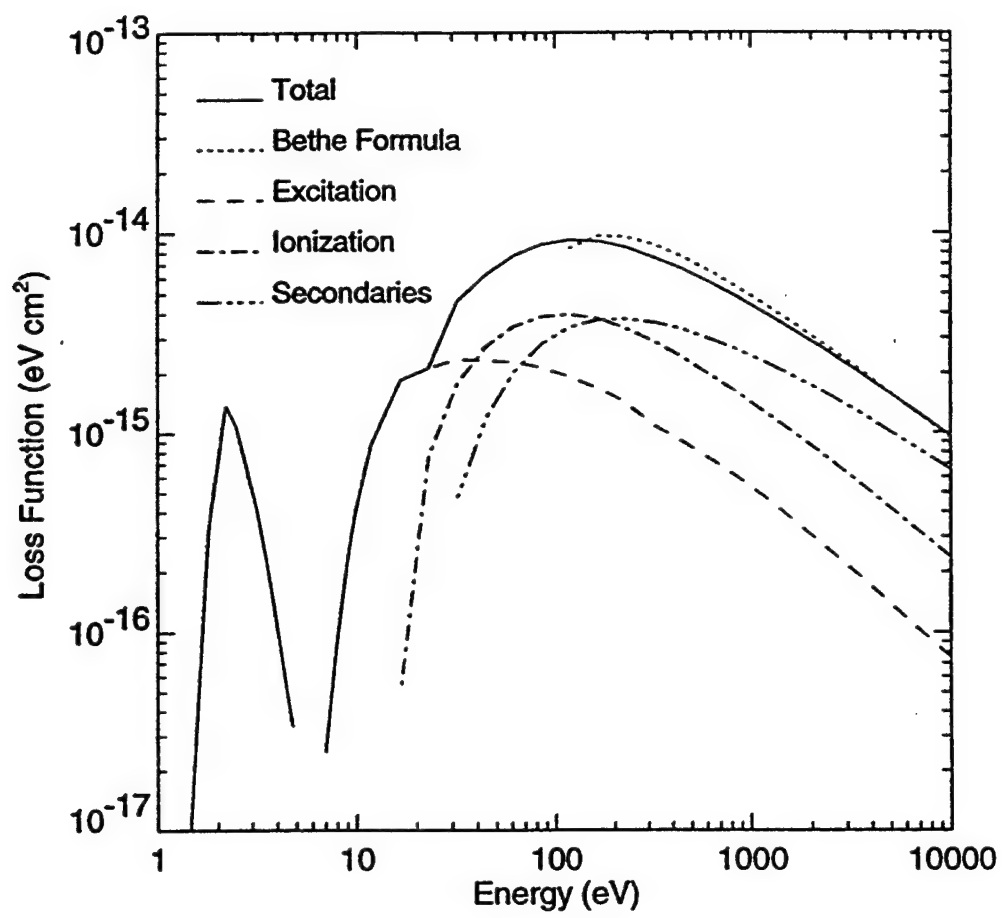
FIGURE 7

FIGURE 8

FIGURE 10
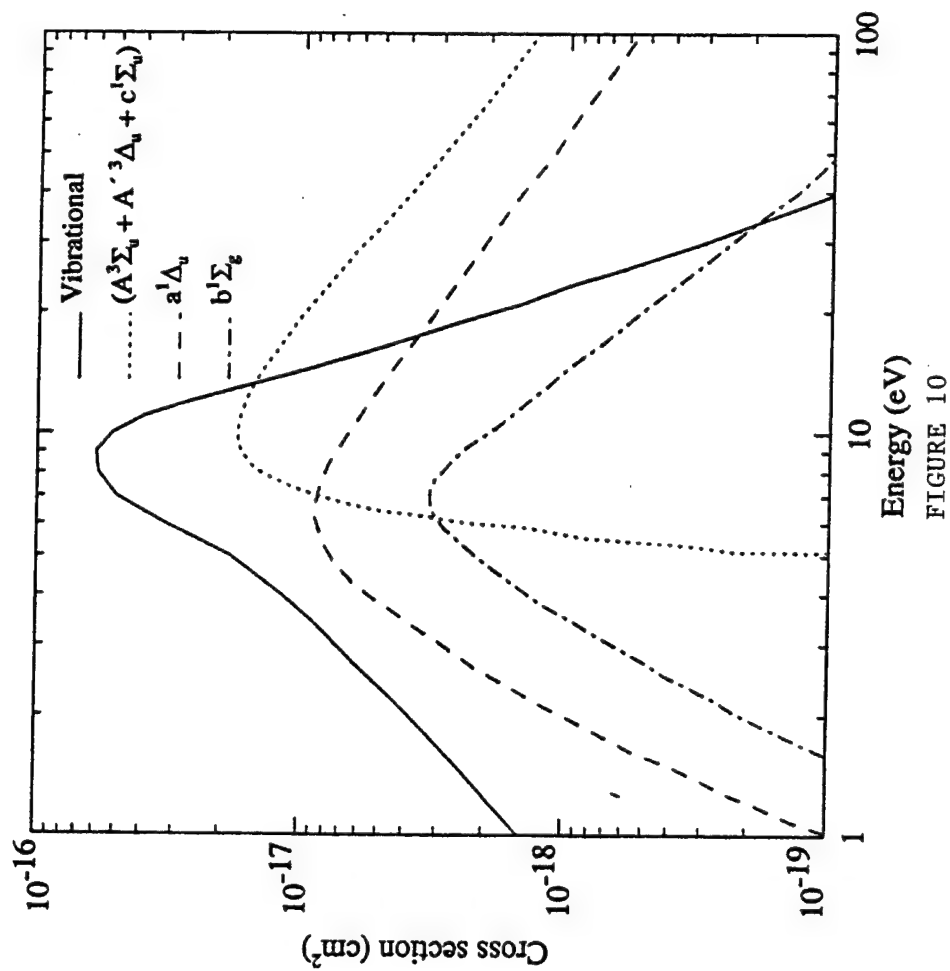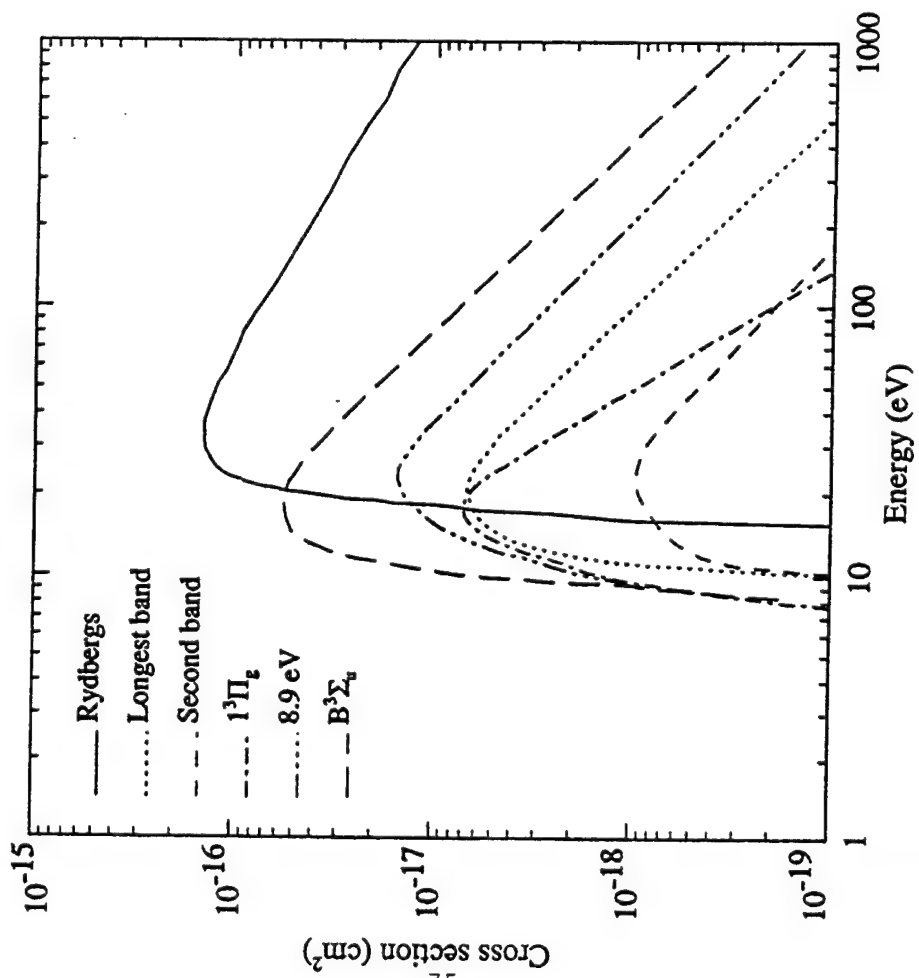
FIGURE 9

74

FIGURE 12

FIGURE 11

75

FIGURE 13

76

FIGURE 15

FIGURE 14

77

FIGURE 17

FIGURE 16

78

FIGURE 18

79
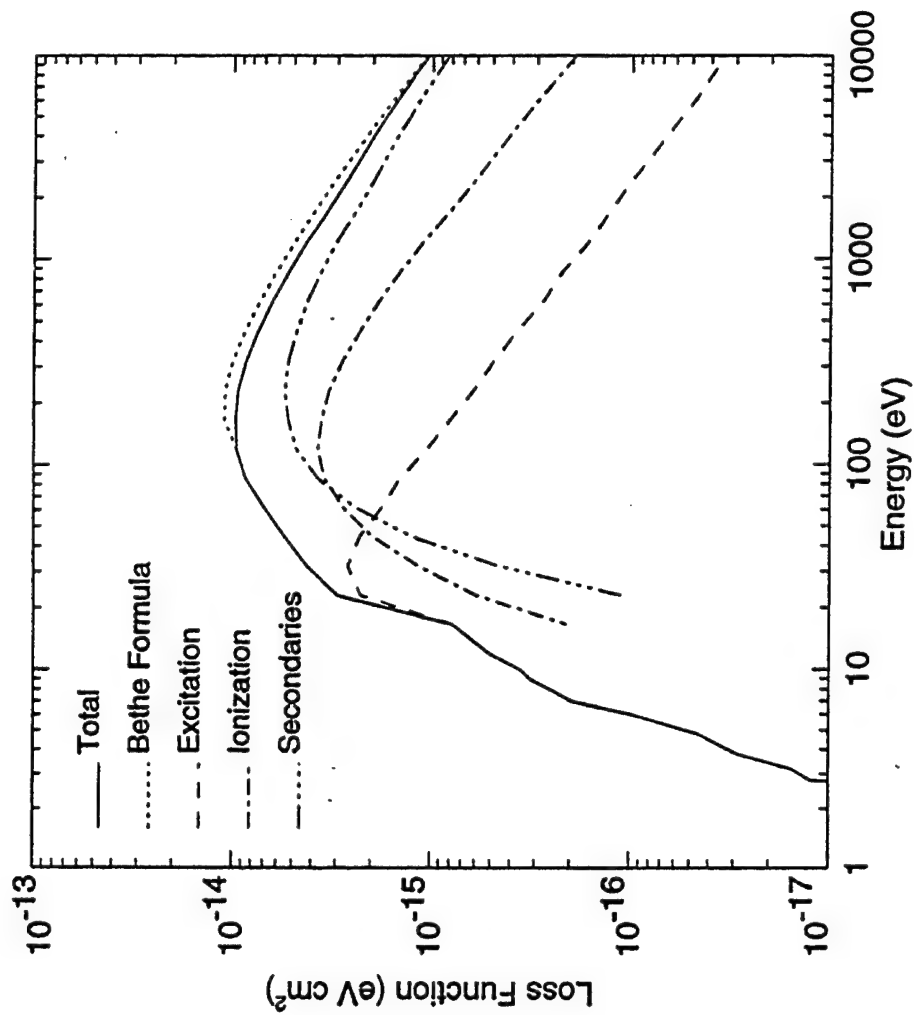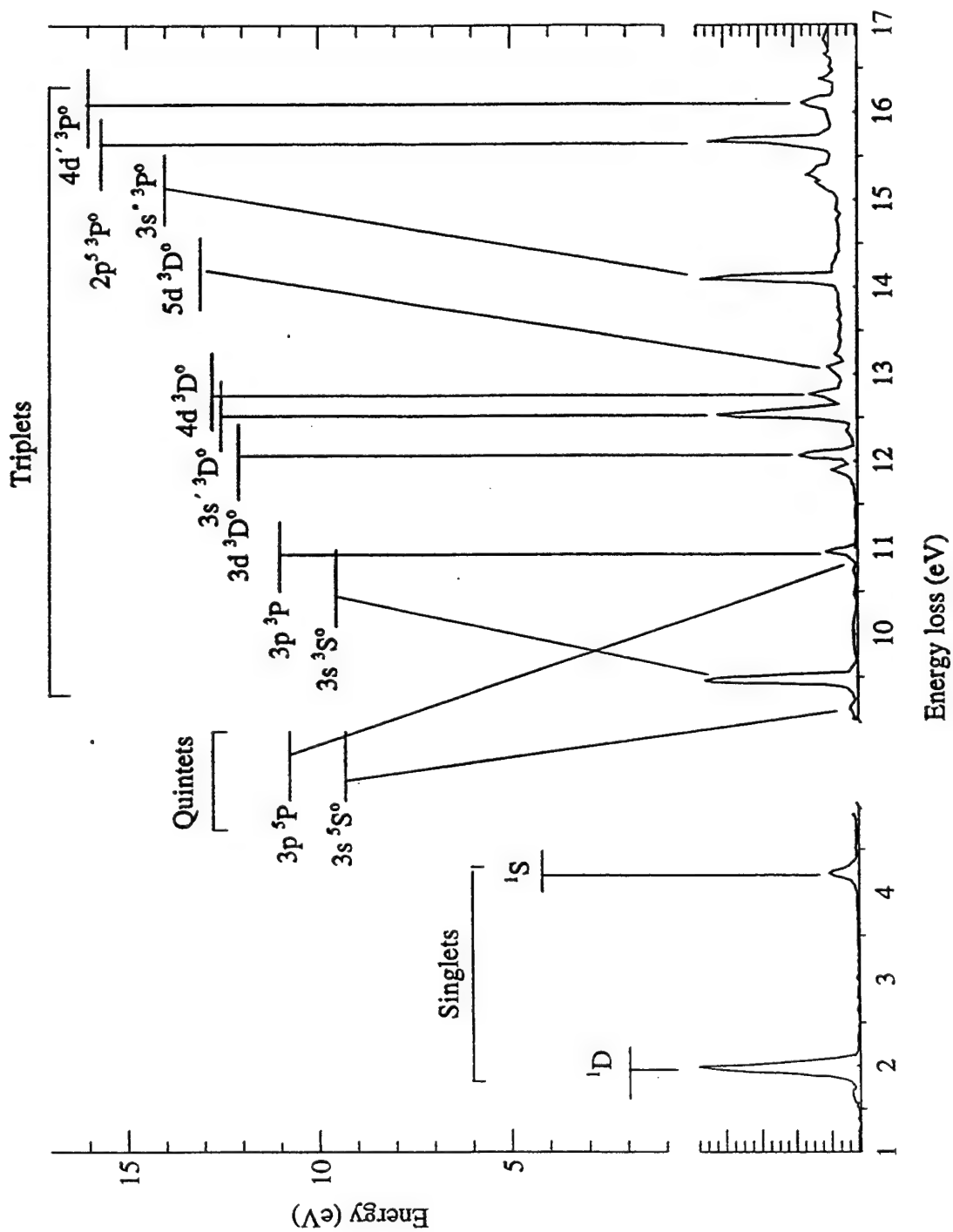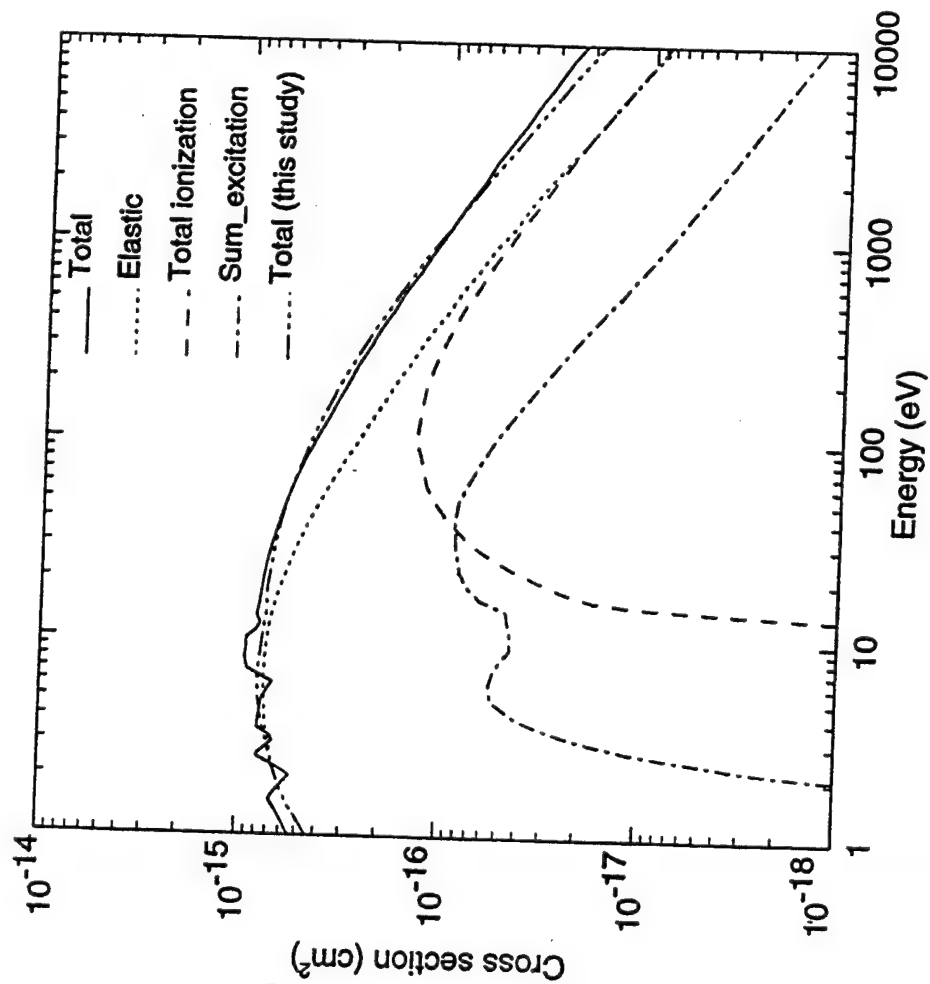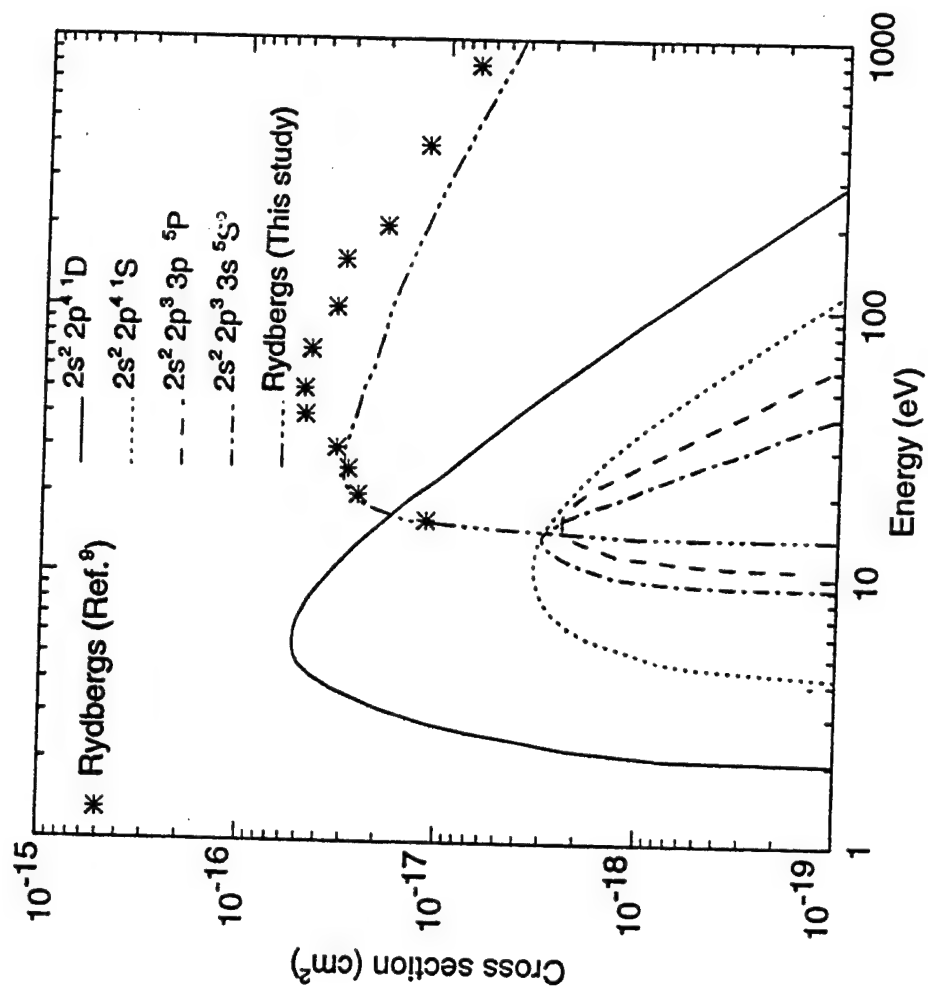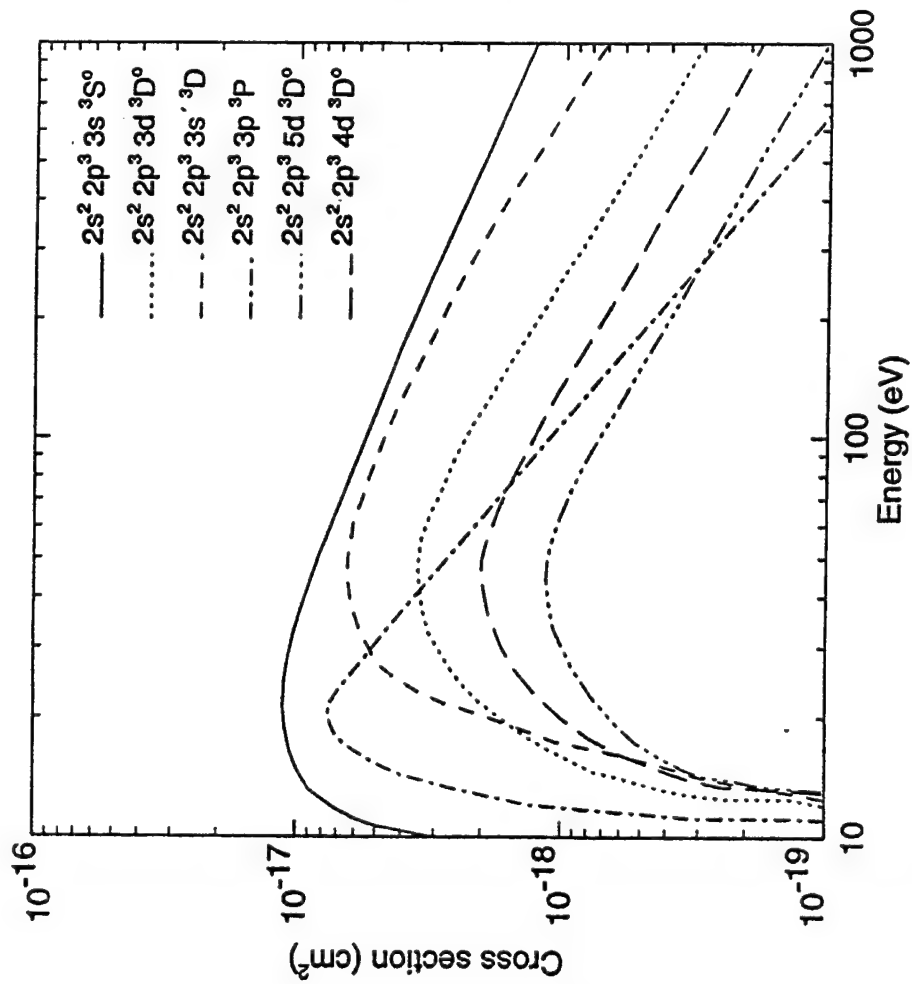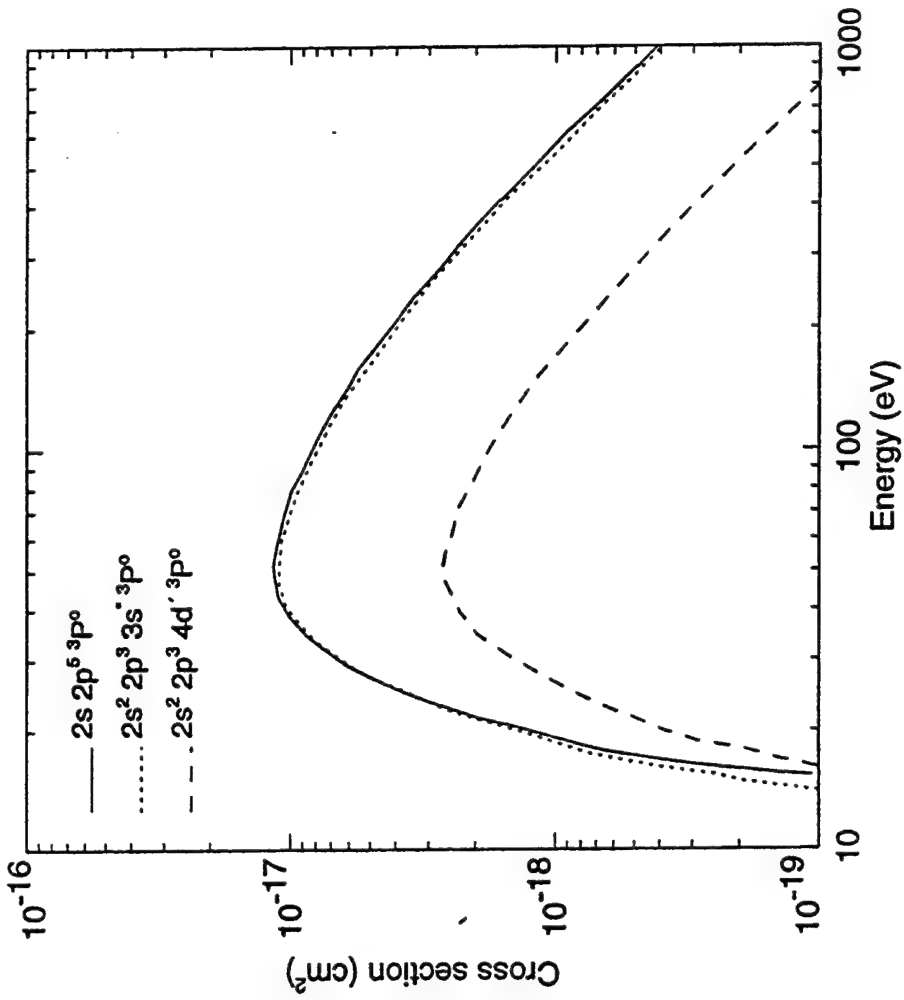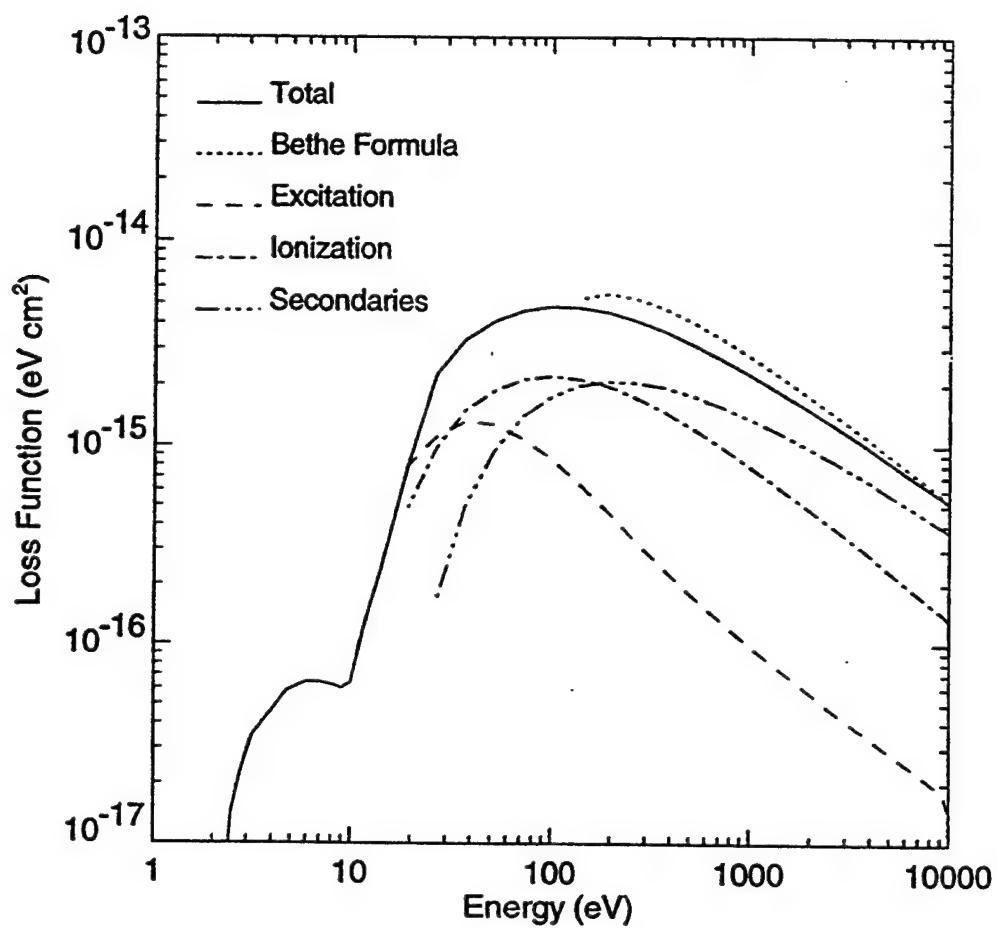
Table 1

Excitation/ Ionization	Threshold (eV)	E_{max} (eV)	σ_{max} cm^2 (10^{-18})	% Contribution to Dissociation	Reference
N_2^+ (*Total*)	15.6	100	252	—	12, 14
N_2 ($X^3\Sigma_g^+$)*vib* (*Total*)	0.9	2.0	1540	—	6
N_2 ($a^1\Pi_g$)	9.1	18.0	26.9	12	51, 59, 60
N_2 ($b'^1\Sigma_u^+$)	14.2	60.0	13.6	83	61
N_2 ($c_4^{'1}\Sigma_u$)	12.9	80.0	12.4	15	61
N_2 ($b^1\Pi_u$)	12.6	40.0	21.2	96	28, 36
N_2 ($c^1\Pi_u$)	12.9	40.0	22.0	100	49, 36
N_2 ($a'^1\Sigma_u^-$)	8.4	15.0	10.4	—	35
N_2 ($a''^1\Sigma_g^+$)	12.3	20.0	5.8	—	35
N_2 ($w^1\Delta_u$)	8.89	13.0	11.7	—	35
N_2 ($A^3\Sigma_u^+$)	6.2	17.0	22.0	—	35
N_2 ($B^3\Pi_g$)	7.4	11.5	29.5	—	35
N_2 ($C^3\Pi_g$)	11.0	14.0	36.0	50	33, 36, 61
N_2 ($W^3\Delta_u$)	7.5	16.5	38.0	—	35
N_2 ($B'^3\Sigma_u^-$)	8.0	15.0	12.5	—	35
N_2 ($E^3\Sigma_g^+$)	12.0	24.0	0.8	—	35, 36
N_2 (*15.8 eV peak*)	16.4	40.0	25.0	100	36
N_2 (*VUV*)	23.7	100	15.5	100	36
N_2 (*17.3 eV peak*)	17.4	40.0	10.5	100	36
N_2 (*N Ryd atoms*)	40.0	88.0	3.4	100	36
N_2 (*N_2 triplet manifold*)	11.0	17.0	12.0	100	36
Other $^1\Pi_u$ *states*	12.6	40.0	30.0	—	36

<p style="text-align:center">Table 2</p>

Excitation/ Ionization	Threshold (eV)	E_{max} (eV)	σ_{max} (10^{-18}) cm^2	Reference
O_2^+ (Total)	12.1	100	291	10, 13, 14
$O_2(X^3\Sigma_g^+)\, v=1$	0.3	8.8	35.1	40
$O_2(X^3\Sigma_g^+)\, v=2$	0.4	9.9	17.6	40
$O_2(X^3\Sigma_g^+)\, v=3$	0.6	9.7	7.7	40
$O_2(X^3\Sigma_g^+)\, v=4$	0.8	9.3	4.5	40
$O_2(1^3\Pi_g)\, SR$	7.6	20.0	6.8	41
$O_2(B^3\Sigma_u)\, SR$	8.3	19.3	60.6	41
$O_2(8.9\ eV\ peak)\, SR$	8.9	24.3	14.5	41
$O_2(second\ band)\,(^3\Sigma)$	10.3	21.8	1.0	65
$O_2(a^1\Delta_u)$	1.0	7.4	10.6	63, 64
$O_2(b^1\Sigma_g^+)$	1.6	6.9	3.5	63, 64
$O_2(longest\ band)\,(^3\Sigma)$	10.0	24.4	6.8	65
$O_2(A^3\Sigma_u^+ + A'^3\Delta_u + c^1\Sigma_u^-)$	4.5	8.0	15.3	7, 64
$O_2(Rydbergs)$	16.0	32.0	140.0	18

<p style="text-align:center">Table 3</p>

Excitation/ Ionization	Threshold (eV)	E_{max} (eV)	σ_{max} (10^{-18}) cm^2	Reference
O^+ (Total)	13.6	100	138	8, 15
$2s^2\,2p^4\quad {}^1D$	2.0	6.0	28.3	47, 69
$2s^2\,2p^4\quad {}^1S$	4.2	9.0	3.3	47, 70
$2s^2\,2p^3\,3s\,{}^5S^\circ$	9.3	13.7	8.9	46
$2s^2\,2p^3\,3s\,{}^3S^\circ$	9.5	29.5	9.1	66
$2s^2\,2p^3\,3p\,{}^5P$	10.7	16.0	3.3	67
$2s^2\,2p^3\,3p\,{}^3P$	11.0	24.0	12.4	67
$2s^2\,2p^3\,3d\,{}^3D^\circ$	12.1	45.6	36.6	66
$2s^2\,2p^3\,3s'\,{}^3D$	12.5	49.0	5.9	68
$2s^2\,2p^3\,4d\,{}^3D^\circ$	12.8	45.1	2.0	68
$2s^2\,2p^3\,5d\,{}^3D^\circ$	13.0	47.5	1.0	68
$2s^2\,2p^3\,4d'\,{}^3P^\circ$	16.0	45.1	2.8	68
$2s^2\,2p^5\quad {}^3P^\circ$	15.0	45.1	13.2	68
$2s^2\,2p^3\,3s''\,{}^3P^\circ$	14.0	44.8	13.3	68
Rydbergs	14.0	25.0	30.0	18

Table A1

Ionization		Dissociation		Vibrational	
E (eV)	σ (10^{-17} cm^2)	E (eV)	σ (10^{-17} cm^2)	E (eV)	σ (10^{-17} cm^2)
---	----	11	.070	----	----
---	----	12	.328	----	----
16	.113	14	1.77	----	----
18	1.33	16	3.32	1.3	.111
20	2.68	20	6.59	1.6	8.84
30	9.78	30	12.08	2.0	101.
50	18.82	50	12.84	2.4	135.
100	25.20	100	11.43	3.0	58.6
200	22.58	200	8.48	4.0	13.7
500	14.55	500	5.03	5.0	2.34
1000	9.21	1000	3.16	6.0	.366

Table A2

$A\,^3\Sigma_u^+$		$B\,^3\Pi_g$		$C\,^3\Pi_g$		$W\,^3\Delta_u$		$B'\,^3\Sigma_u^-$	
E (eV)	σ (10^{-17} cm^2)	E (eV)	σ (10^{-17} cm^2)	E (eV)	σ (10^{-17} cm^2)	E (eV)	σ (10^{-17} cm^2)	E (eV)	σ (10^{-17} cm^2)
6.5	.100	----	----	----	----	----	----	----	----
7.0	.400	7.6	.053	----	----	----	----	----	----
8.0	.700	8.0	.377	----	----	8.0	.200	----	----
9.0	1.00	9.0	1.33	----	----	9.0	.740	9.0	.160
10	1.23	10	2.19	12	.650	10	1.20	10	.350
12	1.65	12	2.93	13	2.10	12	2.10	12	.740
14	2.00	14	2.70	14	4.10	14	3.06	14	1.13
16	2.13	16	2.16	16	2.70	16	3.73	16	1.14
18	2.10	18	1.84	18	2.00	18	3.50	18	.730
20	1.90	20	1.60	20	1.50	20	2.57	20	.540
24	1.40	24	1.31	24	1.03	24	1.57	24	.430
30	.919	30	.973	30	.680	30	.972	30	.337
40	.500	40	.592	40	.380	40	.500	40	.245
50	.262	50	.304	50	.210	50	.262	50	.190
70	.096	70	.125	70	.082	70	.096	70	.114
100	.032	100	.042	100	.027	100	.032	100	.053
150	.009	150	.012	150	.010	150	.010	150	.015
200	.004	200	.003	200	.0034	200	.004	200	.004

Table A3

$a^1\Pi_g$		$b\,^1\Pi_u$		$b'\,^1\Sigma_u^+$		$c'_4\,^1\Sigma_u$		$w\,^1\Delta_u$	
E (eV)	σ $(10^{-17}\,cm^2)$	E (eV)	σ $(10^{-17}\,cm^2)$	E (eV)	σ $(10^{-17}\,cm^2)$	E (eV)	σ $(10^{-17}\,cm^2)$	E (eV)	σ $(10^{-17}\,cm^2)$
----	----	13	.002	15	.013	---	----	9	.010
10	.220	14	.157	16	.089	14	.012	10	.362
12	1.15	16	.526	18	.256	16	.081	12	.981
18	2.69	20	1.21	20	.436	20	.298	14	1.10
30	1.86	30	2.08	30	1.01	30	.719	16	.806
50	1.12	50	2.04	50	1.32	50	1.10	20	.430
100	.559	100	1.63	100	1.26	100	1.20	30	.231
200	.280	200	1.16	200	.978	200	.995	50	.071
500	.111	500	.676	500	.623	500	.629	100	.013
1000	.056	1000	.440	1000	.409	1000	.394	200	.001

Table A4

$c\,^1\Pi_u$		$a'\,^1\Sigma_u^-$		$a''\,^1\Sigma_g^+$		Other $^1\Pi_u$ states	
E (eV)	σ $(10^{-17}\,cm^2)$	E (eV)	σ $(10^{-17}\,cm^2)$	E (eV)	σ $(10^{-17}\,cm^2)$	E (eV)	σ $(10^{-17}\,cm^2)$
----	----	11	.507	13	.031	----	----
13	.002	12	.688	14	.182	13	.002
14	.163	14	.910	16	.368	14	.216
16	.549	16	.824	20	.551	16	.724
20	1.26	20	.558	25	.426	20	1.66
30	2.17	30	.334	30	.304	30	2.86
50	2.13	50	.193	50	.152	50	2.81
100	1.70	100	.096	100	.069	100	2.25
200	1.21	200	.045	200	.033	200	1.59
500	.705	500	.016	500	.013	500	.930
1000	.458	1000	.008	1000	.007	1000	.605

Table A5

15.8 eV peak		VUV		17.3 eV peak		N Rydberg atoms		Triplet manifold	
E (eV)	σ (10^{-17} cm²)	E (eV)	σ (10^{-17} cm²)	E (eV)	σ (10^{-17} cm²)	E (eV)	σ (10^{-17} cm²)	E (eV)	σ (10^{-17} cm²)
--	--	--	--	--	--	--	--	12	.123
--	--	--	--	--	--	--	--	13	.519
17	.225	--	--	--	--	--	--	14	1.03
18	.453	25	.161	18	.120	--	--	16	1.31
20	.852	30	.328	20	.270	--	--	18	.986
25	1.74	40	.529	25	.720	--	--	20	.645
30	2.28	50	.897	30	.970	50	.186	25	.313
50	2.39	70	1.51	50	1.02	70	.327	30	.192
100	1.92	100	1.60	100	.850	100	.348	40	.103
200	1.40	200	1.24	200	.626	200	.275	50	.066
500	.800	500	.712	500	.377	500	.144	70	.027
1000	.510	1000	.456	1000	.232	1000	.061	100	.007

Table B1

Vibrational		Rydbergs		Ionization	
E (eV)	σ (10^{-17} cm^2)	E (eV)	σ (10^{-17} cm^2)	E (eV)	σ (10^{-17} cm^2)
1	.145	----	----	----	----
2	.381	----	----	13	.200
3	.720	17	.281	16	1.09
4	1.17	20	4.18	20	2.93
6	3.24	30	14.09	30	8.08
9	5.98	50	12.36	50	18.24
12	2.59	100	7.59	100	29.08
15	.755	200	4.34	200	27.46
20	.191	500	2.18	500	17.10
30	.030	1000	1.26	1000	10.54

Table B2

$A+A'+c$		$a\,'\Delta_u$		$b\,^1\Sigma_g^+$	
E (eV)	σ (10^{-17} cm^2)	E (eV)	σ (10^{-17} cm^2)	E (eV)	σ (10^{-17} cm^2)
6	.211	----	----	----	----
7	.846	2	.098	2	.021
8	1.41	3	.283	3	.064
10	1.73	4	.548	5	.214
15	1.33	6	.870	7	.324
20	.974	10	.661	9	.247
30	.580	20	.316	13	.117
50	.297	50	.113	20	.052
100	.131	100	.055	30	.024
150	.088	150	.035	50	.009
200	.068	200	.025	100	.002

Table B3

Longest band		Second band		$1\,^3\Pi_g$		8.9 eV		$B\,^3\Sigma u$	
E (eV)	σ (10^{-17} cm^2)	E (eV)	σ (10^{-17} cm^2)	E (eV)	σ (10^{-17} cm^2)	E (eV)	σ (10^{-17} cm^2)	E (eV)	σ (10^{-17} cm^2)
---	---	---	---	---	---	9	.058	---	---
---	---	---	---	8	.017	10	.162	9	.075
11	.083	---	---	9	.059	12	.413	10	.639
12	.212	12	.046	10	.137	15	.918	12	2.98
15	.519	15	.071	11	.210	20	1.42	15	5.29
20	.670	20	.093	13	.431	25	1.49	20	5.58
30	.510	30	.086	18	.700	30	1.27	30	3.91
50	.264	50	.047	24	.502	50	.671	50	1.99
100	.100	100	.020	30	.307	100	.271	100	.748
200	.038	200	.008	50	.095	200	.109	200	.285
500	.011	500	.001	100	.021	500	.034	500	.082
1000	.002	---	---	200	.003	1000	.014	1000	.030

Table C1

^1D		^1S		^5P		^5S		Ionization		Rydbergs	
E (eV)	σ (10⁻¹⁷ cm²)	E (eV)	σ (10⁻¹⁷ cm²)	E (eV)	σ (10⁻¹⁷ cm²)	E (eV)	σ (10⁻¹⁷ cm²)	E (eV)	σ (10⁻¹⁷ cm²)	E (eV)	σ (10⁻¹⁷ cm²)
2.3	.274	---	---	---	---	9.5	.077	---	---	15	.556
3	1.55	4.5	.032	---	---	10	.140	---	---	16	1.53
4	3.95	5	.090	11	.040	11	.205	14	.230	18	2.34
5.5	5.41	6	.190	12	.134	12	.261	16	1.72	20	2.85
8	4.59	8	.302	14	.223	14	.307	20	3.30	25	3.19
10	3.61	11	.336	16	.246	17	.210	30	7.06	30	3.14
15	2.10	15	.293	20	.194	20	.119	50	11.06	50	2.58
20	1.33	20	.223	25	.115	25	.058	100	13.80	100	1.90
30	.681	30	.131	30	.070	30	.029	200	12.22	200	1.28
50	.290	50	.053	50	.019	50	.004	500	7.92	500	.712
100	.081	100	.014	100	.002	100	---	1000	4.99	1000	.436

87

Table C2

3s³S E (eV)	σ (10⁻¹⁷ cm²)	3d³D E (eV)	σ (10⁻¹⁷ cm²)	3s'³D E (eV)	σ (10⁻¹⁷ cm²)	3p³P E (eV)	σ (10⁻¹⁷ cm²)	5d³D E (eV)	σ (10⁻¹⁷ cm²)	4d³D E (eV)	σ (10⁻¹⁷ cm²)
---	---	---	---	13	.014	---	----	---	---	---	---
---	---	12	.010.	14	.028	12	.120	---	---	---	---
10	0.302	13	.037	16	.057	14	.344	---	---	13	.015
12	0.732	14	.057	18	.120	16	.555	14	.024	14	.033
15	.998	16	.091	20	.187	20	.755	16	.043	16	.057
20	1.11	20	.170	25	.415	25	.641	20	.065	20	.100
30	1.05	30	.293	30	.532	30	.517	30	.100	30	.168
50	.836	50	.347	50	.642	50	.275	50	.113	50	.199
100	.557	100	.232	100	.470	100	.114	100	.073	100	.128
200	.369	200	.125	200	.288	200	.050	200	.040	200	.071
500	.206	500	.055	500	.133	500	.014	500	.020	500	.032
1000	.131	1000	.030	1000	.070	---	----	1000	.010	1000	.018

Table C3

$2p^5\,^3P$		$3s''\,^3P$		$4d'\,^3P$	
E (eV)	σ (10^{-17} cm^2)	E (eV)	σ (10^{-17} cm^2)	E (eV)	σ (10^{-17} cm^2)
16	.020	16	.035	----	----
18	.069	18	.084	18	.019
20	.123	20	.137	20	.038
25	.371	25	.360	25	.085
30	.648	30	.632	30	.140
50	1.15	50	1.10	50	.264
100	.828	100	.794	100	.178
200	.420	200	.400	200	.081
500	.120	500	.114	500	.021
1000	.041	1000	.039	800	.010